RUTHENIUM NANOPARTICLES SUPPORTED ON
NANOTUBES/NANOWIRES:
HIGHLY ACTIVE AND LONG LIVED NANOCATALYSTS
IN HYDROLYTIC DEHYDROGENATION OF AMMONIA BORANE

A THESIS SUBMITTED TO
THE GRADUATE SCHOOL OF NATURAL AND APPLIED SCIENCES
OF
MIDDLE EAST TECHNICAL UNIVERSITY

BY

SERDAR AKBAYRAK

IN PARTIAL FULFILLMENT OF THE REQUIREMENTS
FOR
THE DEGREE OF DOCTOR OF PHILOSOPHY
IN
CHEMISTRY

OCTOBER 2016

Approval of the thesis:

**RUTHENIUM NANOPARTICLES SUPPORTED ON
NANOTUBES/NANOWIRES:
HIGHLY ACTIVE AND LONG LIVED NANOCATALYSTS
IN HYDROLYTIC DEHYDROGENATION OF AMMONIA BORANE**

submitted by **SERDAR AKBAYRAK** in partial fulfillment of the requirements for the degree of **Doctor of Philosophy in Chemistry Department, Middle East Technical University** by,

Prof. Dr. Gülbin Dural Ünver _____
Dean, Graduate School of **Natural and Applied Sciences**

Prof. Dr. Cihangir Tanyeli _____
Head of Department, **Chemistry**

Prof. Dr. Saim Özkar
Supervisor, **Chemistry Dept., METU** _____

Examining Committee Members:

Prof. Dr. Gülsün Gökağaç _____
Chemistry Dept., METU

Prof. Dr. Saim Özkar _____
Chemistry Dept., METU

Prof. Dr. Deniz Üner _____
Chemical Engineering Dept., METU

Prof. Dr. Ayşen Yılmaz _____
Chemistry Dept., METU

Prof. Dr. İzzet Morkan _____
Chemistry Dept., Abant İzzet Baysal University

Date: 03/10/2016

I hereby declare that all information in this document has been obtained and presented in accordance with academic rules and ethical conduct. I also declare that, as required by these rules and conduct, I have fully cited and referenced all material and results that are not original to this work.

Name, Last name: Serdar Akbayrak

Signature

ABSTRACT

**RUTHENIUM NANOPARTICLES SUPPORTED ON
NANOTUBES/NANOWIRES:
HIGHLY ACTIVE AND LONG LIVED NANOCATALYSTS
IN HYDROLYTIC DEHYDROGENATION OF AMMONIA BORANE**

Akbayrak, Serdar

Ph.D., Department of Chemistry

Supervisor: Prof. Dr. Saim Özkar

October 2016, 117 pages

Ammonia borane (NH_3BH_3, AB) is one of the most promising solid hydrogen storage materials due to its high hydrogen storage capacity (19.6% wt.), non-toxicity and high stability under ambient conditions. Ammonia borane can release hydrogen upon hydrolysis in the presence of suitable catalysts even at room temperature. Although a large variety of catalysts have been tested in hydrogen generation from the hydrolysis of ammonia borane, the development of efficient, long-lived, reusable catalysts is still an important issue.

This dissertation reports the preparation, characterization and catalytic use of highly active, reusable and long-lived ruthenium catalysts for the hydrolysis of ammonia borane. Ruthenium(0) nanoparticles supported on multiwalled carbon nanotubes (Ru^0/MWCNT) were prepared for the hydrolysis of AB and characterized by advanced analytical techniques including ICP-OES, XRD, TEM, SEM, EDX, and XPS. The results reveal that ruthenium(0) nanoparticles of size in the range 1.4−3.0 nm are well-dispersed on multiwalled carbon nanotubes. Ru^0/MWCNT were found to be highly active catalyst in hydrogen generation from the hydrolysis of AB with a turnover frequency value of 329 min^{-1} at 25.0 ± 0.1 °C.

For comparison, ruhenium(0) nanoparticles were also formed on an inorganic nanowire, xonotlite $(Ca_6(Si_6O_{17})(OH)_2)$. Ruhenium(0) nanoparticles supported on xonotlite $(Ru^0/X\text{-}NW)$ were prepared by the ion exchange of Ru^{3+} ions with Ca^{2+} cations in the lattice of xonotlite nanowire followed by their reduction with sodium borohydride in aqueous solution at room temperature. $Ru^0/X\text{-}NW$ was also characterized by the same analytical methods. $Ru^0/X\text{-}NW$ are found to be a long lived catalyst with a TTO value of 134,100 in hydrolysis of ammonia borane $25.0 \pm 0.1°C$. The comparisons in terms of activity, life-time and reusability were also extended to the ruthenium(0) nanoparticles supported on hydroxyapatite (HAp) and silica coated cobalt ferrite $(CoFe_2O_4)$ supported ruthenium catalysts. Ru^0/HAp and $Ru^0/SiO_2\text{-} CoFe_2O_4$ catalysts were found to be highly active in hydrolysis of AB with a TOF value of 137 min^{-1} and 172.5 min^{-1}, respectively. Ru^0/HAp provides a TTO value of 87,000 in hydrolysis of ammonia borane at $25.0 \pm 0.1°C$. $Ru^0/SiO_2\text{-} CoFe_2O_4$ catalyst was found to be highly reusable catalyst in hydrolysis of AB retaining 94% of its initial catalytic activity even after tenth use.

Keywords: Catalyst, Ruthenium, Carbon Nanotube, Nanowire, Hydoxyapatite, Silica Coating, Magnetically Separable Catalyst, Hydrolysis of Ammonia Borane, Hydrogen Generation.

ÖZ

NANOTÜPLERLE/NANOTELLERLE DESTEKLENMİŞ RUTENYUM NANOPARÇACIKLARI: AMONYAK BORANIN HİDROLİTİK DEHİDROJENLENMESİNDE YÜKSEK AKTİFLİKLİ VE UZUN ÖMÜRLÜ NANOKATALİZÖRLER

Akbayrak, Serdar

Doktora, Kimya Bölümü

Tez Yöneticisi: Prof. Dr. Saim Özkar

Ekim 2016, 117 sayfa

Amonyak boran (NH_3BH_3, AB) yüksek hidrojen taşıma kapasitesine (kütlece %19.6) sahip olmasından, zehirsiz olmasından ve ortam koşullarında yüksek dayanıklılık göstermesinden dolayı önemli katı hidrojen depolayıcı malzemelerden biridir. Amonyak boran uygun katalizörlerin varlığında oda sıcaklığında bile hidrolizle hidrojen salabilmektedir. Amonyak boranın hidrolizinden hidrojen eldesinde pek çok katalizörün test edilmesine rağmen, etkili, uzun ömürlü ve tekrar kullanılabilir katalizörlerin geliştirilmesi hala önemli bir konudur.

Bu tezde amonyak boranın hidrolizi için oldukça aktif, tekrar kullanılabilir ve uzun ömürlü rutenyum katalizörlerinin hazırlanmasını ve tanımlanmasını sunuyoruz. Çok katmanlı karbon nanotüp destekli rutenyum nanaparçacıkları (Ru^0/MWCNT) amonyak boranın (AB) hidrolizi için hazırlanmış ve ICP-OES, XRD, TEM, SEM, EDX ve XPS içeren ileri analitik yöntemlerle tanımlanmıştır. Elde edilen sonuçlar 1.4-3.0 nm boyut aralığına sahip rutenyum nanoparçacıklarının çok katmanlı karbon nanotüp yüzeyine iyice dağıldığını göstermektedir. Ru^0/MWCNT amonyak boran hidrolizinden hidrojen eldesinde çok aktif bir katalizör olup 25.0 ± 0.1 °C'de 329 çevrim frekansına sahiptir.

Kıyaslama için rutenyum nanoparçacıkları inorganik bir nanotel olan xonotlit üzerinde de oluşturulmuştur ($Ca_6(Si_6O_{17})(OH)_2$). Ru^0/X-NW, Ru^{3+} iyonları ile xonotlit nanotellerindeki Ca^{2+} iyonlarının yer değiştirmesiyle ve oda sıcaklığında sodyum borhidrür ile indirgenmesiyle hazırlanmıştır. Ru^0/X-NW de aynı analitik yöntemlerle tanımlanmıştır. Ru^0/X-NW'nin 25.0 ± 0.1 °C'de amonyak boranın hidrolizinde 134,100 çevrim sayısı ile uzun ömürlü bir katalizör olduğu bulunmuştur. Aktiflik, ömür ve tekrar kullanılabilirlik yönünden kıyaslamalar hidroksiapatit ve silika ile kaplanmış $CoFe_2O_4$ destekli rutenyum katalizörleri ile de genişletilmiştir. Ru^0/HAp ve Ru^0/SiO_2-$CoFe_2O_4$ katalizörlerinin 137 ve 172.5 çevrim sayısı ile amonyak boran hidrolizinde oldukça aktif oldukları da bulunmuştur. Ru^0/HAp 25.0 ± 0.1 °C'de amonyak boranın hidrolizinde 87,000 çevrim sayısına sahiptir. Ru^0/SiO_2- $CoFe_2O_4$ katalizörünün amonyak boranın hidrolizinde on kez kullanımdan sonra bile ilk aktifliğinin % 94'ünü koruyarak tekrar kullanılabilir olduğu bulunmuştur.

Anahtar Kelimeler: Katalizör, Rutenyum nanoparçacıkları, Karbon nanotüp, Nanotel, Hidroksiapatit, Silika kaplama, Manyetik Olarak Ayrılabilir Katalizörler, Amonyak Boran Hidrolizi, Hidrojen Üretimi.

To my wife

ACKNOWLEDGEMENT

TABLE OF CONTENTS

LIST OF TABLES

TABLES

LIST OF FIGURES

FIGURES

LIST OF ABBREVIATIONS

TOF :   Turnover Frequency

TTO :   Total Tornover Number

E_a :   Apparent Activation Energy

NPs: Nano particles

CNT: Carbon Nanotube

SWCNT: Singlewall Carbon Nanotube

MWCNT: Multiwall Carbon Nanotube

HAp: Hydroxyapatite

X-NW: Xonotlite Nanowire

AB: Ammonia borane

BET: Brunauer-Emmett-Teller

SEM: Scanning electron microscopy

STM: Scanning tunnelling microscopy

AFM: Atomic force microscopy

TEM: Transmission electron microscopy

XRD: X-ray diffraction

XPS: X-ray photoelectron spectroscopy

EDS: Energy dispersive spectroscopy

ICP: Inductively coupled plasma

NMR: Nuclear magnetic resonance spectroscopy

EXAFS: Extended X-ray absorption fine structure

CHAPTER 1

INTRODUCTION

1.1. Hydrogen

The use of hydrogen as an energy carrier is anticipated to facilitate the transition from fossil fuels to the renewable energy sources, on the way towards a sustainable energy future [1]. Secure storage and effective release of hydrogen are very important in the application of hydrogen energy. Tremendous efforts have been devoted to research and development on materials that can hold sufficient hydrogen in terms of gravimetric and volumetric densities and have suitable thermodynamic and kinetic properties [2]. Long-term exploration shows that the most effective and safest way of storing hydrogen is to use solid media such as sorbent materials [3] or hydrides [4]. Chemical hydrides provide a higher energy density for H_2 storage as compared to the gas or liquid H_2 tank systems. Many chemical hydrides have been tested as hydrogen storage materials for onboard applications [5,6] to achieve the total system targets of DOE Center of Excellence [7,8]. Recent reports have shown that B–N adducts need to be considered as hydrogen storage materials because of their high content of hydrogen with multiple nature, the protic N–H and hydridic B–H hydrogen [2]. Among B-N adducts, ammonia borane ($H_3N·BH_3$, AB) appears to be an appropriate hydrogen storage materials because of its high hydrogen content of 19.6 wt %, high stability under ambient conditions, and nontoxicity [9].

Hydrogen stored in the AB complex can be released by either thermal dehydrogenation or solvolysis. Thermal dehydrogenation process has some

drawbacks: i) it requires long induction time (~3h) and high temperature (Eq.1-4) [10], ii) various byproducts, such as ammonia and borazine ($B_3N_3H_6$) can be formed during reaction.

$$NH_3BH_3(s) \rightarrow NH_3BH_3(l) \qquad\qquad\qquad\qquad\qquad Eq.\ 1$$

$$NH_3BH_3(l) \rightarrow 1/n\ [NH_2\text{-}BH_2]_n(s) + H_2(g) \qquad T \approx 100\ ^\circ C \quad Eq.\ 2$$

$$1/n\ [NH_2\text{-}BH_2]_n(s) \rightarrow 1/n\ [NH\text{-}BH]_n(s) + H_2(g) \qquad T \approx 150\ ^\circ C \quad Eq.\ 3$$

$$1/n\ [NH\text{-}BH]_n(s) \rightarrow BN(s) + H_2(g) \qquad\qquad T \approx 1200\ ^\circ C \quad Eq.\ 4$$
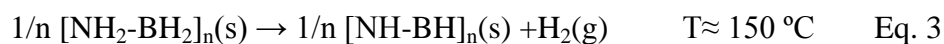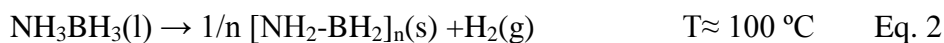
Solvolysis (hydrolysis or methanolysis) [10] appears to be favorable for hydrogen generation from AB at ambient temperature. AB is relatively stable to hydrolysis in aqueous solution. Therefore, the hydrolytic dehydrogenation of AB occurs at an appreciable rate only in the presence of suitable catalyst at room temperature (Eq.5). Hydrolysis of ammonia borane can be monitored by ^{11}B-NMR whereby NH_3BH_3 exhibits a quartet around $\delta=-24.0$ ppm while borate product (BO_2^-) exhibits a singlet around $\delta=10.0$ ppm (Fig.1). Regarding the nature of boron containing product of hydrolysis, we adopted the use BO_2^- (aq) ion as hydrolysis product [11]. When dissolved in aqueous solution, BO_2^- ion [12] will be converted first to $B(OH)_4^-$ ion which can undergo condensation to polyborate species as confirmed by ^{11}B NMR spectroscopy [13].

$$NH_3BH_3(aq) + 2H_2O(l) \rightarrow NH_4^+(aq) + BO_2^-(aq) + 3H_2(g) \qquad Eq.\ 5$$

(a)

(b)
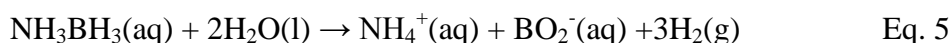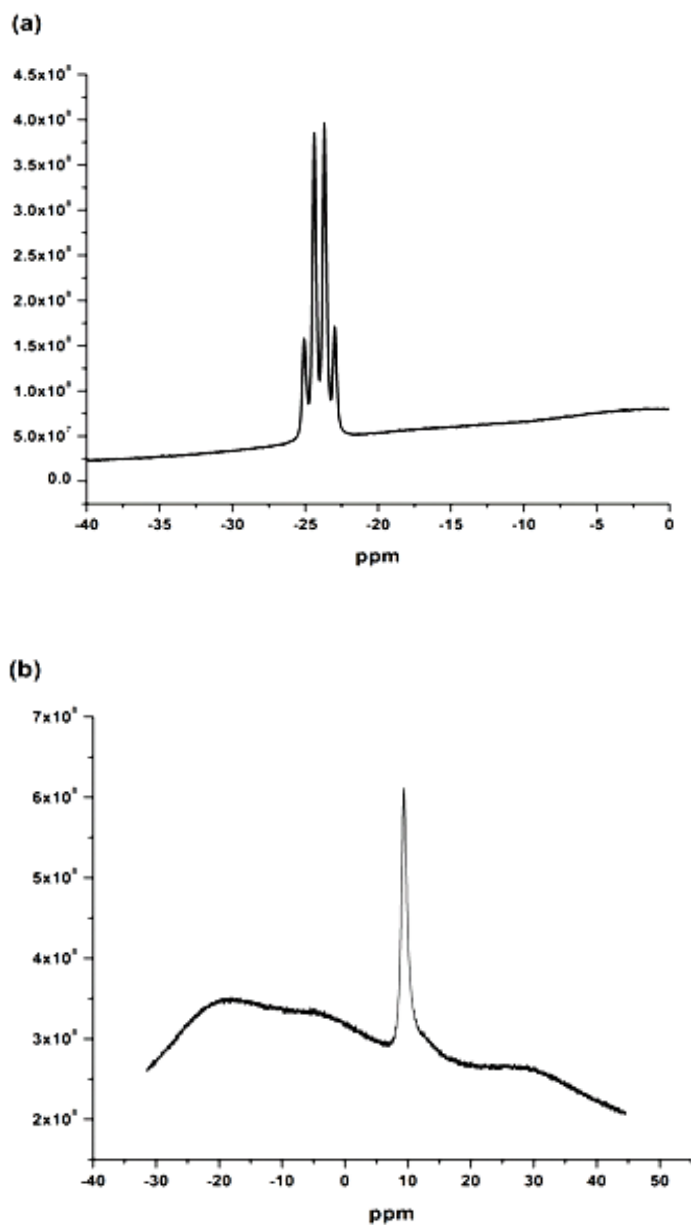
Figure 1. ^{11}B-NMR spectra of (a) aqueous ammonia borane and (b) the reaction solution after the hydrolysis of AB.

1.2. Catalysis and Metal Nanoparticles

Catalysts can provide a selective route for the desired product by opening faster reaction pathways. In fact, they make the reaction go faster. Metal nanoparticles, having the particle size smaller than 100 nm, have been widely used in catalysis because they have large fraction of surface atoms which results in much higher

catalytic activity compared to the bulk metal. They provide high activity and selectivity in many chemical reactions such as hydrogenation of aromatics, oxidation of alcohols, amination, hydrolysilation, Heck-Suzuki coupling [14]. Metal nanoparticles are usually isolable, redispersible, and reusable catalysts and, thus, also meet some requirements of the modern concept of green catalysis [15,16].

Metal nanoparticles can be prepared by "top-down" and "bottom-up" approaches [17]. In the former approach bulk material is cut into pieces in nanoscale by using special techniques such as ball milling, electron beam lithography [18]. In the latter approach metal nanoparticles are obtained by assembling the atoms or molecules by various methods such as chemical reduction, chemical vapor deposition and atomic layer deposition techniques [19].

However, the aggregation of nanoparticles to the bulk metal is still the most important problem that should be overcome in their catalytic application. In fact, it is well known that metal nanoparticles of high surface energy tend to aggregate into large particles in the absence of stabilizing agents [20].
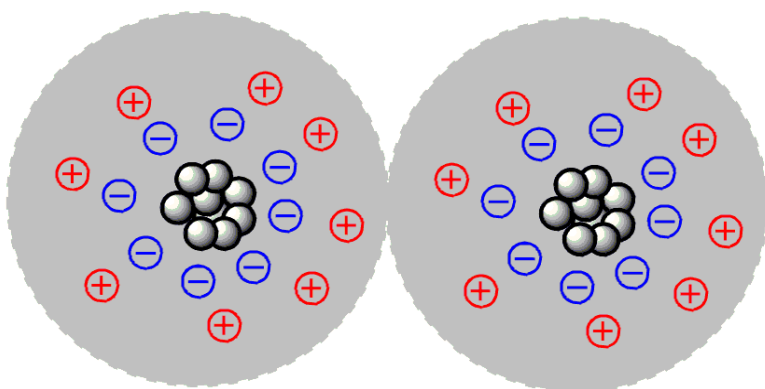
Figure 2. Illustration of electrostatic stabilization
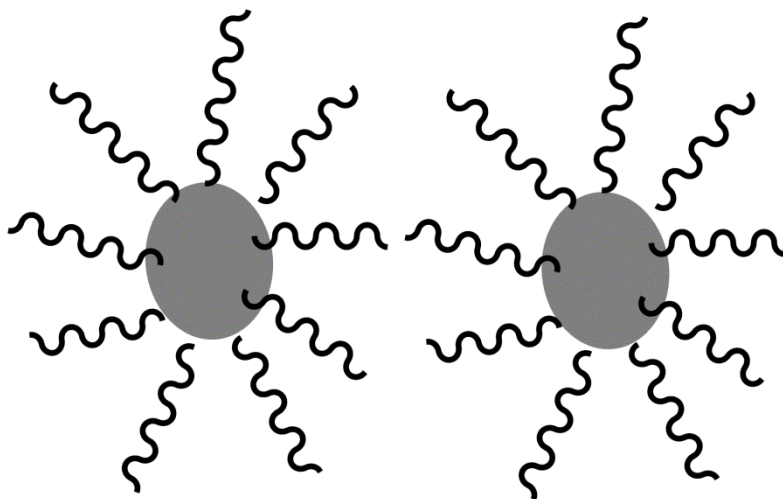
Figure 3. Illustration of steric stabilization

Electrostatic stabilization and steric stabilization are the well known methods for stabilizing of metal nanoparticles. In the former one, anions and cations from the starting materials remain in solution, and associate with the nanoparticles [21]. The particles are surrounded by an electrical double layer [22] (Fig. 2) and a Coulombic repulsive force between individual particles was achieved, which prevents the aggregation of particles [23] (Fig. 2).

Steric stabilization of metal NPs is achieved by coating the nanoparticles with layers of protecting groups (amines, polymers, thiols etc., with long alkyl chains) which provide steric barrier and thus prevents close contact of metal nanoparticles to each other [24] (Fig 3).

Activity and stability of nanoparticles catalysts can be improved by preventing the metal nanoparticles agglomeration using suitable stabilizing agents [24]. Metal NPs can also be stabilized by supporting on carbonecous materials (carbon, graphene, carbon nanotube), metal oxides or oxide surfaces (TiO_2, CeO_2, SiO_2, Al_2O_3), porous materials (MOFs, zeolite). These materials may provide the preparation of metal nanoparticles with controllable size and size distribution. However, the choice of supporting material for a desired reaction is critical [25].

There has been growing interest on carbon based supporting materials such as carbon black, carbon nanotubes (CNTs), graphene. CNTs are cylindrical nanostructures composed of sheet(s) of carbon atoms. They can be divided into two categories

namely, single-wall carbon nanotubes (SWCNTs) and multi-wall carbon nanotubes (MWCNTs) (Fig.4).
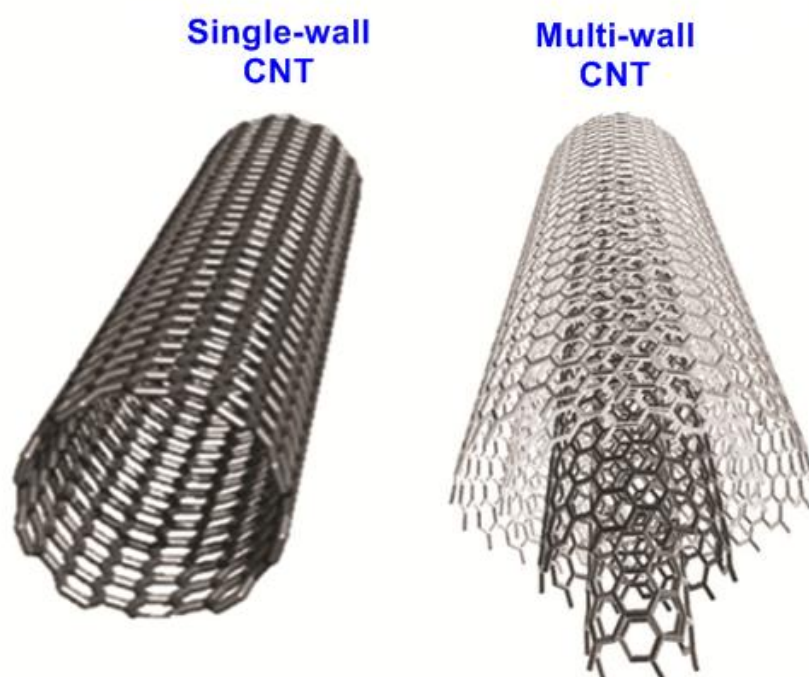
Figure 4. Schematic representation of carbon nanotubes [27].

Carbon nanotubes have exceptional structural, electronic and mechanical properties [26], which makes them an ideal material to be used in many fields [27]. Carbon nanotubes appear to be very attractive materials as catalyst supports in liquid phase reactions as they provide high dispersion of nanoparticles, significantly increase contact surface between the reactants and active sites, and greatly minimize the diffusion limitations, compared with traditional catalyst supports [28]. Since graphene, a 2-D sheet of sp^2-hybridized carbon, have the similar properties with the CNTs, much attention has been paid to graphene in the field of catalysis. However, difficulties in preparation of graphene from graphite using Hummers method [29] makes CNTs ideal candidate as a catalyst support among the members of carbon family.

The morphology, shape, structure, size, arrangement of atoms, crystal structure and material composition of the catalysts can be investigated using advance analytical tools as shown in Fig. 5. Scanning electron microscopy (SEM), atomic force

microscopy (AFM), transmission electron microscopy (TEM), X-ray diffraction (XRD), X-ray photoelectron spectroscopy (XPS), energy dispersive spectroscopy (EDS), inductively coupled plasma (ICP), nuclear magnetic resonance spectroscopy (NMR), extended X-ray absorption fine structure (EXAFS), scanning tunneling microscopy (STM) are widely used techniques in catalysis field.
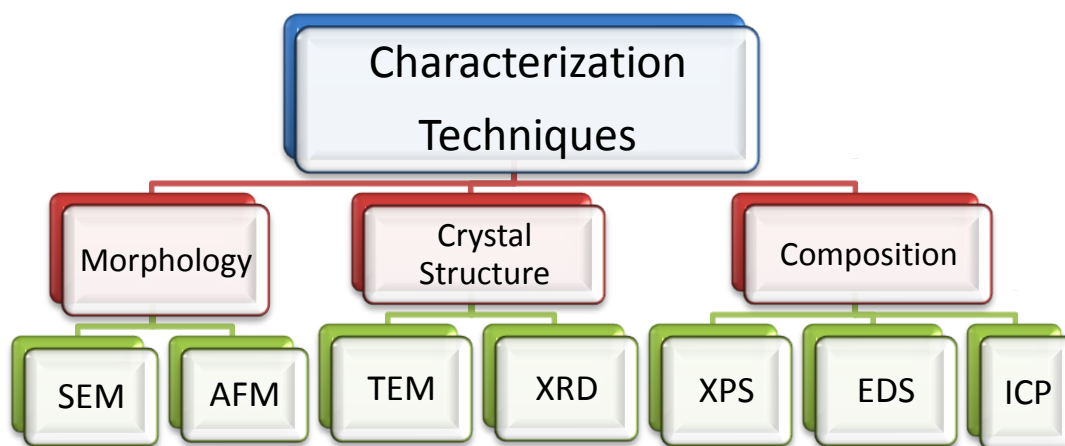
Figure 5. Schematic presentation of characterization techniques for the catalysts.

1.3. The Motivation of the Dissertation

Among the transition metal nanoparticles ruthenium is one of the most active catalysts in many chemical reactions such as alcohol oxidations [30], hydrogenation of aromatics [31], hydrogen generation from sodium borohydride [32] and ammonia borane [33]. Therefore, ruthenium based catalysts were selected to be used in hydrogen generation from the hydrolysis of ammonia borane in this study. To the best of our knowledge commercial Ru/Carbon, published in 2009, was the first ruthenium containing carbon based catalyst used in hydrolysis of AB [34]. That report encouraged us to prepare ruthenium nanoparticles supported on multi-walled carbon nanotubes (Ru^0/MWCNT) due to the unique properties of CNTs mentioned above. Ru^0/MWCNTs show remarkable catalytic activity with a TOF value of 329 (mol H$_2$×(mol Ru)$^{-1}$×min^{-1}) in hydrolysis of AB at 25.0 °C. The reusability and

lifetime experiments show that Ru^0/MWCNTs are still active catalyst in the hydrolysis of ammonia borane even after the fourth run preserving 41% of their initial catalytic activity and also providing 26400 turnovers in the hydrolysis of AB at room temperature before deactivation (Chapter 3). To achieve more stable catalysts in hydrolysis of AB as compared to the Ru^0/MWCNTs we considered to develop various ruthenium catalysts on different supporting materials. In this respect, Ru NPs were supported on xonotlite nanowire (Ru^0/X-NW) which is one dimensional inorganic counterparts of carbon nanotubes. Ru^0/X-NW showed superior catalytic life time (TTO= 134,100 mol H_2/mol Ru) (Chapter 4). All the results of Ru^0/X-NW were also compared to the one obtained by ruthenium(0) nanoparticles supported on the surface of bulk hydroxyapatite (Ru^0/HAp) (Chapter 5). Ru^0/HAp provide 87,000 turnovers and maintain 92% of their initial catalytic activity even after the fifth run of hydrolysis of ammonia borane at room temperature. However, isolation of these catalysts by filtration and centrifugation is difficult and material loss is inevitable during the isolation process. Therefore, magnetically separable and highly reusable Ru NPs were also developed in this dissertation (Chapter 6). Ruthenium(0) nanoparticles supported on magnetic silica-coated cobalt ferrite (Ru^0/SiO_2-$CoFe_2O_4$) were prepared and used as catalyst for the hydrolysis of AB. Ru^0/SiO_2-$CoFe_2O_4$ are reusable catalysts in hydrogen generation from the hydrolysis of AB retaining 94 % of their original catalytic activity after the tenth use.

Briefly, in this dissertation, various ruthenium based catalysts were successfully prepared and characterized by using advanced analytical tools including TEM, SEM, EDS, XRD, XPS, ICP-OES. The catalysts were tested in hydrogen generation from the hydrolysis of ammonia borane. Highly active, long-lived and reusable catalysts were developed for hydrogen generation from the hydrolysis of ammonia borane.

CHAPTER 2

EXPERIMENTAL

2.1. Materials

Ruthenium(III) chloride trihydrate ($RuCl_3 \cdot 3H_2O$) and ammonia borane (AB, 97%), hydroxyapatite (HAp, 99%), $Ca(NO_3)_2 \cdot 4H_2O$ (98%), $Na_2SiO_3 \cdot 9H_2O$ (99%), Iron(III) chloride ($FeCl_3$), tetraethylorthosilicate (TEOS, 98%), ammonium hydroxide (NH_4OH), sodium hydroxide (NaOH), cobalt(II) chloride ($CoCl_2$), were purchased from Aldrich. Multiwalled carbon nanotubes (MWCNTs) with a diameter of 150 nm were purchased from Electrovac, Kalosterneuburg, Austria.

2.2. Characterization

Metal contents of the catalysts were determined by Inductively Coupled Plasma Optical Emission Spectroscopy (ICP-OES, Leeman-Direct Reading Echelle). Transmission electron microscopy (TEM) was performed on a JEM-2100F (JEOL) microscope operating at 200 kV. Samples were examined at magnification between 400 and 700 K. The X-ray photoelectron spectroscopy (XPS) analysis was performed on a Physical Electronics 5800 spectrometer equipped with a hemispherical analyzer and using monochromatic Al Kα radiation of 1486.6 eV, the X-ray tube working at 15 kV, 350W and pass energy of 23.5 keV. ^{11}B NMR spectra were recorded on a Bruker Avance DPX 400 with an operating frequency of 128.15 MHz for [11]B. X-Ray Diffraction pattern of the samples were characterized by Rigaku Mini-Flex XRD (2θ range= 10-80°, scanning rate= 1 degree/minute) with a radiation source of Cu-K$_\alpha$ line (λ=1,54056 Å). BET surface area of the samples was analyzed by using a Micromeritics ASAP2020.

2.3. Impregnation of Ru^{3+} ions on Multiwalled Carbon Nanotubes (Ru^{3+}/MWCNT)

Multiwalled carbon nanotubes were refluxed in a mixture of HNO_3 (36 mL)/H_2SO_4 (54 mL) at 80 °C for 6 h. The mixture was then filtered and washed with distilled water until the pH value of filtrate reached 7. The functionalized multiwalled carbon nanotubes were dried at 120 °C for 12 h in the oven. The dried MWCNTs (100 mg) were stirred in 100 mL of an aqueous solution of 6.56 mg of $RuCl_3 \cdot 3H_2O$ for 72 h at room temperature. The sample was then filtered using a funnel with sintered glass filter and washed with 100 mL of distilled water and the remnant was dried at 120 °C for 12 h in the oven

2.4. In situ formation of ruthenium(0) nanoparticles supported on multiwalled carbon nanotubes (Ru^0/MWCNT) and concomitant hydrolytic dehydrogenation of AB

Ruthenium(0) nanoparticles supported on multiwalled carbon nanotubes (Ru^0/MWCNT) were *in situ* generated from the reduction of Ru^{3+}/MWCNT during the catalytic hydrolysis of AB. Before starting the catalyst formation and concomitant catalytic hydrolysis of AB, a jacketed reaction flask (20 mL) containing a Teflon-coated stir bar was placed on a magnetic stirrer (Heidolph MR-301) and thermostatted to 25.0 ± 0.1°C by circulating water through its jacket from a constant temperature bath. Then, a graduated glass tube (60 cm in height and 3.0 cm in diameter) filled with water was connected to the reaction flask to measure the volume of the hydrogen gas to be evolved from the reaction (Fig.6).
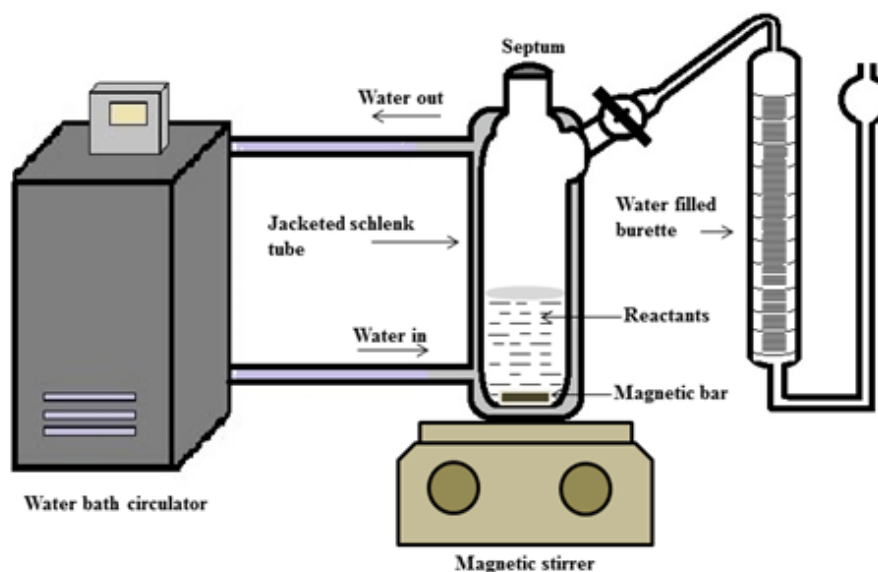
Figure 6. Schematic diagram of the reaction setup used for AB hydrolysis.

Next, 10 mg powder of Ru^{3+}/MWCNT (1.91 wt % Ru) was dispersed in 10 mL of distilled water in the reaction flask thermostatted at 25.0 ± 0.1 °C. Then, 31.8 mg of AB (1.0 mmol $H_3N.BH_3$) was added into the flask and the reaction medium was stirred at 1000 rpm. After a short induction period of less than 1.0 min, ruthenium(0) nanoparticles were formed and the catalytic hydrolysis of AB started. The volume of hydrogen gas evolved was measured by recording the displacement of water level every 30 s at constant atmospheric pressure of 693 Torr. The reaction was stopped when no more hydrogen evolution was observed. In each experiment, the resulting solutions were filtered and the filtrates were analyzed by ^{11}B NMR and conversion of AB to metaborate anion was confirmed by comparing the intensity of signals in the ^{11}B NMR spectra of the filtrates.

2.5. Determination of the most active ruthenium loading for Ru^0/MWCNT used in hydrolytic dehydrogenation of AB

The catalytic activity of Ru^0/MWCNT samples with various ruthenium loading in the range of 0.7−2.8% wt was tested in hydrogen generation from the hydrolysis of AB starting with 0.216 mM Ru and 100 mM AB in 10 mL solution at 25.0 ± 0.1 °C. The highest catalytic activity was achieved by using 1.91% wt ruthenium-loaded multiwalled carbon nanotubes. For all the tests reported hereafter, ruthenium loading of 1.91% wt. was used unless otherwise stated.

11

2.6. Determination of activation energy for hydrolytic dehydrogenation of AB catalyzed by Ru^0/MWCNT

In a typical experiment, the hydrolysis reaction was performed starting with 10 mL of 100 mM (31.8 mg) AB solution and 10 mg of Ru^{3+}/MWCNT (1.91% wt. ruthenium, [Ru] = 0.189 mM) at various temperatures (20, 25, 30, 35, 40 °C) in order to obtain the activation energy (Ea).

2.7. Reusability of Ru^0/MWCNT in hydrolytic dehydrogenation of AB

After the complete hydrolysis of AB started with 10 mL of 100 mM AB (31.8 mg $H_3N.BH_3$), and 30 mg Ru^{3+}/MWCNT (1.91% wt. ruthenium, [Ru] = 0.567 mM) at 25.0 ± 0.1 °C, the catalyst was filtered through a sintered glass funnel and washed with 100 mL water and dried in the oven at 120 °C. The isolated samples of Ru^0/MWCNT were weighed and redispersed in 10 mL solution of 100 mM AB for a subsequent run of hydrolysis at 25.0 ± 0.1 °C.

2.8. Determination of the catalytic lifetime of Ru^0/MWCNT in hydrolytic dehydrogenation of AB

The catalytic lifetime of Ru^0/MWCNT in the hydrolysis of AB was determined by measuring the total turnover number (TTO). Such a lifetime experiment was started with a 100 mL solution containing 0.0189 mM Ru^{3+}/MWCNT and 30 mM AB at 25.0 ± 0.1°C. When all the AB present in the solution was completely hydrolyzed, more AB was added and the reaction was continued in this way until no hydrogen gas evolution was observed.

2.9. Preparation of xonotlite nanowire [$Ca_6(Si_6O_{17})(OH)_2$]

Xonotlite nanowire (X-NW) was prepared by following the procedure described elsewhere [35]. The $Ca(NO_3)_2 \cdot 4H_2O$ and $Na_2SiO_3 \cdot 9H_2O$ were dissolved in distilled water, respectively to obtain 0.5 M solutions. The reactant molar ratio of Ca/Si was kept at 1.0. The $Ca(NO_3)_2$ solution was added dropwise into Na_2SiO_3 solution at room temperature under stirring to obtain a white suspension. Then the suspension was transferred into the Teflon-lined stainless-steel autoclaves and heated at 200 °C for 24 h, followed by cooling down to room temperature naturally. After the hydrothermal treatment, the suspension was filtrated and washed with distilled water and anhydrous ethanol for three times, respectively. After washing, the remaining

liquid was removed by vacuum filtration, and the obtained powders (xonotlite nanowires) were dried at 120 °C for 24 h.

2.10. Preparation of ruthenium(0) nanoparticles supported on xonotlite nanowire (Ru⁰/X-NW)

Ruthenium(III) cations were introduced onto the xonotlite nanowires by ion exchange of 400 mg xonotlite nanowires in 100 mL aqueous solution of 21.83 mg $RuCl_3 \cdot 3H_2O$. This slurry was stirred at room temperature for three days. The Ru^{3+}/X-NW sample was isolated by centrifugation and washed with 100 mL of distilled water and the remnant was dried under vacuum (10^{-3} Torr) at 80 °C. Then, 200 mg Ru^{3+} exchanged xonotlite nanowires was added into 100 mL of 75 mg $NaBH_4$ solution. When the hydrogen generation from the reaction solution ended ($\sim$1 h), the solid powders were isolated again by centrifugation and washed three times with 20 mL of deionized water to remove metaborate anions and dried under vacuum. The samples of Ru^0/X-NW were bottled as black powders. Ruthenium content of the Ru^0/X-NW sample was found to be 1.37% wt by ICP-OES analysis.

2.11. Determination of activation energy for hydrolytic dehydrogenation of AB catalyzed by Ru⁰/X-NW

In a typical experiment, the hydrolysis reaction was performed starting with 10 mL of 100 mM (31.8 mg) AB solution and 20 mg Ru^0/X-NW (1.37% wt. ruthenium, [Ru] = 0.271 mM) at various temperatures (20, 25, 30, 35, 40 °C) in order to obtain the activation energy.

2.12. Determination of the catalytic lifetime of Ru⁰/X-NW in hydrolytic dehydrogenation of AB

The catalytic lifetime of Ru^0/X-NW in the hydrolysis of AB was determined by measuring the total turnover number (TTO). Such a lifetime experiment was started with a 50 mL solution containing 0.0542 mM Ru^0/X-NW and 30 mM AB at 25.0 ± 0.1 °C. When all the ammonia borane present in the solution was completely hydrolyzed, more AB was added and the reaction was continued in this way until no hydrogen gas evolution was observed.

2.13. Preparation of ruthenium(III) exchanged hydroxyapatite (Ru^{3+}/HAp)

Hydroxyapatite, $Ca_{10}(PO_4)_6(OH)_2$, (500 mg) was added to a solution of $RuCl_3.xH_2O$ (57.7 mg) in 100 mL H_2O in a 250 mL round bottom flask. This slurry was stirred at room temperature for three days. The Ru^{3+}/HAp sample was filtered by using Whatman-1 filter paper, washed with 100 mL of distilled water and the remnant was dried under vacuum (10^{-3} torr) at 80 °C.

2.14. Determination of the most active ruthenium loading for Ru^0/HAp used in hydrolytic dehydrogenation of AB

The catalytic activity of Ru^0/HAp samples with various ruthenium loading in the range of 1.0–8.0% wt. was tested in hydrogen generation from the hydrolysis of AB starting with 0.784 mM Ru and 100 mM AB in 10 mL solution at 25.0 ± 0.1 °C. The highest catalytic activity was achieved by using 3.96% wt. ruthenium loaded hydroxyapatite. For all the tests reported hereafter, ruthenium loading of 3.96% wt. was used unless otherwise stated.

2.15. Determination of activation energy for hydrolytic dehydrogenation of AB catalyzed by Ru^0/HAp

In a typical experiment, the hydrolysis reaction was performed starting with 10 mL of 100 mM (31.8 mg) AB solution and 10 mg Ru^{3+}/HAp (3.96% wt. ruthenium, [Ru] = 0.392 mM) at various temperatures (20, 25, 30, 35, 40 °C) in order to obtain the activation energy.

2.16. Reusability of Ru^0/HAp in hydrolytic dehydrogenation of AB

After the complete hydrolysis of AB started with 10 mL of 100 mM AB (31.8 mg H_3NBH_3), and 30 mg Ru^{3+}/HAp (3.96% wt. ruthenium, [Ru] = 1.175 mM) at 25.0 ± 0.1 °C, the catalyst was isolated as dark-grey powder by centrifugation and dried under vacuum (10^{-3} torr) at 80 °C after washing with 100 mL of water. The isolated samples of Ru^0/HAp were weighed and redispersed in 10 mL solution of 100 mM AB for a subsequent run of hydrolysis at 25.0 ± 0.1 °C.

2.17. Determination of the catalytic lifetime of Ru^0/HAp in hydrolytic dehydrogenation of AB

The catalytic lifetime of Ru^0/HAp in the hydrolysis of AB was determined by measuring the total turnover number (TTO). Such a lifetime experiment was started

with a 100 mL solution containing 0.784 mM Ru^0/HAp and 30 mM AB at 25.0 ± 0.1 °C. When all the ammonia borane present in the solution was completely hydrolyzed, more AB was added and the reaction was continued in this way until no hydrogen gas evolution was observed.

2.18. Preparation of magnetic silica-coated cobalt ferrite (SiO_2-$CoFe_2O_4$)

The preparation of magnetic cobalt ferrite nanoparticles was carried out by modification of previously established procedure [36]. The detailed information on the preparation and characterization of silica-coated cobalt ferrite can be found elsewhere [37]. In a typical experiment 25 mL of 0.4 M iron(III) chloride and 25 mL of 0.2 M of cobalt(II) chloride solutions were mixed at room temperature. Then, in a separate vessel 25 mL of 3.0 M sodium hydroxide solution was prepared and slowly added to the salt solution. After complete addition of NaOH solution, a black suspension was obtained. The mechanical stirring was continued for 1 h at 80 °C. Then the solution was cooled to room temperature and the black precipitates were collected by using an external magnet. The supernatant was removed and the particles were washed 3 times with deionized water–ethanol solution and then the particles were dispersed in 50 mL of water. Silica coating was applied by using a modified version of Stober method [38]. For the preparation of silica coating, 200 mL ethanol, 1 mL TEOS and 0.5 mL of NH_4OH were added to the reaction mixture and subsequently 50 mL cobalt ferrite colloid was added to the mixture and the mixture was stirred for 4 h at room temperature. After the formation of the thick silica shell, particles were collected with a magnet and washed 3 times with deionized water. The resulting silica-coated cobalt ferrite nanoparticles (SiO_2-$CoFe_2O_4$) were separated by using a permanent magnet and washed with excess ethanol and dried at 120 °C for 12 h in the oven.

2.19. Impregnation of ruthenium(III) ions on magnetic silica-coated cobalt ferrite [Ru^{3+}/SiO_2-$CoFe_2O_4$]

SiO_2-$CoFe_2O_4$ (100 mg) was added to a solution of $RuCl_3 \cdot 3H_2O$ (5.65 mg) in 20 mL H_2O in a 50 mL beaker. This slurry was stirred at room temperature for 12 h and then, all supernatant solution was removed by using a permanent magnet. Next, the resulting particles Ru^{3+}/SiO_2-$CoFe_2O_4$ were washed with 20 mL of deionized water

and isolated by using a permanent magnet and the remnant was dried at 120 °C for 12 h in the oven.

2.20. In situ formation of ruthenium(0) nanoparticles supported on magnetic silica-coated cobalt ferrite [Ru^0/SiO_2-$CoFe_2O_4$] and concomitant catalytic hydrolysis of AB

Ruthenium(0) nanoparticles supported on magnetic silica-coated cobalt ferrite were *in situ* generated from the reduction of Ru^{3+}/SiO_2-$CoFe_2O_4$ during the catalytic hydrolysis of AB. 10 mg powder of Ru^{3+}/SiO_2-$CoFe_2O_4$ (1.96 wt.% Ru) was dispersed in 10 mL distilled water in the reaction flask thermostated at 25.0 ± 0.1°C. Then, 31.8 mg AB (1.0 mmol H_3NBH_3) was added into the flask and the reaction medium was stirred at 1000 rpm. After adding ammonia borane, ruthenium(0) nanoparticles were formed and the catalytic hydrolysis of AB started immediately.

2.21. Determination of activation energy for hydrolytic dehydrogenation of AB catalyzed by Ru^0/SiO_2-$CoFe_2O_4$

In a typical experiment, the hydrolysis reaction was performed starting with 10 mL of 100 mM (31.8 mg) AB solution and 10 mg Ru^{3+}/SiO_2-$CoFe_2O_4$ (1.96% wt. ruthenium, [Ru] = 0.186 mM) at various temperatures (25, 30, 35, 40 °C) in order to obtain the activation energy.

2.22. Reusability of Ru^0/SiO_2-$CoFe_2O_4$ in hydrolytic dehydrogenation of AB

After the complete hydrolysis of AB started with 10 mL of 100 mM AB (31.8 mg H_3NBH_3), and 60 mg Ru^{3+}/SiO_2-$CoFe_2O_4$ (1.96% wt. ruthenium, [Ru] = 0.744 mM) at 25.0 ± 0.1°C, the catalyst was isolated using a permanent magnet. Ru^0/SiO_2-$CoFe_2O_4$ were magnetically attracted to the bottom of the reaction vessel by a magnet, and the upper solution was removed and the catalyst was washed with 10 mL of water before every run in the reusability test. After washing, the catalyst was isolated again and the isolated sample of Ru^0/SiO_2-$CoFe_2O_4$ redispersed in 10 mL solution of 100 mM AB for a subsequent run of hydrolysis at 25.0 ± 0.1°C.

CHAPTER 3

Ruthenium(0) Nanoparticles Supported on Multiwalled Carbon Nanotubes

Most of the transition metal catalysts are in the form of nanoparticles that suffer in long-term stability because of the aggregation into clumps and ultimately to the bulk metal, despite using the best stabilizers [24], which leads to a decrease in catalytic activity and lifetime. With high external surface area and aspect ratio [39,40], carbon nanotubes appear to be very attractive as catalyst supports in liquid phase reactions as they provide high dispersion of nanoparticles, significantly increase contact surface between the reactants and active sites, and greatly minimize the diffusion limitations, compared with traditional catalyst supports. In this dissertation, we aimed to develop highly active, reusable and long-lived ruthenium catalysts in hydrogen generation from hydrolysis of ammonia borane. Therefore, ruthenium(0) nanoparticles supported on multiwalled carbon nanotubes were prepared as catalysts used in hydrolysis of ammonia borane.

3.1. Hydrolytic dehydrogenation of ammonia borane catalyzed by Ru^0/MWCNTs

Ruthenium(0) nanoparticles supported on multiwalled carbon nanotubes were *in situ* generated during the hydrolysis of ammonia borane. Ruthenium(III) ions were impregnated on the acid treated MWCNT from the aqueous solution of ruthenium(III) chloride and then reduced by AB at room temperature. When AB solution is added to the suspension of ruthenium(III) ions impregnated on carbon nanotubes, both reduction of ruthenium(III) to ruthenium(0) and hydrogen release

from the hydrolysis of AB occur concomitantly. The progress of ruthenium(0) nanoparticles formation and concomitant dehydrogenation of ammonia borane was followed by monitoring the changes in H_2 pressure. Figure 7 shows the plot of equivalent H_2 generated versus time for the hydrolysis of AB starting with Ru^{3+}/MWCNT precatalyst (0.378 mM Ru) and 100 mM AB in 10 mL aqueous solution at $25.0 \pm 0.1°C$. After a short induction period of 1.0 min, the hydrogen generation starts and continues almost linearly until the release of 3 equiv. H_2 per equivalent of AB.
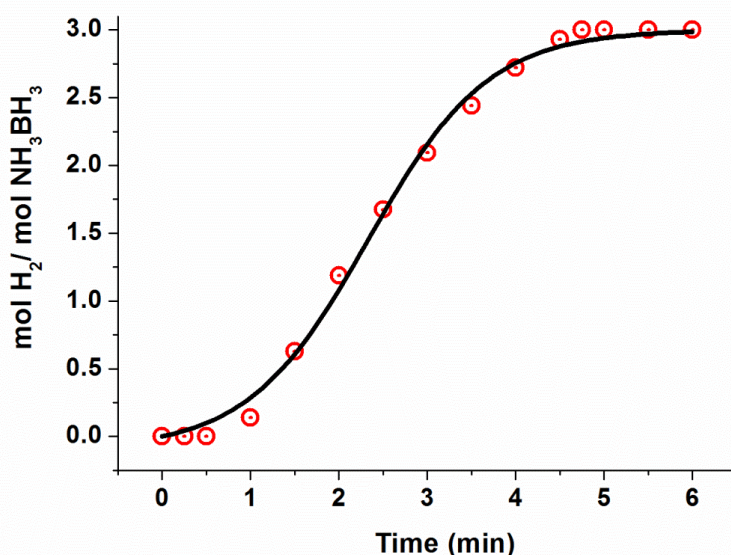
Figure 7. Plot of equivalent H_2 generated versus time for the hydrogen generation from the hydrolysis of ammonia borane (AB) starting with 20 mg Ru^0/MWCNT (with a loading of 1.91% wt. Ru) as catalyst and 1.0 mmol AB in 10 mL of aqueous solution at $25.0 \pm 0.1°C$. The sigmoidal curve fits well to the two-step mechanism for the ruthenium(0) nanoparticle formation.

The observation of an induction period and a sigmoidal shape of dehydrogenation curve indicates the formation of ruthenium(0) nanoparticles with a two-step, nucleation and autocatalytic growth mechanism [41,42]. The formation kinetics of the $Ru(0)_n$ nanoparticle catalyst can be obtained using the hydrogen release from AB as reporter reaction [43], given in Scheme 1, in which P is the added precursor Ru^{3+}/MWCNT and Q is the growing $Ru(0)_n$ nanoparticles on the surface of MWCNT. The hydrogen generation from the hydrolysis of AB will accurately report on and amplifies the amount of $Ru(0)_n$ nanoparticle catalyst, Q, present if the dehydrogenation rate is fast in comparison to the rate of nanoparticles formation. It

was shown that the dehydrogenation is zero-order in [AB] when the substrate to catalyst ratio is large enough to ensure that the dehydrogenation reporter reaction is fast relative to the rate of slower nanoparticle formation k_1 and k_2 steps (Scheme 1).

Sigmoidal kinetics can be seen in Figure 7 and fit well by the Finke- Watzky two-step, nucleation, and autocatalytic growth mechanism of nanoparticle formation [41]. The observation of a sigmoidal dehydrogenation curve and its curve-fit to the slow, continuous nucleation, $P \rightarrow Q$ (rate constant k_1) followed by autocatalytic surface growth, $P + Q \rightarrow 2Q$ (rate constant k_2) kinetics are very strong evidence for the formation of metal(0) nanoparticles catalyst from a soluble transition-metal complex in the presence of reducing agent [41]. The rate constants determined from the nonlinear least-squares curve-fit function (given in Appendix) are $k_1 = 4.6 \times 10^{-2}$ min^{-1} and $k_2 = 5.0 \times 10^2 \, M^{-1} \, min^{-1}$. The mathematically required correction has been made to k_2 for the stoichiometry factor of 1058 as described elsewhere [42], but not for the "scaling factor"; that is no correction has been made for the changing the number of Ru atoms on the growing metal surface.

The ruthenium(0) nanoparticles supported on multiwalled carbon nanotubes (Ru^0/MWCNT), *in situ* formed during the hydrolysis of AB, could be isolated from the reaction solution as powder by filtration and characterized by ICP-OES, XRD, SEM, EDX, TEM, and XPS techniques. Ruthenium content of Ru^0/MWCNT was determined by ICP-OES.

$$P \xrightarrow{k_1} Q$$

$$P + Q \xrightarrow{k_2} 2Q$$

$$H_3NBH_3 \, (aq) + 2H_2O(l) \xrightarrow{\text{fast}} NH_4^+(aq) + BO_2^-(aq) + 3H_2(g)$$
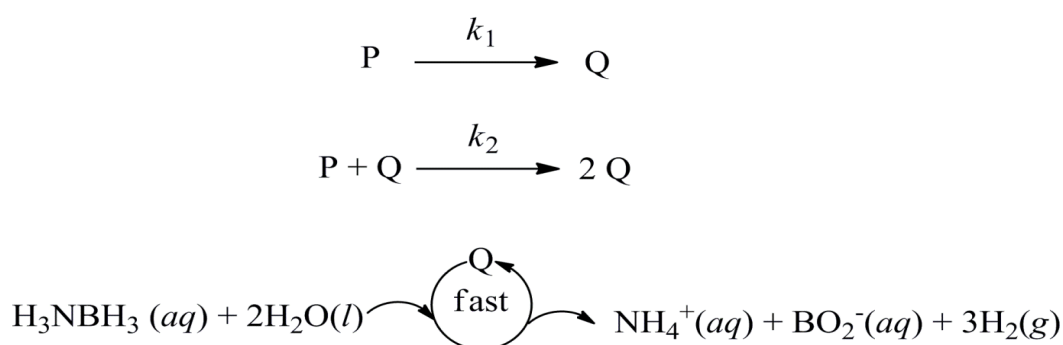
Scheme 1. Illustration of the hydrolysis of ammonia borane as reporter reaction for the formation of ruthenium(0) nanoparticles: P is the precursor ruthenium(III) ion impregnated on MWCNTs and Q is the growing Ru(0)$_n$ nanoparticles.

The XRD patterns of pristine MWCNT, acid-treated MWCNT and Ru^0/MWCNT are given altogether in Figure 8 for comparison. A comparison of the XRD patterns of

pristine MWCNT and acid-treated MWCNT given in panels a and b in Figure 8, respectively, clearly shows that there is no change in the characteristic diffraction peaks of multiwalled carbon nanotubes after acid treatment indicating that MWCNTs were not severely damaged by refluxing in the mixture of HNO_3/H_2SO_4 [44]. The diffraction peaks at 26.2°, 43.3°, and 54.5° could be well-indexed as (002), (100), and (004) diffractions of graphite structure, respectively [45]. XRD patterns of acid treated MWCNT (Figure 8b) and Ru^0/MWCNT with a ruthenium loading of 1.91% wt. Ru (Figure 8c) are almost identical. There is no observable peak attributable to ruthenium nanoparticles in Figure 8c, probably as a result of low ruthenium loading of materials [46].
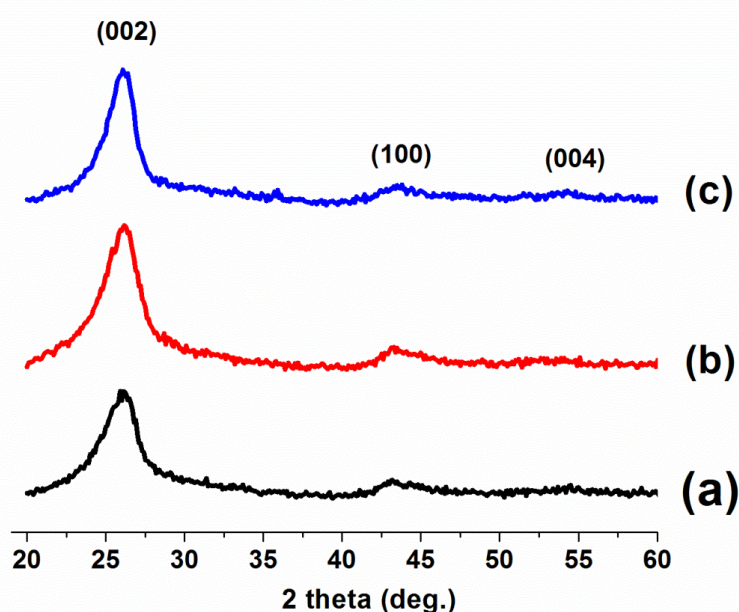
Figure 8. XRD patterns of (a) pristine MWCNT, (b) acid-treated MWCNT, (c) Ru^0/MWCNT with a 1.91 % wt. Ru loading.

The BET nitrogen adsorption analysis gave the surface area of pristine MWCNT, acid treated MWCNT and Ru^0/MWCNT as 13.2, 41 and 31 m^2g^{-1}, respectively. The noticeable decrease in the surface area of acid treated carbon nanotubes upon ruthenium loading may imply the existence of ruthenium(0) nanoparticles on the surface.
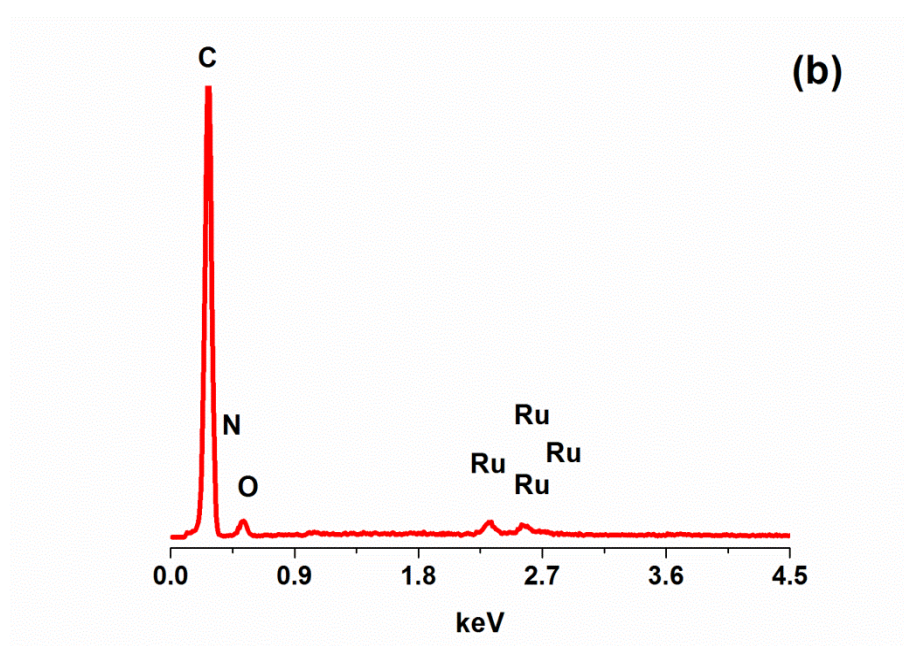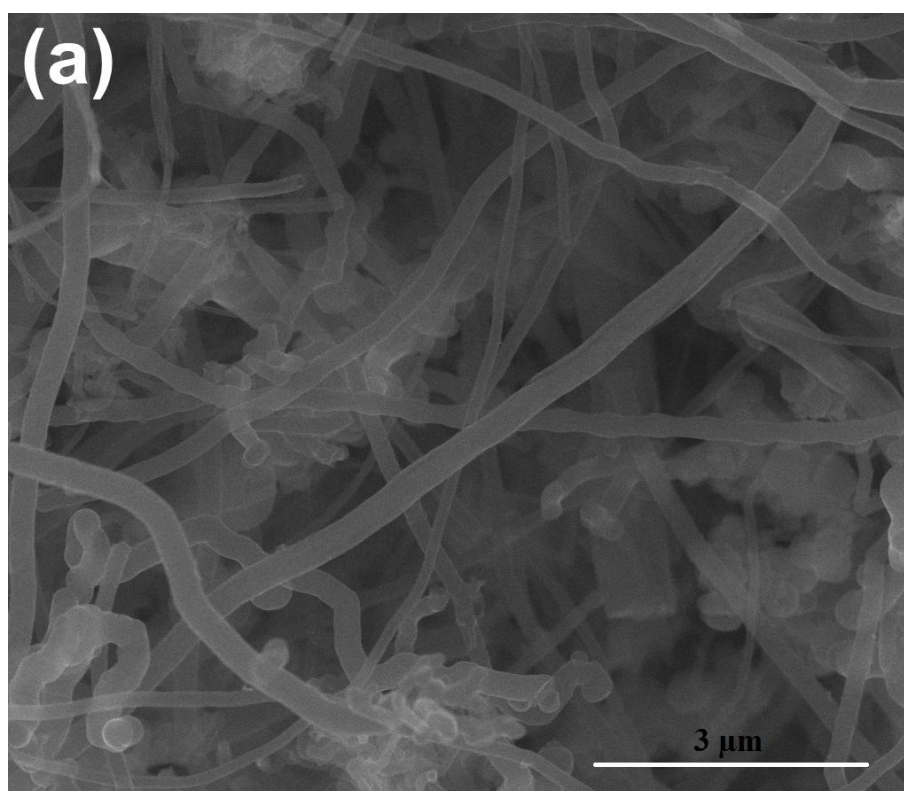
Figure 9. (a) SEM image (The scale bar is 3 μm), (b) SEM-EDX spectrum of Ru^0/MWCNT with a 1.91% wt. Ru loading.

Figure 9 exhibits the SEM image and SEM-EDX spectrum of Ru^0/MWCNT with a ruthenium loading of 1.91% wt. indicating that ruthenium is the only element

detected in the sample in addition to the surface elements of carbon nanotubes (N, C, O) because of functional groups formed after acid treatment.

Figure 10 shows the TEM images of acid treated MWCNTs and Ru^0/MWCNT taken with different magnifications. From the TEM images given in Figures 10b−e, one can see that (i) highly dispersed ruthenium(0) nanoparticles are formed on the surface of MWCNTs with particle size in the range 1.4−3.0 nm (mean diameter: 2.5 ± 0.8 nm, histogram in Figure 10f) and (ii) neither the acid treatment nor the impregnation of ruthenium(III) followed by reduction to ruthenium(0) causes any damage to the wall of carbon nanotubes in agreement with the XRD results.
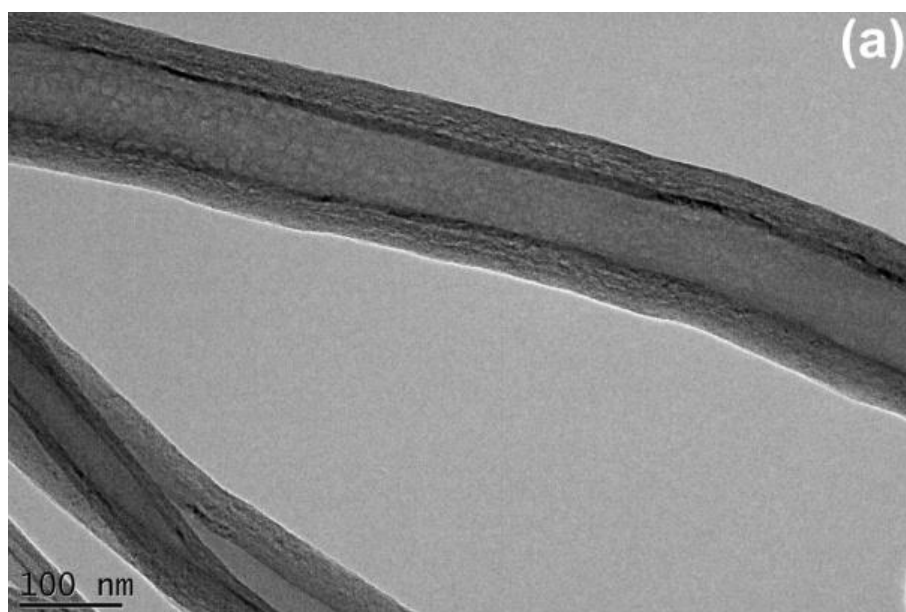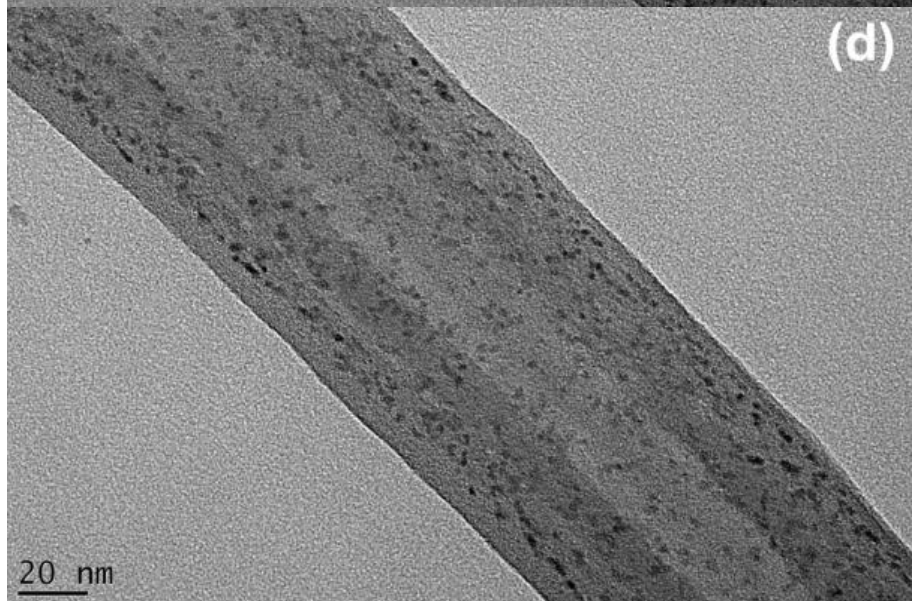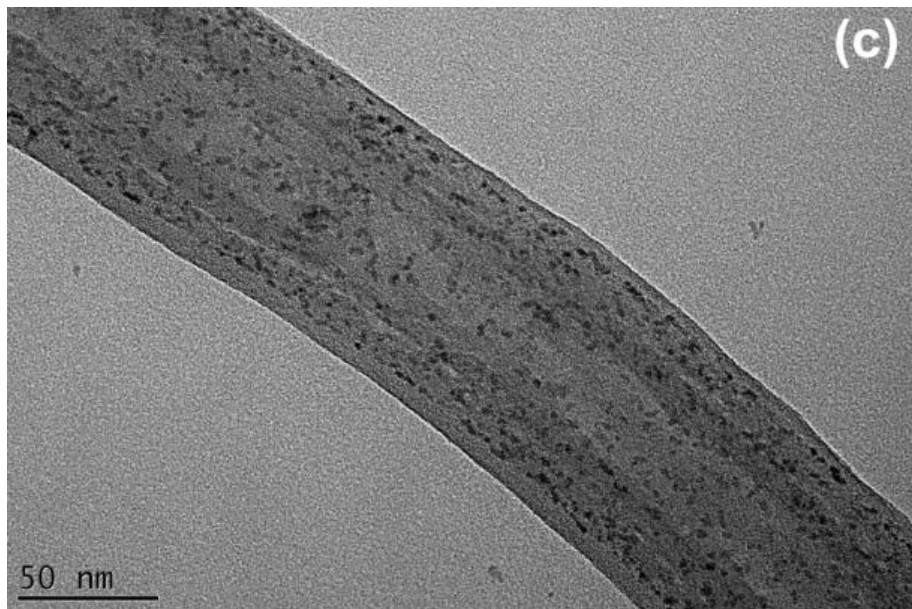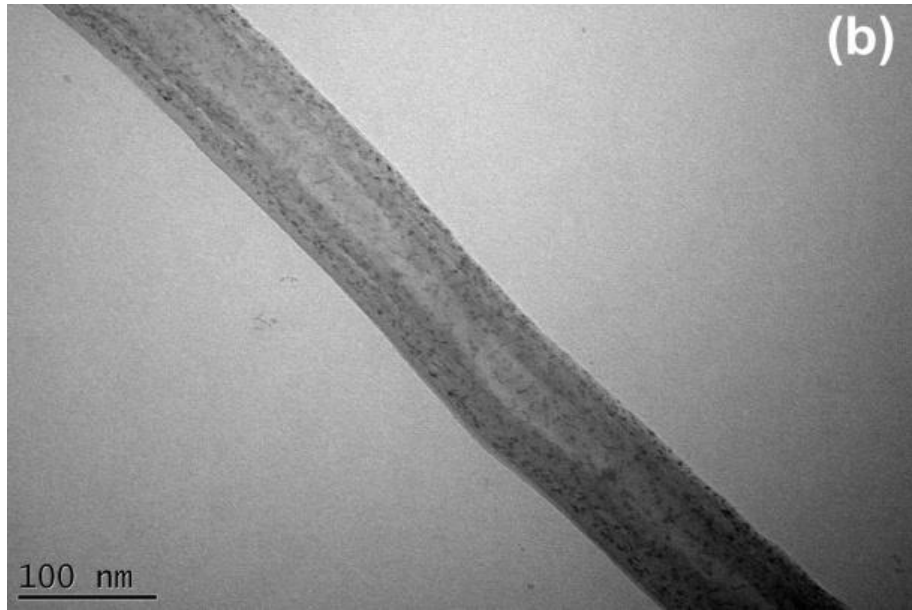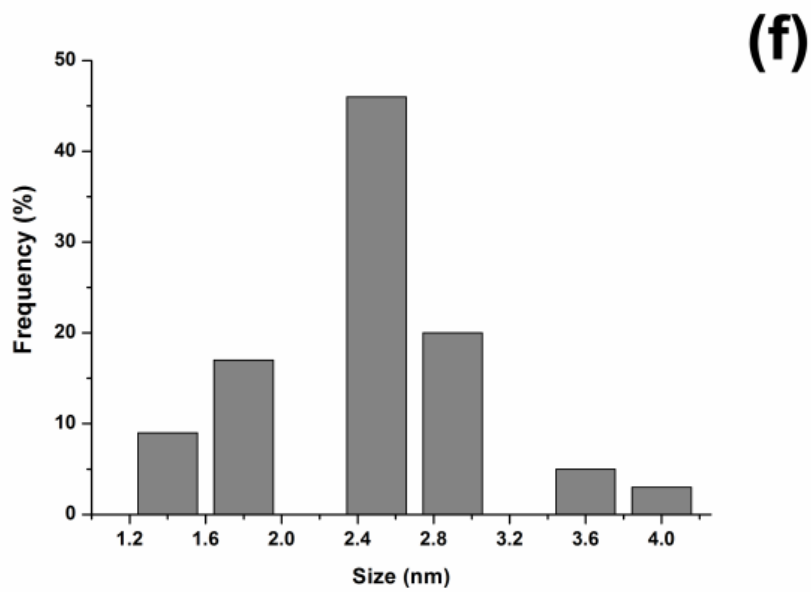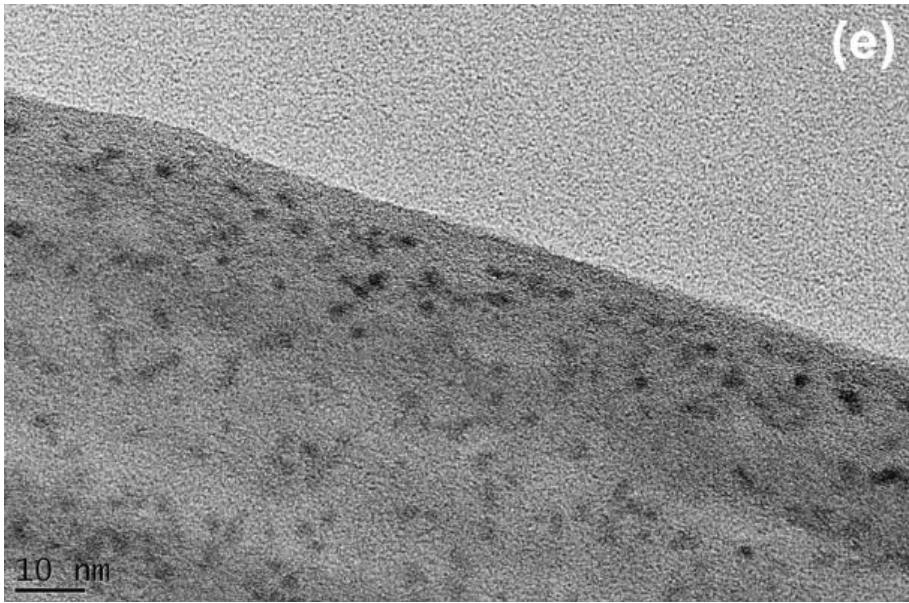
Figure 10. TEM images of (a) the acid-treated MWCNTs (the scale bar is 100 nm) and Ru^0/MWCNT with a 1.91% wt. Ru loading in different magnifications with scale bars of (b) 100, (c) 50, (d) 20, (e) 10 nm, and (f) the corresponding histogram for the particle size distribution.
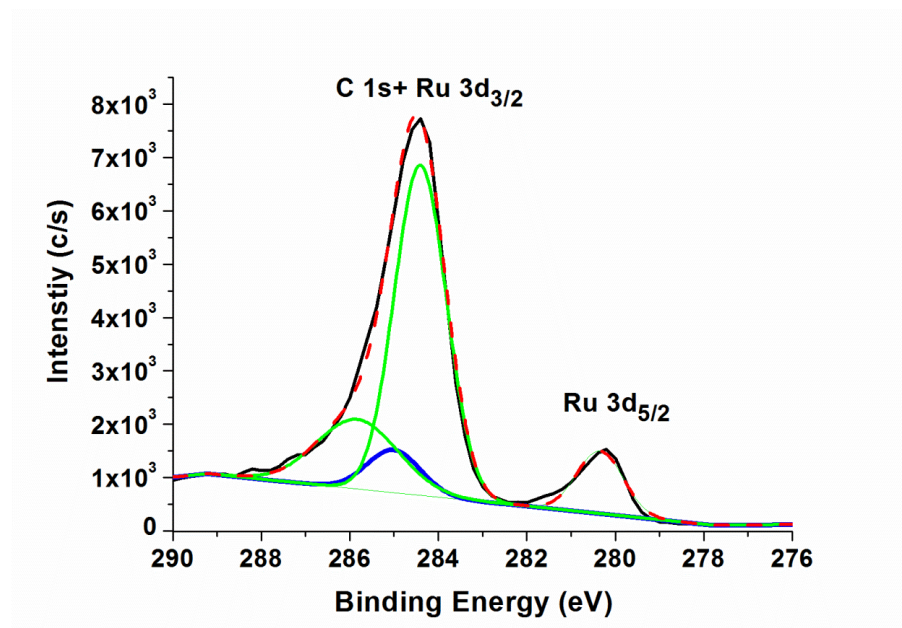
Figure 11. Ru 3d XPS spectrum of Ru^0/MWCNT with a 1.91% wt. Ru loading.

The composition of Ru^0/MWCNT formed *in situ* during the hydrolysis of AB and the oxidation state of ruthenium were also studied by XPS technique. High-resolution X-ray photoelectron spectrum of a Ru^0/MWCNT sample with metal loading of 1.91% wt. Ru given in Figure 11 shows two prominent bands at 284.4 and 280.2 eV, which can readily be assigned of Ru(0) 3d$_{3/2}$ and 3d$_{5/2}$, respectively, in the nanoparticles by comparing with values of ruthenium metal 285 and 280 eV, respectively [47]. It is noteworthy that the Ru(0) 3d$_{3/2}$ peak at 284.4 eV overlaps with the C 1s peak at 283.9 eV coming from multiwalled carbon nanotubes with a percent atomic ratio of 14.63 (C 1s/Ru 3d). Because of this overlap, only the peak at 280.2 eV can with certainty be assigned to Ru(0) 3d$_{5/2}$. The higher energy peaks might be of carbon or ruthenium.

3.1.1. Catalytic activity of Ru^0/MWCNT in hydrolytic dehydrogenation of ammonia borane

Before starting with the investigation on the catalytic activity of Ru^0/MWCNT in the hydrolysis of AB, a control experiment was performed to check whether the acid treated MWCNTs show any catalytic activity in the hydrolysis of AB at the same temperature. In a control experiment starting with 1.0 mmol of AB and 10 mg of powder of MWCNT (the same amount as the one used in catalytic activity tests) in 10 mL of water at 25.0 ± 0.1°C or 40.0 ± 0.1°C, no hydrogen generation was

observed in 1 h at both temperatures. This observation indicates that the hydrolysis of AB does not occur in the presence of MWCNTs in the temperature range used in this study. Ru^0/MWCNTs are found to be highly active catalyst in the hydrolysis of ammonia borane generating 3.0 equivalent H_2 gas per mol of AB in the same temperature range.

Expectedly, the catalytic activity depends on the ruthenium loading of catalyst materials. A series of experiments were performed starting with 10 mL solution of 100 mM AB and 0.216 mM Ru using Ru^{3+}/MWCNT sample with various ruthenium loading (0.73, 1.47, 1.91, 2.26, 2.83% wt. Ru) in appropriate amount to provide the same ruthenium concentration in all of the experiments. The catalytic activity in the hydrolysis of AB at 25.0 ± 0.1 °C shows variation with the ruthenium loading as shown in Figure 12. The Ru^0/MWCNT sample with ruthenium loading of 1.91% wt. Ru provides the highest catalytic activity in hydrogen generation from the hydrolysis of AB at 25.0 ± 0.1°C. As the ruthenium loading further increases, the catalytic activity of Ru^0/MWCNT decreases, most probably due to the agglomeration of nanoparticles, resulting in a decrease in the surface area and the accessibility of active sites [48]. For all the experiments performed in this study, ammonia test was applied following the procedure described elsewhere [42] and no ammonia generation was detected.
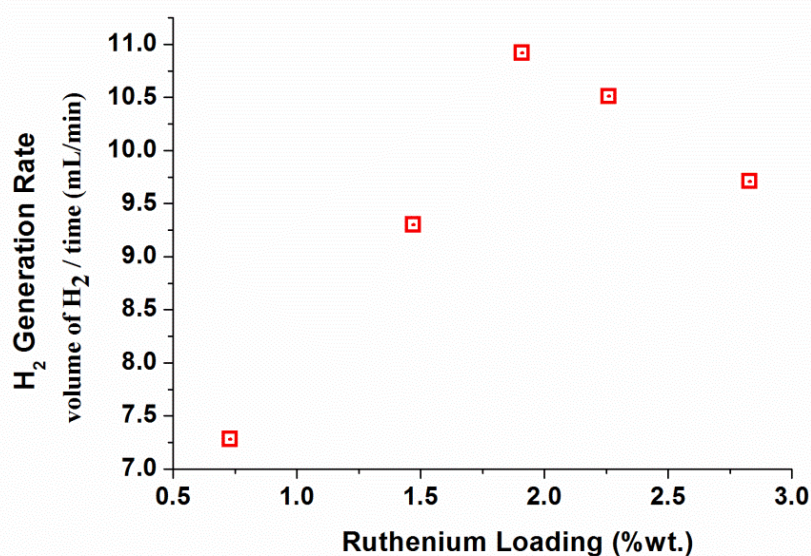
Figure 12. Rate of hydrogen generation versus Ru loading in weight percentage for the hydrolysis of AB (100 mM) catalyzed by Ru^0/MWCNT with various Ru loading (0.216 mM Ru) at 25.0 ± 0.1°C.
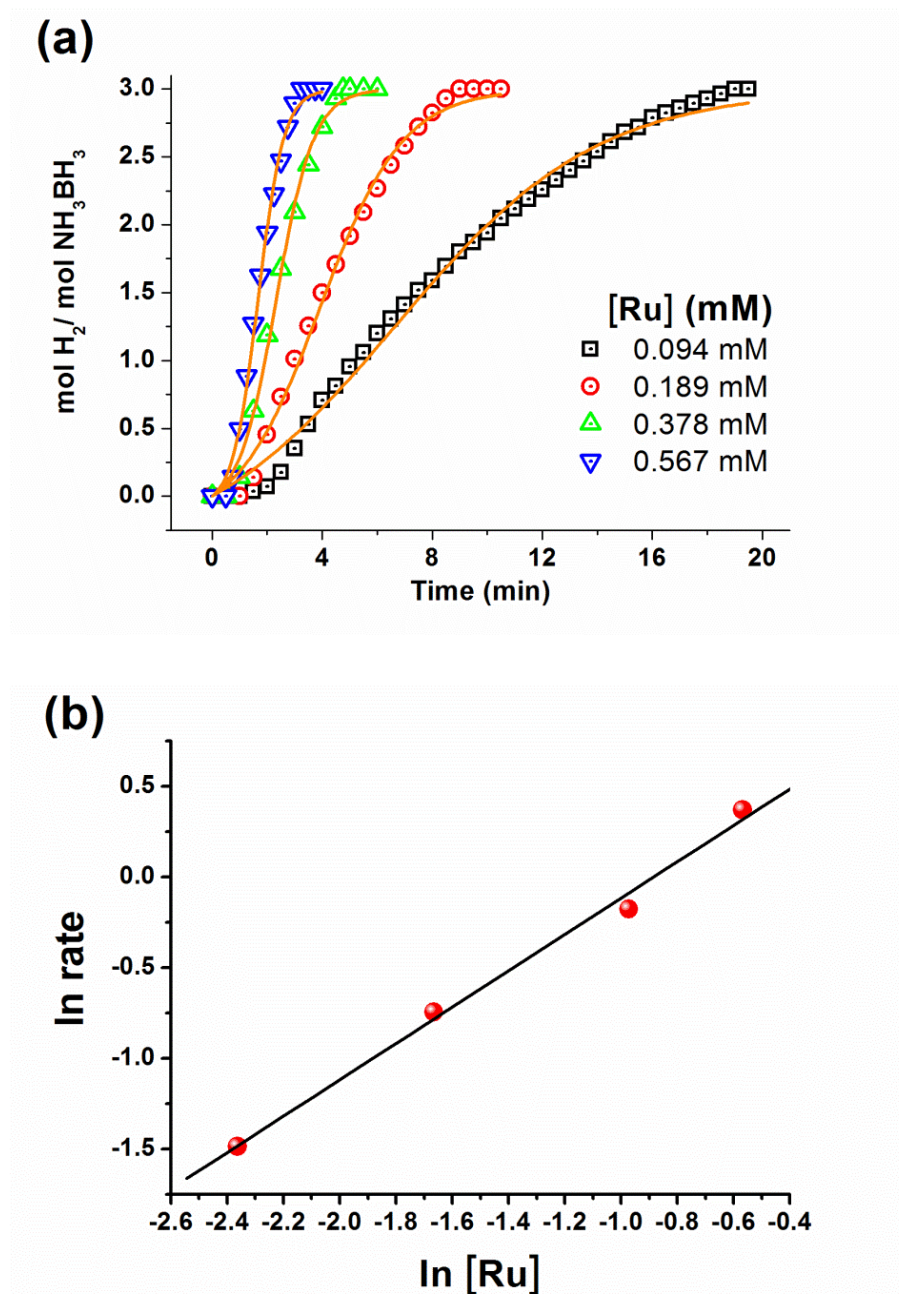
Figure 13. (a) mol H_2/mol H_3NBH_3 versus time graph depending on the ruthenium concentration in Ru^0/MWCNT for the hydrolysis of AB (100 mM) at $25.0 \pm 0.1°C$, (b) the plot of hydrogen generation rate versus the concentration of Ru, both in logarithmic scale. $\ln(\text{rate}) = 1.002 \ln[Ru] + 0.88$.

Fig. 13a shows the evolution of equivalent hydrogen per mole of AB versus time plot for the hydrolysis of AB (100 mM) using Ru^0/MWCNT with a loading of 1.91% wt. Ru as catalyst in different ruthenium concentration at 25.0 ± 0.1 °C. In each experiment, hydrogen evolution starts after a short induction period of less than 2 minutes and continues almost linearly until complete conversion of the substrate generating 3.0 equivalents of H_2 per mole of AB. All the experimental data fit well to the 2-step mechanism yielding the rate constants k_1 of the slow, continuous

27

nucleation (P → Q) and k_2 of the autocatalytic surface growth (P + Q → 2Q) for the formation of ruthenium(0) nanoparticles catalyst from the reduction of ruthenium(III) ions during the hydrolysis of AB (Table 1). It is observed that the rate constant k_1 for the nucleation and the rate constant k_2 for autocatalytic surface growth slightly change with the increasing concentration of ruthenium.

Figure 13b shows the plot of hydrogen generation rate versus initial concentration of ruthenium, both in logarithmic scale, which gives a straight line with a slope of 1.0 indicating that hydrolysis of AB is first-order with respect to the ruthenium concentration. The turnover frequency (TOF) for hydrogen generation from the hydrolysis of AB (100 mM) at 25.0 ± 0.1 °C was determined from the hydrogen generation rate in the linear portion of plots given in Fig. 13a for experiments starting with 100 mM AB plus Ru^0/MWCNTs with a loading of 1.91 % wt. Ru. The TOF value of Ru^0/MWCNTs catalyst is as high as 329 min^{-1} (mol H_2/ mol Ru. min) in hydrolysis of AB at 25.0 ± 0.1 °C (see the appendix for the TOF calculation). As clearly seen from the TOF values of the reported ruthenium catalysts and that of the carbon based catalysts in literature listed in Table 2 and Table 3, respectively, Ru^0/MWCNTs provide comparable catalytic activity in hydrolysis of AB. The TOF values of catalysts listed in Table 2 and Table 3 show variations for different supporting materials.

Table 1. The rate constants k_1 of the slow, continuous nucleation, P → Q, and k_2 of the auto-catalytic surface growth, P + Q → 2Q for the formation of ruthenium(0) nanoparticles catalyst from the ruthenium(III) ions during the hydrolysis of AB at various concentration of ruthenium. [a] TOF values were not corrected by the fraction of active sites.

Ru [mM]	k_1 (s^{-1})	k_2 ($M^{-1}s^{-1}$)	k_2/k_1	TOF[a]
0.094	$6.36 \times 10^{-4} \pm 4.23 \times 10^{-5}$	$1.38 \pm 7.46 \times 10^{-2}$	2.18×10^{3}	329
0.189	$7.64 \times 10^{-4} \pm 8.53 \times 10^{-5}$	$1.82 \pm 1.11 \times 10^{-1}$	2.38×10^{3}	309
0.378	$7.71 \times 10^{-4} \pm 1.27 \times 10^{-4}$	$2.09 \pm 1.34 \times 10^{-1}$	2.71×10^{3}	274
0.567	$9.46 \times 10^{-4} \pm 1.51 \times 10^{-4}$	$2.06 \pm 1.20 \times 10^{-1}$	2.17×10^{3}	252

TOF values can also show variation in different catalysts concentration. In our study, we observed a decrease in TOF values with the increasing initial concentration of ruthenium in the Ru^0/MWCNTs catalyst as shown in Table 1. The inverse dependence of the TOF on the precatalyst concentration is a known phenomenon in literature [49] which indicates that the lower concentration of precatalyst forms smaller particles exhibiting higher catalytic activity for some reactions [50,51]. In

fact, inverse relationship between the apparent turnover frequency and the concentration of precatalyst or catalyst has been reported for different reactions with different catalysts such as hydrogenation by cobalt(III) acetylacetonate [52], alcohol oxidation by palladium(II) acetate [53], hydrogenation of styrene by osmium [54], Heck reaction by palladium [55,56], heterolysis by cobalt [57], cyclohexene hydrogenation by iridium [51], and methanolysis by rhodium [49]. With one exception of iridium hydrogenation catalyst [51], in all the reports the inverse dependence has been ascribed to the increasing size of nanoparticles. However, only in the case of methanolysis of ammonia borane catalyzed by rhodium nanoparticles, experimental evidence has been provided showing that the inverse dependence is due to the increasing particles size [49].

Table 2. The turnover frequency (TOF; *mol H₂ .(mol Ru)⁻¹(min)⁻¹*), total turnover number (TTO; *mol H₂.(mol Ru)⁻¹*) and activation energy (Eₐ; *kJ/mol*) values of reported ruthenium catalysts used in hydrogen generation from the hydrolysis of AB. The surface area and the average particle size of ruthenium based catalysts were also given for comparison (hyphen - means the data is not given). TOF and TTO values were given for the hydrolysis of AB at room temperature.

Catalyst	TOF (min⁻¹)	Ea (kj/mol)	Surface Area (m²/g)	Average Ru Particle size (nm)	Life Time (TTO)	Ru/AB molar ratio	Ref.
RuNi/TiO₂ (anatase+rutile)	914	28.1	39.7	2.3	153000	0.001	[58]
Ru/TiO₂ (anatase+rutile)	604	37.7	39.7	1.7	104500	0.001	[58]
Ru/graphene	600	12.7	-	1.9	-	0.002	[59]
Ru/Carbon black (Ketjenblack EC-300)	429.5	34.81	800	1.7	-	0.00425	[34]
Ru⁰/CeO₂	361	51	48	-	135100	0.00095	[60]
Ru⁰/MWCNT	329	33	31	2.5	26400	0.00094	[61]
Ru/SBA-15	316	34.8	438	3.0±0.8	-	0.002	[62]
Ru/g-C₃N₄ (Graphitic carbon nitride)	313	37.4	25	2.8	-	0.0017	[63]
RuCuNi/CNTs	311.5	36.67	-	1.35	-	0.0015	[64]
Ru-MIL 53(Al)	266.9	33.7	932.1	2.0	-	0.004	[65]
Ru-MIL 53(Cr)	260.8	28.9	1096.5	2.0	-	0.004	[65]
Ru@TiO₂	241	70	-	2.3±0.7	71500	0.0006	[66]
Ru@MIL-96	231	48	211.2	2.0		0.0039	[67]
Ru/nanodiamond	229	50.7	-	3.7	13474	0.0033	[68]
Ru@SiO₂	200	38	193	2.0		0.0025	[69]
Ru(0)/PSSA-co-MA	180	54	-	1.9±0.7	51720	0.005	[70]
Ru@MIL-101	178	51	2089	1.6	-	0.008	[71]
Ru(0)/SiO₂-CoFe₂O₄	172.5	45.6	-	-	-	0.00097	[72]
Ru/HfO₂	170	65	15.8	3.5±0.6	175600	0.00396	[73]
Ru/HAp	137	58	-	4.7±0.7	87000	0.00392	[74]
Ru⁰/X-NW	135	77	70	4.4±0.4	134100	0.00271	[75]
RuCu/graphene	135	30.59	-	-	-	0.004	[76]
Commercial Ru/Carbon (3.0%wt)	113	76	1000	-	-	0.00178	[77]
Ru/graphene	100	11.7	-	1.7	-	0.010	[78]
Ru NPs@ZK-4	90.2	28	380	2.9±0.9	36700	0.0005	[79]
Ru@Al₂O₃	83.3	46	40	2.5	-	0.00375	[80]
Ru(0)NP/laurate	75	47	-	2.6±1.2	5900	0.0005	[81]
Nanoporous Ru (Ru₂₀Al₈₀)	26.7	66.5	27.4	-	21000	0.01	[82]
Meta stable Ru NPs	21.8	27.5	-	2.2	-	0.00250	[83]

Table 3. The turnover frequency and activation energy values of reported carbon based catalysts used in hydrogen generation from the hydrolysis of AB (TOF values were given for the hydrolysis of AB at room temperature).

Catalyst	TOF (mol H_2 mol metal^{-1}min^{-1})	Ea (kj/mol)	Ref.
Rh/CNT	706	32	[84]
Ru/graphene	600	12.7	[59]
Pt/CNTs-O-HT	468	-	[85]
Ru/Carbon black (Ketjenblack EC-300)	429.5	34.81	[34]
Pd@Co/graphene	408.9	-	[86]
Ru@Co/graphene	344	-	[87]
Ru@Ni/graphene	339.5	36.59	[88]
Ru^0/MWCNT	329	33	[61]
Ru@Co/C	319.7	21.16	[89]
Ru/g-C$_3$N$_4$ (Graphitic carbon nitride)	313	37.4	[63]
RuCuNi/CNTs	311.5	36.67	[64]
Ru@Ni/C	250.1	37.87	[89]
Ru/nanodiamond	229	50.7	[68]
RuCu/graphene	135	30.59	[76]
Commercial Ru/Carbon (3.0%wt)	113	76	[90]
Ag@Co/graphene	102.4	20.03	[91]
Ru/graphene	100	11.7	[78]
Ag@Ni/graphene	77	49.56	[91]
RGO-Cu$_{75}$Pd$_{25}$	29.9	45	[92]
RGO-Ni$_{30}$Pd$_{70}$	28.7	45	[93]
RGO-Pd	26.3	40	[94]
200 ALD cycle Ni /CNT	26.2	-	[95]
Ni/CNT	23.53	-	[96]
Co$_{35}$Pd$_{65}$/C	22.7	27.5	[97]
CoNi/RGO	19.54	39.89	[98]
CoNi/graphene	16.4	13.49	[99]
Ag@CoNi/graphene	15.89	36.15	[100]
Co/graphene	13.9	32.72	[101]
Ag$_{0.5}$@Co$_{0.5}$/graphene	10.5	39.33	[102]
CuCo/graphene	9.18	-	[103]
Ni/C	8.8	-	[104]
RGO-Cu$_{0.2}$@Co$_{0.8}$	8.36	-	[105]
RGO/Pd	6.25	51	[106]
Ag/C/Ni	5.32	38.91	[107]
RGO-Cu	3.61	-	[108]

Table 4. The rate constants k_1 of the slow, continuous nucleation, P → Q, and k_2 of the autocatalytic surface growth, P + Q → 2Q for the formation of ruthenium(0) nanoparticles catalyst from the reduction of Ru^{3+} ions during the hydrolysis of AB at various temperature.

Temperature (°C)	k_1 (s^{-1})	k_2 (M^{-1}s^{-1})	k_2 / k_1
20	$5.56 \times 10^{-4} \pm 5.68 \times 10^{-5}$	$1.12 \pm 6.75 \times 10^{-2}$	2.01×10^3
25	$9.45 \times 10^{-4} \pm 9.37 \times 10^{-5}$	$1.59 \pm 1.01 \times 10^{-1}$	1.68×10^3
30	$1.66 \times 10^{-3} \pm 1.51 \times 10^{-4}$	$1.41 \pm 1.19 \times 10^{-1}$	8.47×10^2
35	$2.54 \times 10^{-3} \pm 3.29 \times 10^{-4}$	$2.49 \pm 2.74 \times 10^{-1}$	9.78×10^2
40	$4.15 \times 10^{-3} \pm 5.08 \times 10^{-4}$	$3.45 \pm 3.94 \times 10^{-1}$	8.31×10^2

The kinetics of ruthenium(0) nanoparticle formation and concomitant hydrogen generation from the hydrolysis of ammonia borane were also followed at various temperature in order to get an idea on the energy barrier for the slow nucleation and autocatalytic surface growth of metal(0) nanoparticles as well as for the hydrolysis reaction. Fig. 14a shows the evolution of equivalent H_2 per mole of AB versus time plot for the hydrolysis of AB starting with Ru^{3+}/MWCNTs precatalyst (0.189 mM Ru) and 100 mM AB at five different temperatures. For each temperature, experimental data curve-fit well to the 2-step mechanism yielding the rate constants k_1 of the slow, continuous nucleation (P → Q) and k_2 of the autocatalytic surface growth (P + Q → 2Q) for the formation of ruthenium(0) nanoparticles catalyst from the ruthenium(III) ions during the hydrolysis of ammonia borane (Table 4). From the Arrhenius plots constructed by using the values of rate constants k_1 and k_2 at various temperatures in Fig. 14b and c, one can obtain the activation energy, $E_a = 77 \pm 7$ kJ/mol for the nucleation and $E_a = 41 \pm 2$ kJ/mol for the autocatalytic surface growth of ruthenium(0) nanoparticles, respectively. The large value of k_2/k_1 ratio also given in Table 4 is indicative of the high level kinetic control in the formation of ruthenium(0) nanoparticles from the reduction of the precursor ruthenium(III) ions on the surface of MWCNTs.

Activation energy for hydrogen generation from the hydrolysis of AB catalyzed by Ru^0/MWCNTs could be determined by evaluating the temperature dependent kinetic data presented in Fig. 14a. The rate constants for the hydrogen generation at different temperature were calculated from the slope of linear portion of each plot given in Fig. 14a and used for the calculation of activation energy ($E_a = 33 \pm 2$ kJ/mol) from the Arrhenius plot in Fig. 14d. The activation energy for the hydrolysis of ammonia borane catalyzed by Ru^0/MWCNTs is comparable to the literature values reported

for the same reaction using other ruthenium catalysts listed in Table 2 and Table 3. The results indicate that apparent activation energy values show variation according to the catalyst. There is no observable relation between the catalytic activity and E_a values of the reported catalyst used in hydrolysis of ammonia borane.
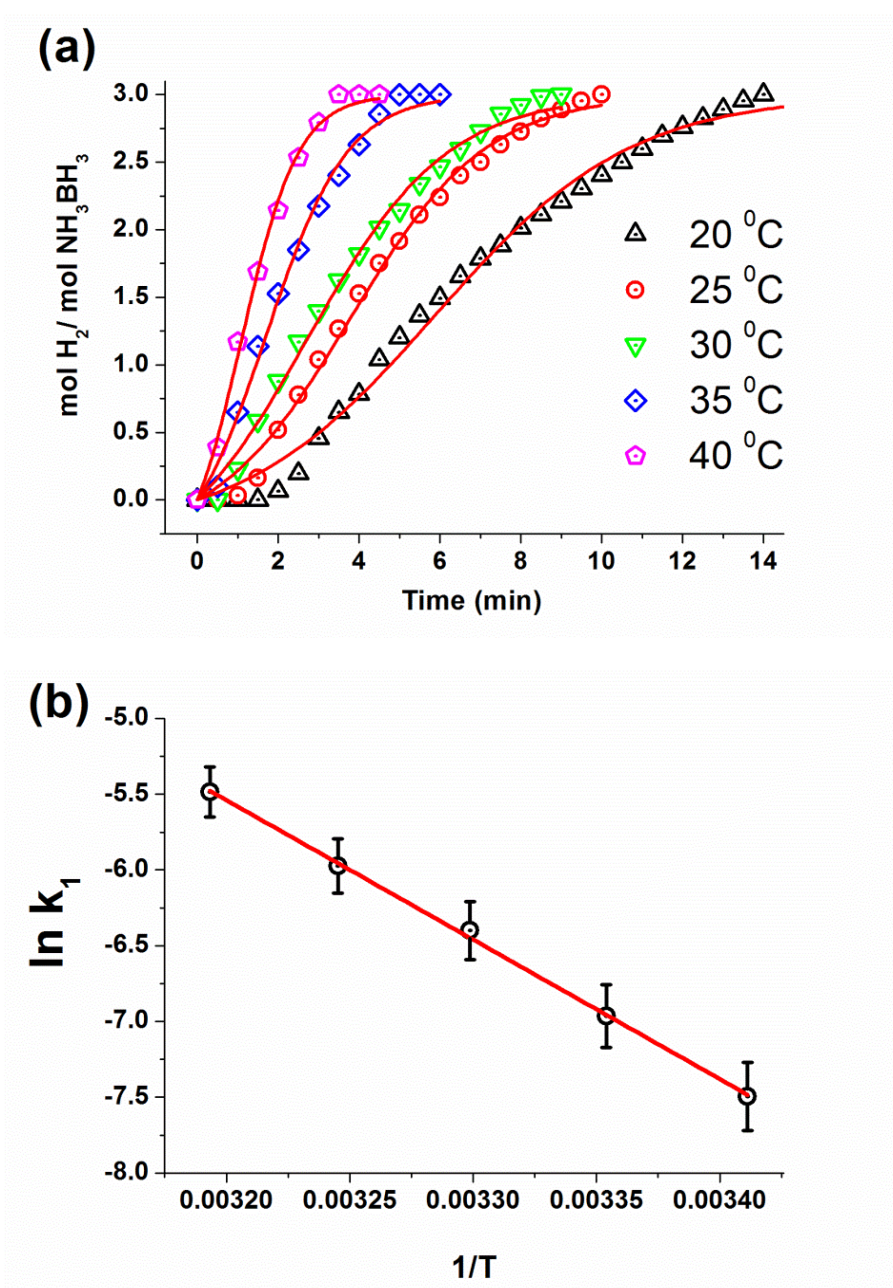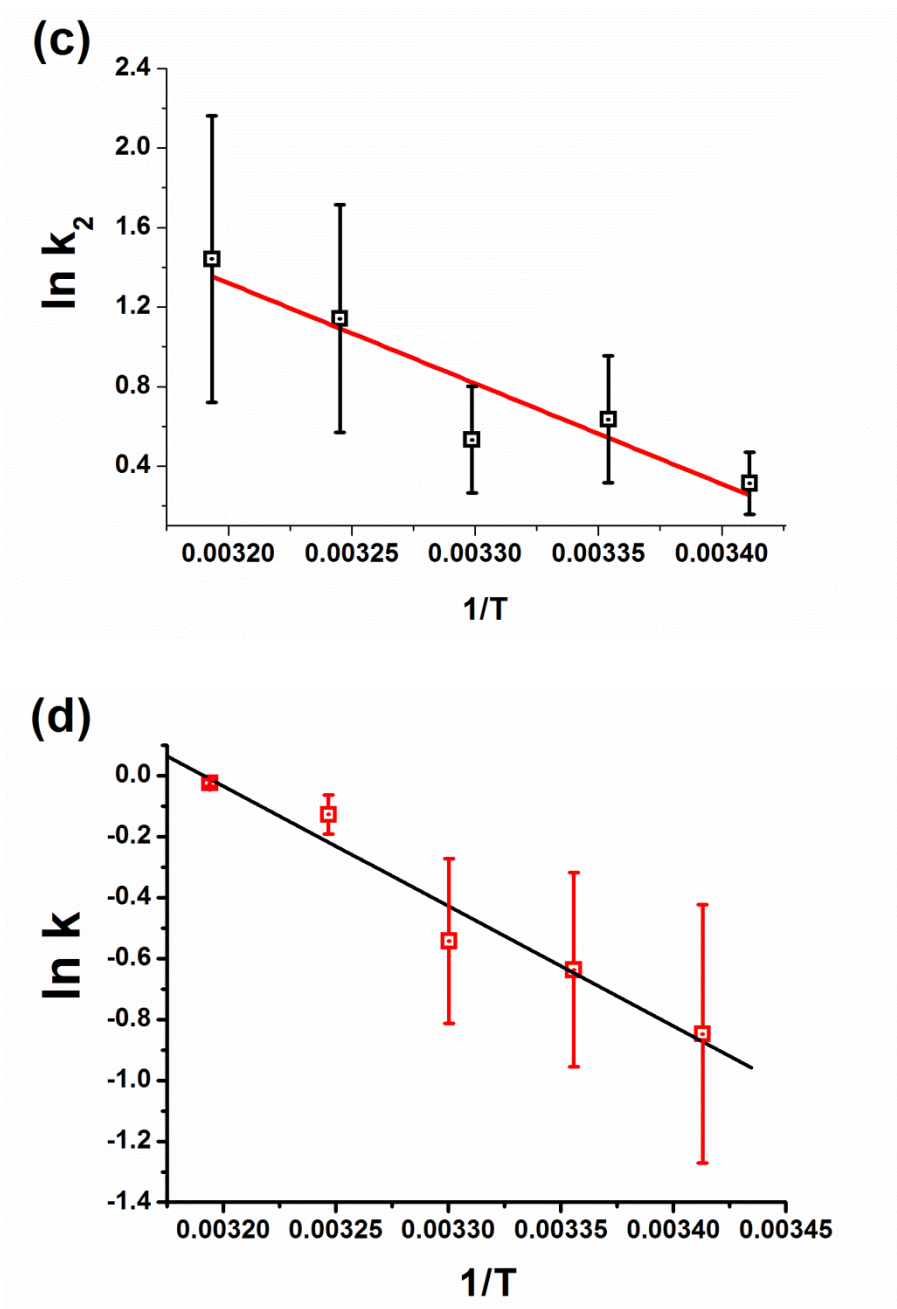
Figure 14. (a) mol H_2/mol H_3NBH_3 versus time graph for the hydrolysis of AB (100 mM) using Ru^0/MWCNT([Ru] = 0.189 mM) as catalyst at different temperatures, (b) The Arrhenius plot for nucleation of ruthenium(0) nanoparticles, $\ln(k_1) = -9205.04/T + 23.91$, (c) The Arrhenius plot for the autocatalytic surface growth of ruthenium(0) nanoparticles, $\ln(k_2) = -4943.7/T + 16.9$. (d) The Arrhenius plot for hydrogen generation from the catalytic hydrolysis of ammonia borane, $\ln(k_{obs}) = -3941.72/T + 12.57$.
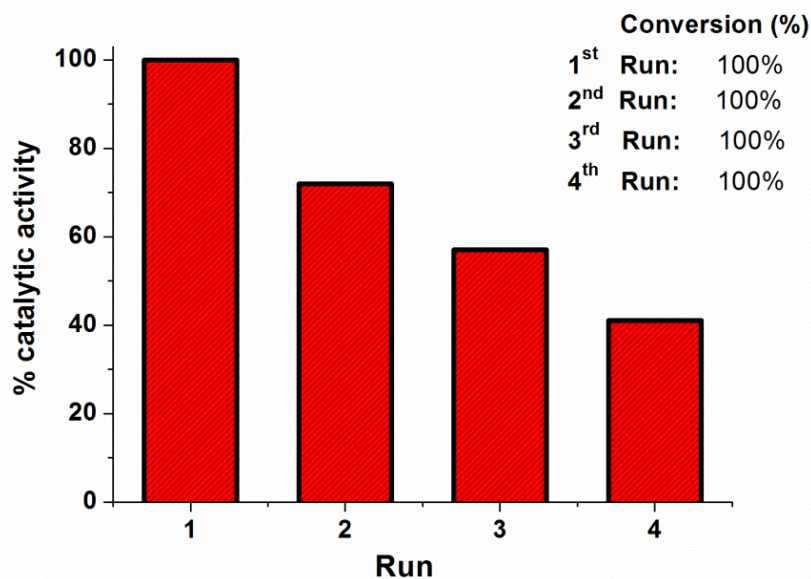
Figure 15. Percentage of initial catalytic activity of Ru^0/MWCNT ([Ru] = 0.567 mM) in successive runs after the reuse for the hydrolysis of ammonia borane (100 mM).

Reusability test of Ru^0/MWCNTs was performed using the catalyst isolated from the reaction solution after a previous run of hydrolysis of AB. After the completion of hydrogen generation from the hydrolysis of AB starting with 0.567 mM Ru^{3+}/MWCNT plus 100 mM AB in 10 mL aqueous solution at 25.0 ± 0.1°C, the catalyst was isolated by filtering and washing with water and dried in the oven at 80 °C. The whole powder materials were weighed and then redispersed in 10 mL of solution containing 100 mM AB and a second run hydrolysis was started immediately and continued until the completion of hydrogen evolution. This was repeated four times.

Figure 15 shows the percentage of initial catalytic activity of Ru^0/MWCNTs in the subsequent catalytic hydrolysis of 100 mM ammonia borane performed by using the catalyst isolated after the previous run of hydrolysis at 25.0 ± 0.1 °C. The reusability tests reveal that Ru^0/MWCNTs are still active in the subsequent runs of hydrolysis of ammonia borane providing a release of 3.0 equivalent H_2 per mole of NH_3BH_3. After the fourth run hydrolysis of ammonia−borane, Ru^0/MWCNTs preserve 41% of their initial catalytic activity. TEM images of Ru^0/MWCNT after the forth reuse in the hydrolysis of ammonia borane (Figure 16) show that ruthenium(0) nanoparticles aggregate on MWCNT after the forth reuse. The aggregation of metal nanoparticles causes a decrease in the surface area of nanoparticles. Therefore, the decrease in

catalytic activity in successive runs can be attributed to the agglomeration of nanoparticles on the surface of carbon nanotubes during the isolation and redispersion processes, as the material loss has already been taken into account in calculating the activity in each run.
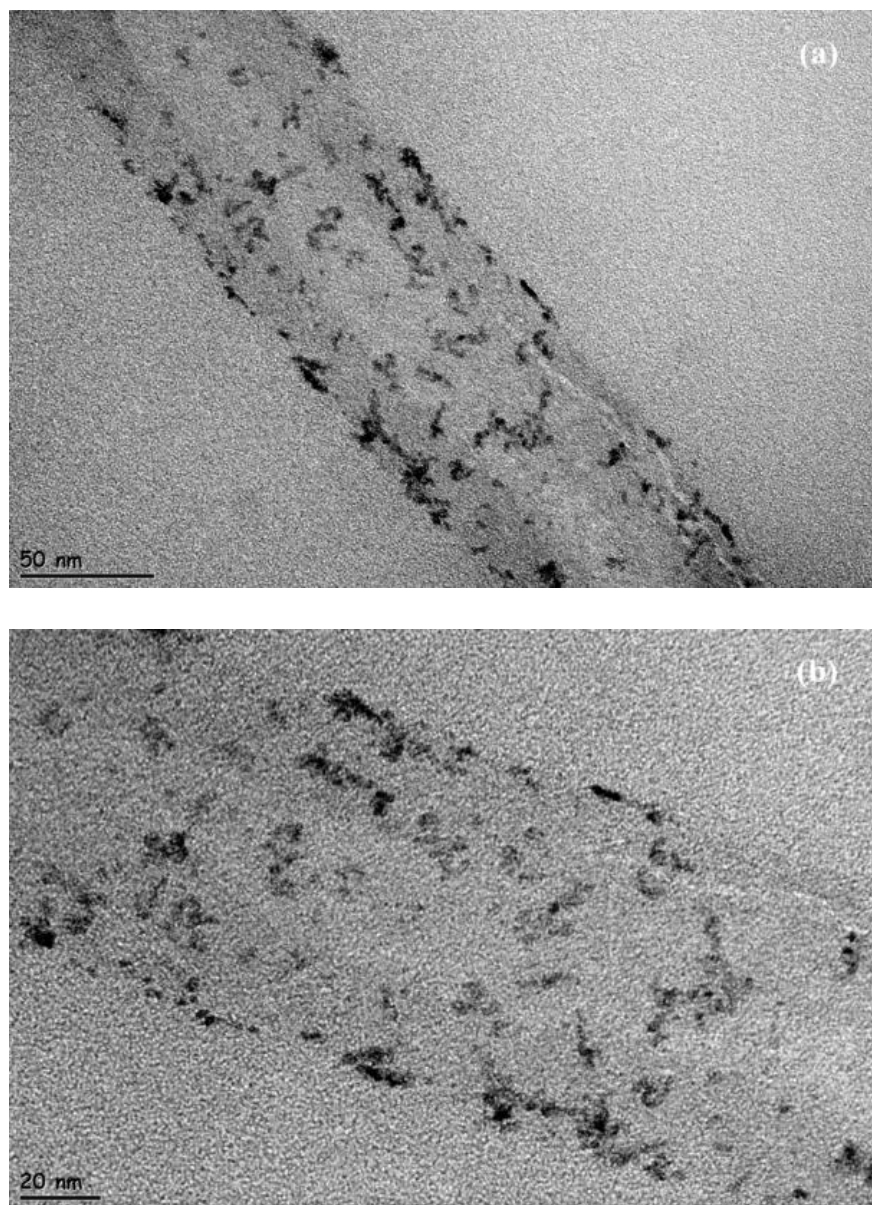
Figure 16. TEM image of Ru^0/MWCNT after the 4th use at the scale bar of (a) 50 nm, (b) 20 nm

Catalytic lifetime of Ru^0/MWCNTs was measured by the total turnover number (TTO) in the hydrolysis of ammonia borane. A catalyst lifetime experiment starting with 1.89 μmol Ru in 100 mL of solution of AB at 25.0 ± 0.1 °C reveals a minimum

TTO value of 26400 turnovers over 29 h in the hydrolysis of AB before deactivation of the catalyst. Ru^0/MWCNTs provide comparable TTO value for the hydrolysis of AB as compared to the other ruthenium catalysts listed in Table 2. An initial TOF value of 329 min^{-1} was obtained; however, the average TOF value was calculated to be 15 min^{-1} in the catalytic lifetime experiment. The observation that the TOF value decreases as the reaction proceeds indicates the deactivation of ruthenium(0) nanoparticles catalyst. After the lifetime experiment, the resulting solution was filtered and the ruthenium concentration of filtrate was found to be 0.085 ppm as determined by ICP-OES. This indicates that 96% of ruthenium nanoparticles still remain on the surface of carbon nanotubes after lifetime experiment. Therefore, the deactivation of Ru^0/MWCNTs catalyst can be attributed to a decrease in accessibility of active sites of ruthenium nanoparticles due the passivation of metal surface by metaborate ions which accumulate in solution as the reaction proceeds.

CHAPTER 4

Ruthenium(0) Nanoparticles Supported on Xonotlite Nanowire

Activity and stability of nanoparticles catalysts can be improved by preventing the metal nanoparticles agglomeration using suitable stabilizing agents. Although carbon materials provide a high external surface area, the aggregation of metal nanoparticles can frequently be seen. To achieve more durable catalysts in hydrogen generation from the hydrolysis of AB as compared to the Ru^0/MWCNTs we considered to prepare ruthenium NPs supported on xonotlite nanowire which is one-dimensional inorganic analog of carbon nanotubes.

4.1. Hydrolytic dehydrogenation of ammonia borane catalyzed by Ru^0/X-NW

The preparation of Ru^0/X-NW comprises the ion-exchange of Ru^{3+} ions with Ca^{2+} ions in the lattice of xonotlite nanowire, followed by the reduction of the Ru^{3+}-exchanged xonotlite nanowire with sodium borohydride in aqueous solution at room temperature. Fig. 17 exhibits the SEM image, SEM-EDX spectrum and TEM images of xonotlite nanowire indicating that (i) xonotlite nanowire has an average diameter of 36 nm and length of 1.4 μm, and (ii) there is no impurity detected in addition to the framework elements of xonotlite nanowire (Ca, Si, O).
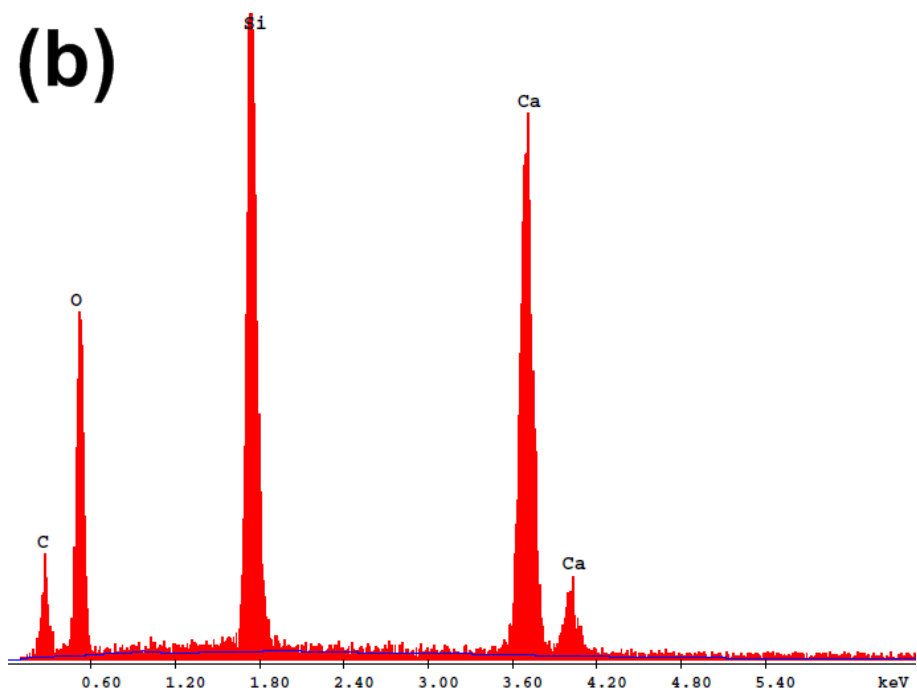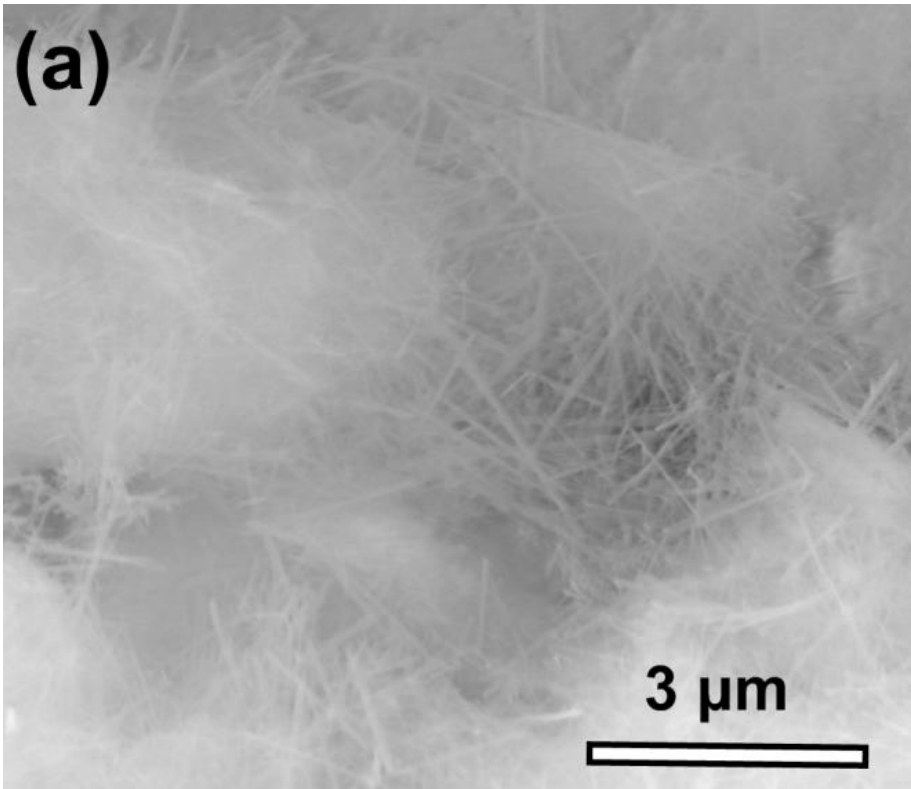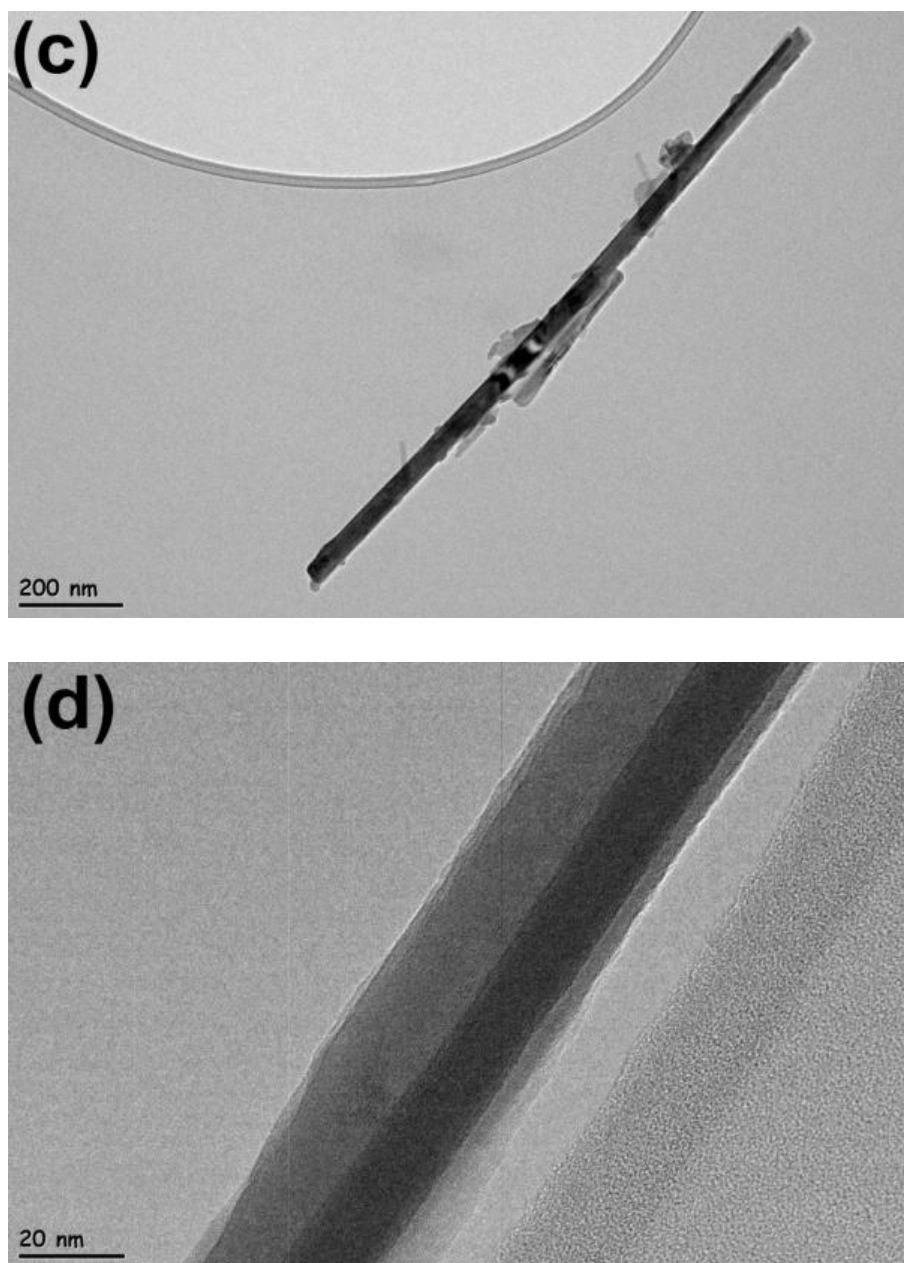
Figure 17. (a) SEM image, (b) SEM-EDX spectrum, and (c-d) TEM images of xonotlite nanowire with two different magnifications.

Ruthenium(0) nanoparticles supported on xonotlite nanowire (Ru^0/X-NW) were isolated from the reaction solution by centrifugation, copious washing with water, and drying under vacuum (10^{-3} Torr) at 80 °C and characterized by ICP-OES, XRD, SEM, SEM-EDX, TEM, XPS and the N$_2$ adsorption– desorption technique. Ruthenium content of Ru^0/X-NW was found to be 1.37% wt. by ICP-OES.
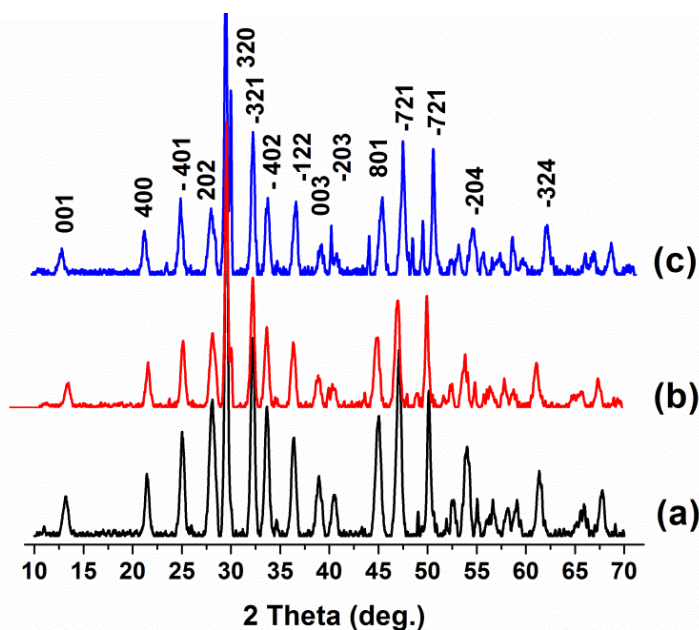
Figure 18. Powder XRD patterns of (a) xonotlite nanowire, (b) Ru^{3+}/X-NW, (c) Ru^0/X-NW with a 1.37% wt. Ru loading.

Fig. 18 shows the XRD pattern of xonotlite nanowire powders, the ruthenium(III) ion exchanged xonotlite (Ru^{3+}/X-NW) and ruthenium(0) nanoparticles supported on xonotlite (Ru^0/X-NW) with a ruthenium loading of 1.37% wt. Ru. It can be seen that all the peaks in Fig. 18a match the standard values of xonotlite (JCPDS no. 23-0125) in terms of positions (2 theta) of the peaks [35]. The comparison of the XRD patterns for three samples clearly shows that there is no change in the characteristic diffraction peaks of xonotlite nanowire. This observation indicates that the host material remains intact after ion-exchange and reduction of ruthenium(III) ions without noticeable alteration in the framework lattice or loss in the crystallinity. There is no observable peak attributable to ruthenium nanoparticles in Fig. 18 b and 18 c, probably as a result of low ruthenium loading on xonotlite nanowire.

The BET nitrogen adsorption analysis gave the surface area of xonotlite nanowire and Ru^0/X-NW as 72.89 and 69.75 $m^2\ g^{-1}$, respectively. This slight decrease in the surface area of xonotlite nanowire upon ruthenium loading may imply the existence of ruthenium(0) nanoparticles on the surface.

42

(a)

5 µm

(b)

1 µm
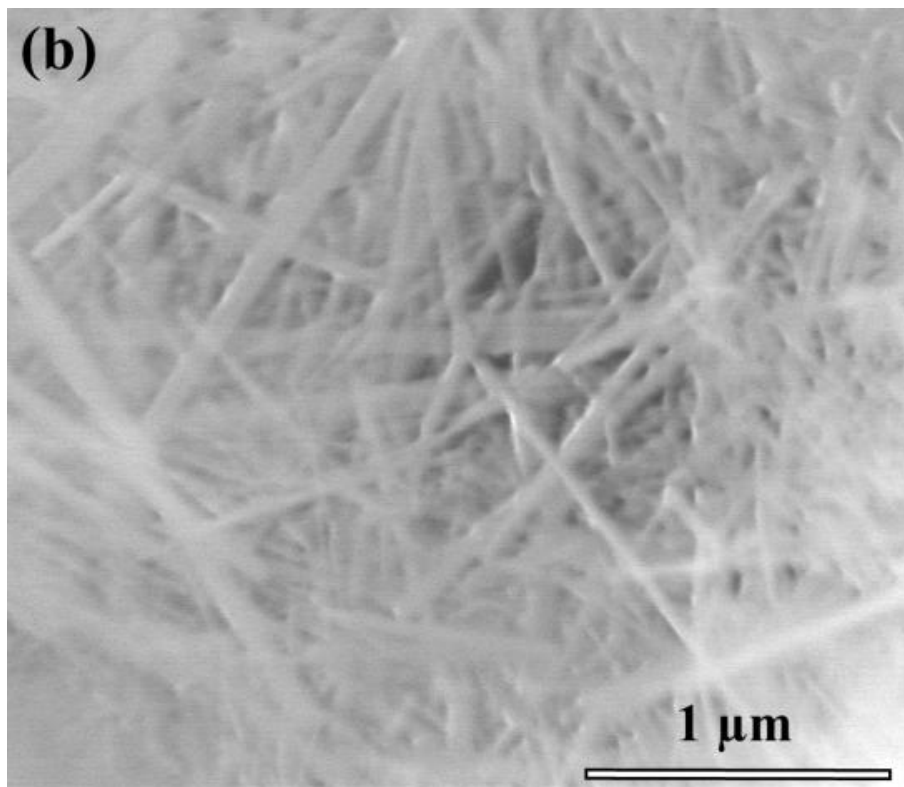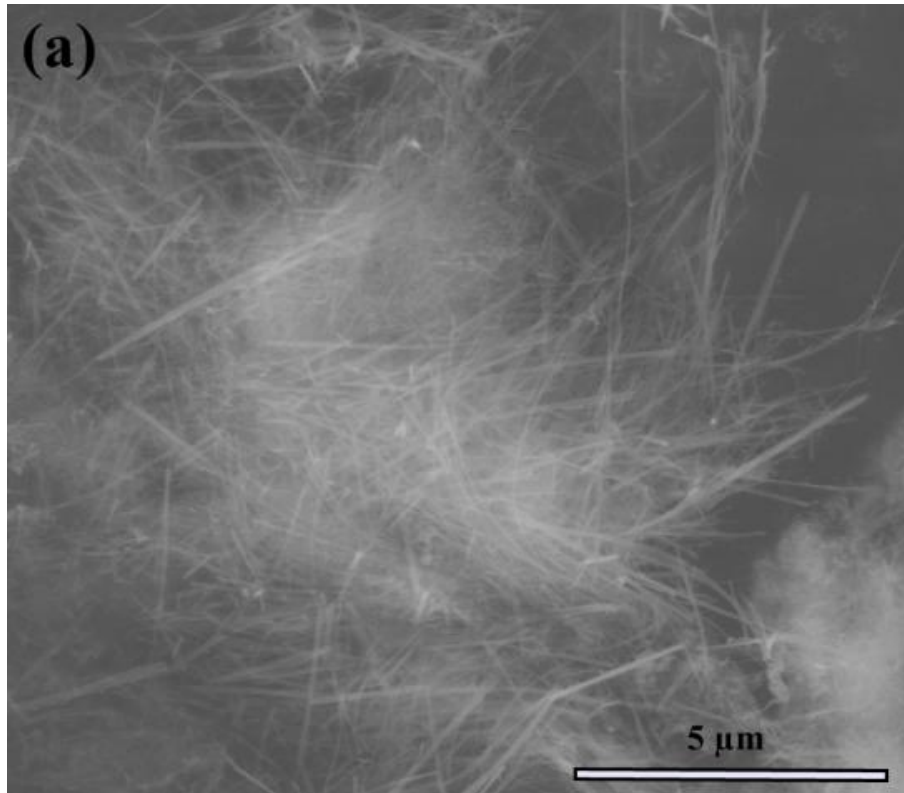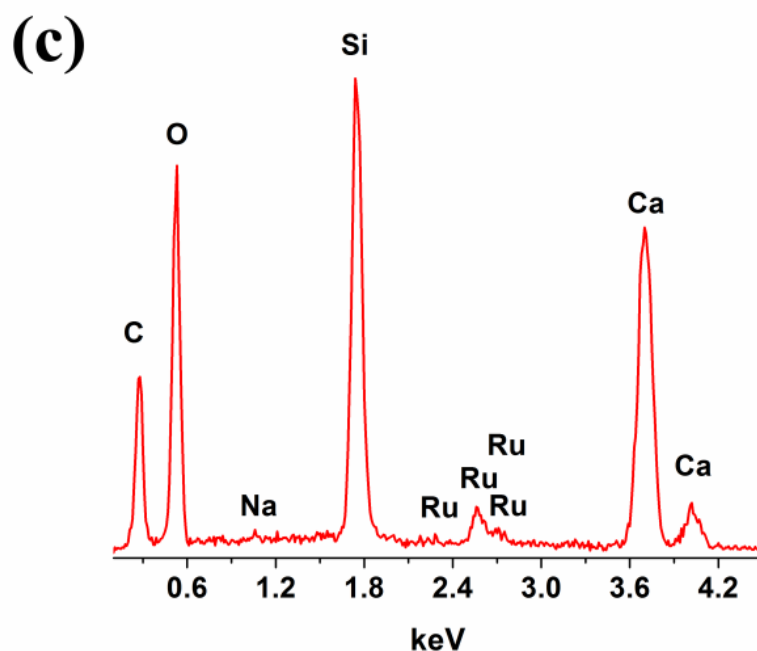
Figure 19. (a) and (b) SEM images of Ru^0/X-NW in different magnifications, (c) SEM-EDX spectrum of Ru^0/X-NW with a 1.37% wt. Ru loading.

Fig. 19 exhibits the SEM image and SEM-EDX spectrum of Ru^0/X-NW with a ruthenium loading of 1.37% wt. indicating that ruthenium and sodium are the elements detected in the sample in addition to the framework elements of xonotlite nanowire (Ca, Si, O). The existence of sodium element in the SEM-EDX spectrum can be attributed to the fact that the cation sites left by Ru^{3+} ions upon reduction are reoccupied by sodium cations coming from sodium borohydride [31].

Fig. 20 shows the TEM images of xonotlite nanowire and Ru^0/X-NW with a ruthenium loading of 1.37% wt. taken with different magnifications, which indicate that (i) highly dispersed ruthenium(0) nanoparticles with particle size in the range 3.6–5.9 nm are formed on the surface of xonotlite nanowire (mean diameter: 4.4 ± 0.4 nm in Fig. 20 c), (ii) ion-exchange of ruthenium(III) followed by reduction to ruthenium(0) causes no change in the framework lattice of the xonotlite nanowire in agreement with the XRD results.
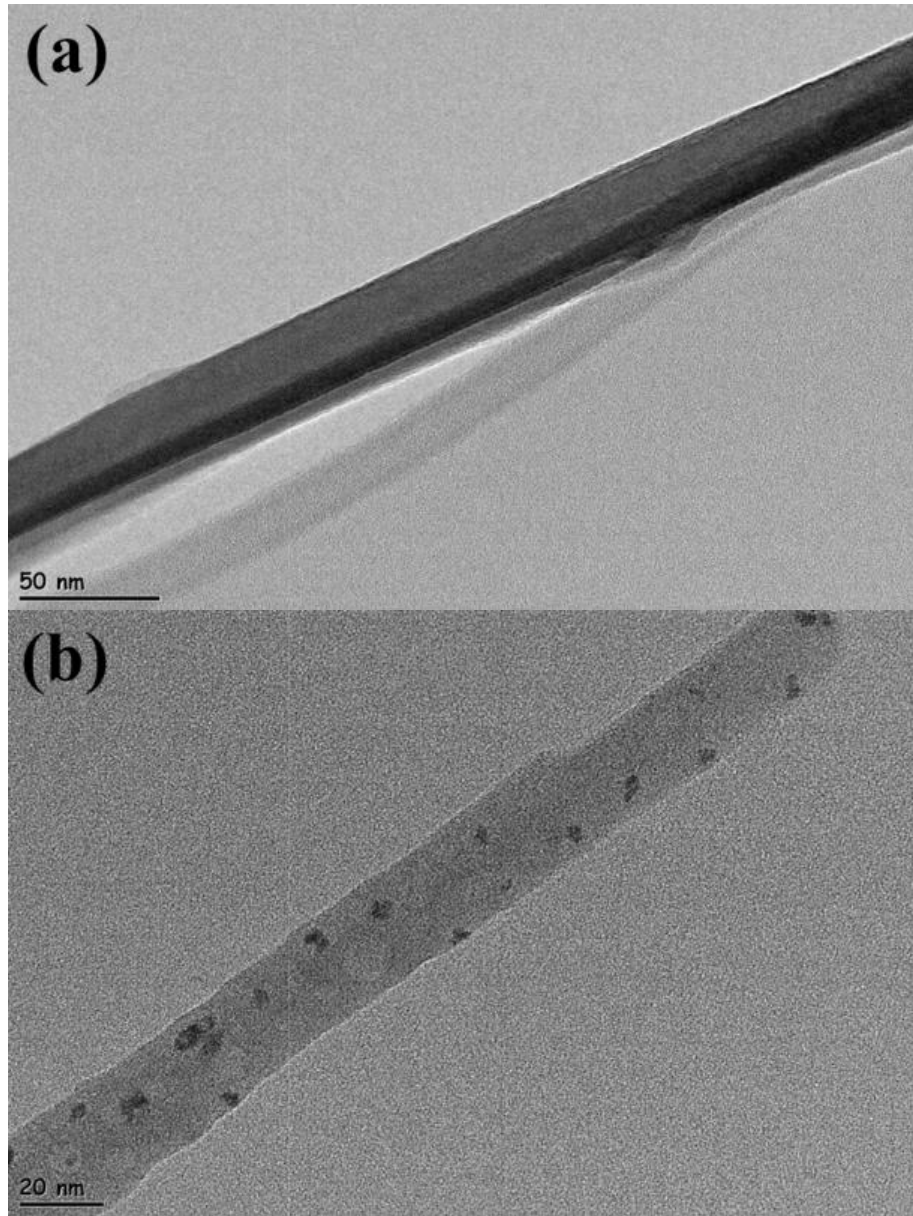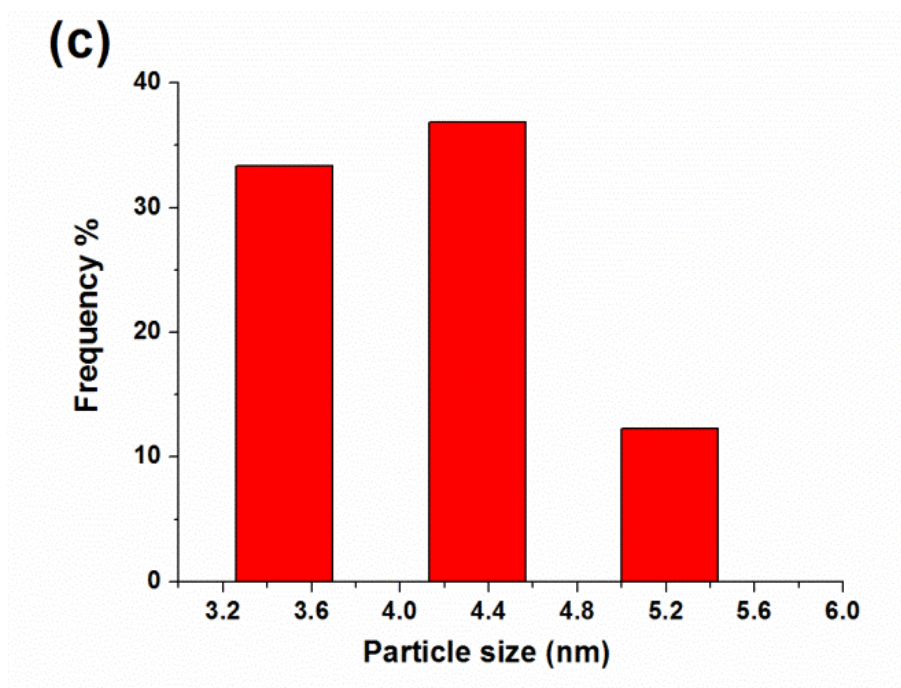
Figure 20. (a) TEM image of xonotlite nanowire with the scale bar of 50 nm, (b) TEM image of Ru^0/X-NW with a ruthenium loading of 1.37% wt. with the scale bar of 20 nm. (c) Histogram of Ru^0/X-NW showing particle size distribution.

The surface composition of Ru^0/X-NW with a ruthenium loading of 1.37% wt was also studied by XPS technique. The survey-scan X-ray photoelectron spectrum of Ru^0/X-NW given in Fig. 21a shows all the framework elements of xonotlite nanowire in agreement with the SEM-EDX result. High-resolution X-ray photoelectron spectrum of a Ru^0/X-NW sample with metal loading of 4.0% wt. Ru given in Fig. 21b shows two prominent bands at 284.4 and 280.9 eV, which can readily be assigned of ruthenium oxides $3d_{3/2}$ and $3d_{5/2}$, respectively [109]. However, it is noteworthy that oxidation of Ru(0) during the XPS sampling procedure is a well known fact.

46
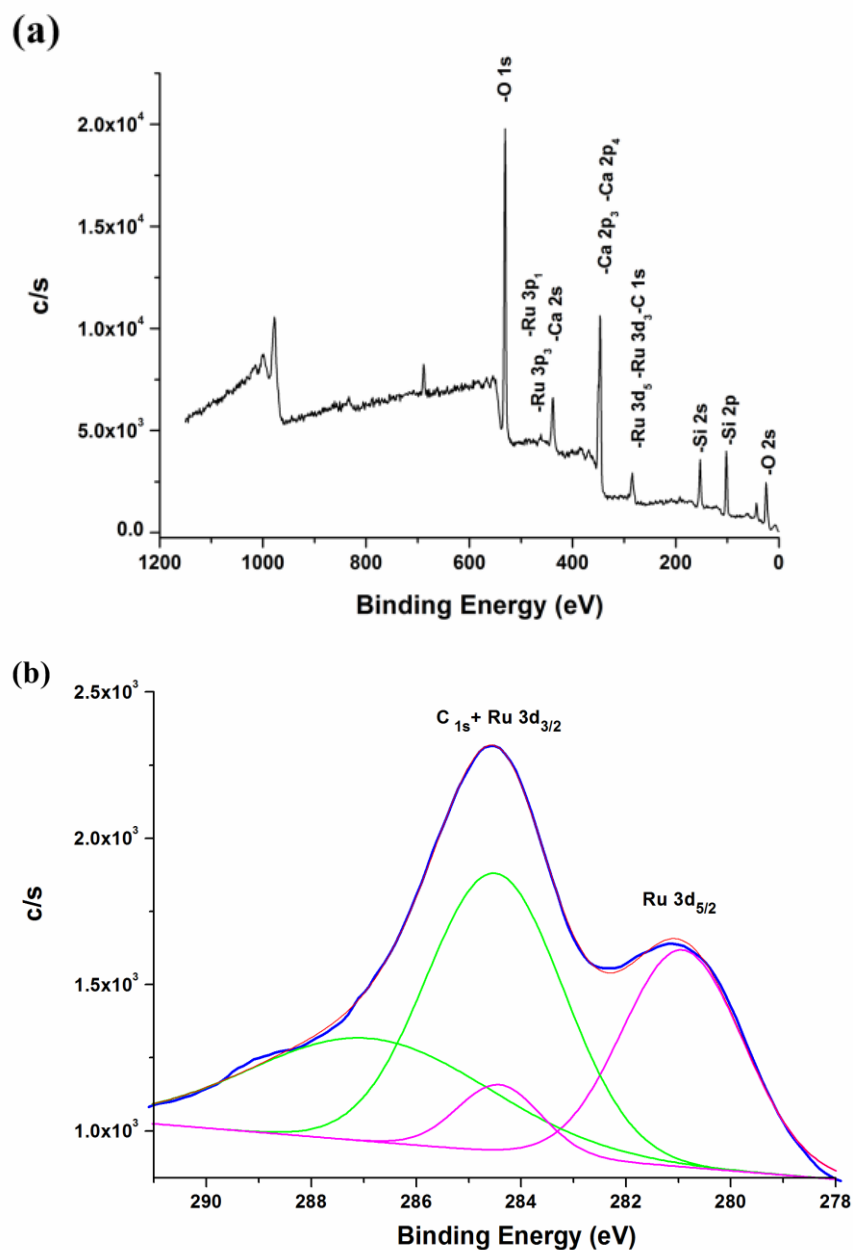
Figure 21. (a) X-ray photoelectron (XPS) spectrum of Ru^0/X-NW with a ruthenium loading of 1.37% wt. (b) Ru 3d XPS spectrum of Ru^0/X-NW with a ruthenium loading of 4.0 % wt.

4.1.1. Catalytic activity of Ru^0/X-NW in hydrolytic dehydrogenation of ammonia borane

Before starting with the investigation on the catalytic activity of Ru^0/X-NW in the hydrolysis of AB, a control experiment was performed to check whether xonotlite nanowire show any catalytic activity in the hydrolytic dehydrogenation of AB at the same temperature. In a control experiment starting with 1.0 mmol of AB and 20 mg of powder of xonotlite nanowire (the same amount as the one used in catalytic

47

activity tests) in 10 mL of water at 25.0 ± 0.1 °C or 40.0 ± 0.1 °C, no hydrogen generation was observed in 1 h at either temperatures. This observation indicates that the hydrolysis of AB does not occur in the presence of xonotlite nanowire in the temperature range used in this study. Ru[0]/X-NW are found to be highly active catalyst in the hydrolysis of AB generating 3.0 equivalent H_2 gas per mol of AB in the same temperature range.
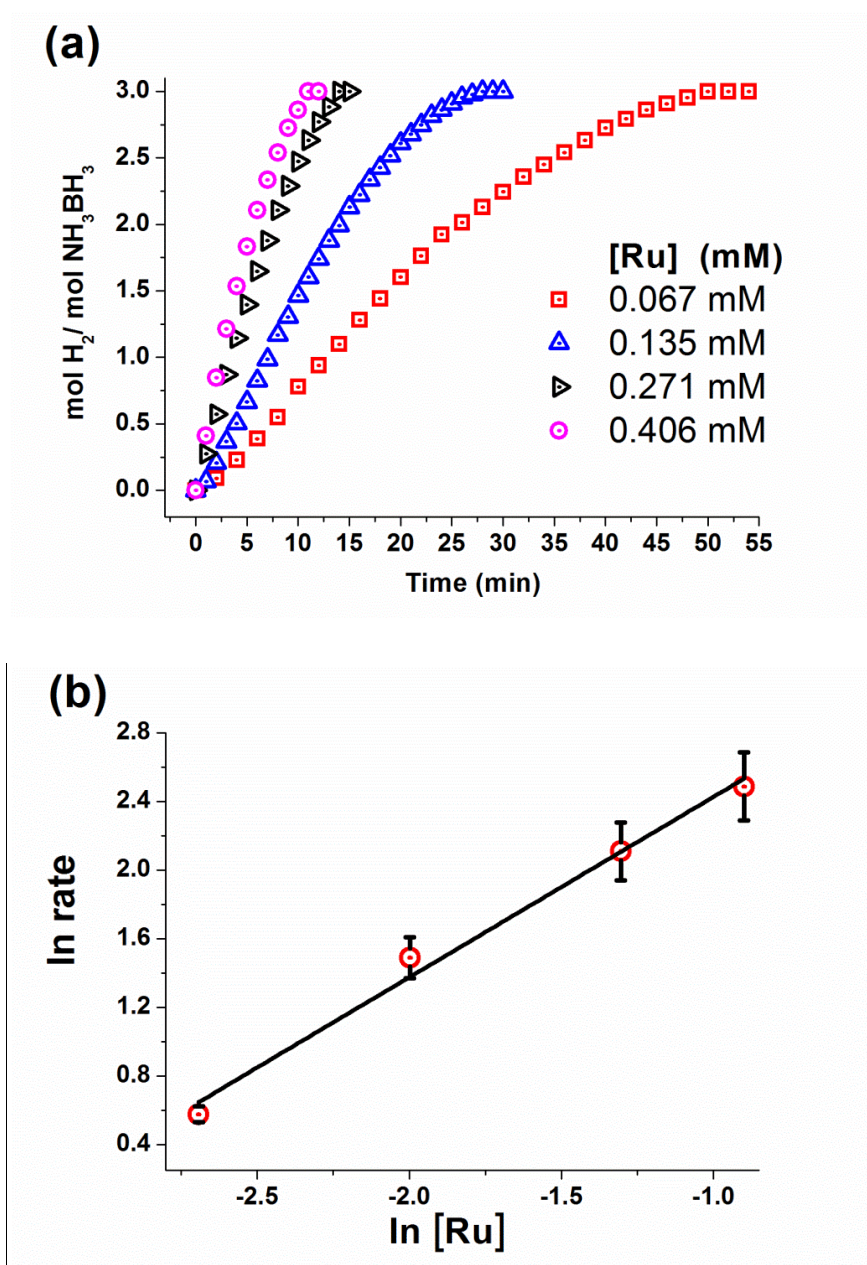
Figure 22. (a) mol H_2 /mol $H_3N.BH_3$ versus time graph depending on the ruthenium concentration in Ru[0]/X-NW for the hydrolytic dehydrogenation of AB (100 mM) at 25.0 ± 0.1 °C, (b) The plot of hydrogen generation rate versus the concentration of Ru, both in logarithmic scale; ln(rate) = 1.05 ln[Ru] + 3.48.

Fig. 22a shows the evolution of equivalent hydrogen per mole of AB versus time plot for the hydrolytic dehydrogenation of AB (100 mM) using Ru^0/X-NW as catalyst in different ruthenium concentration at 25.0 ± 0.1 °C. The hydrogen generation rate was determined from the linear portion of each plot. For all tests a complete hydrogen release (mol H_2/mol $H_3NBH_3 = 3$) was observed. Fig. 22b shows the plot of hydrogen generation rate versus initial concentration of ruthenium, both in logarithmic scale, which gives a straight line with a slope of 1.05 indicating that hydrolysis of AB is first order with respect to the ruthenium concentration.

The turnover frequency (TOF) for hydrogen generation from the hydrolytic dehydrogenation of AB (100 mM) at 25.0 ± 0.1 °C was determined from the hydrogen generation rate in the linear portion of plots given in Fig. 22a for experiments starting with 100 mM AB plus Ru^0/X-NW with a loading of 1.37% wt. Ru. The TOF value of Ru^0/X-NW catalyst is as high as 135 min^{-1} (mol H_2/mol Ru min) in the hydrolytic dehydrogenation of ammonia-borane at 25.0 ± 0.1 °C. As clearly seen from the TOF values of the reported ruthenium catalysts listed in Table 2 (see chapter 3), Ru^0/X-NW provide comparable catalytic activity in hydrolysis of AB.

The catalytic hydrolytic dehydrogenation of ammonia borane was carried out at various temperature in the range of 20–40 °C starting with Ru^0/X-NW (loading = 1.37% wt. Ru and [Ru] = 0.271 mM) plus 100 mM AB in 10 mL of water. The rate constants for the hydrogen generation at different temperatures were calculated from the slope of the linear part of each plot given in Fig. 23a and used for the calculation of activation energy (Ea = 77 ± 2 kJ mol^{-1}) from the Arrhenius plot, which is shown in Fig. 23b. The activation energy for the hydrolytic dehydrogenation of ammonia-borane catalyzed by Ru^0/X-NW is comparable to the literature values reported for the same reaction using other ruthenium catalysts (Table 2, see chapter 3).

Figure 23. (a) The evolution of equivalent hydrogen per mole of AB versus time plot for the hydrolytic dehydrogenation of AB starting with Ru^0/X-NW (0.271 mM Ru) and 100 mM AB at various temperatures. (b) The Arrhenius plot for the Ru^0/X-NW catalyzed hydrolytic dehydrogenation of AB. ln k = −9309.91(1/T) + 30.24.
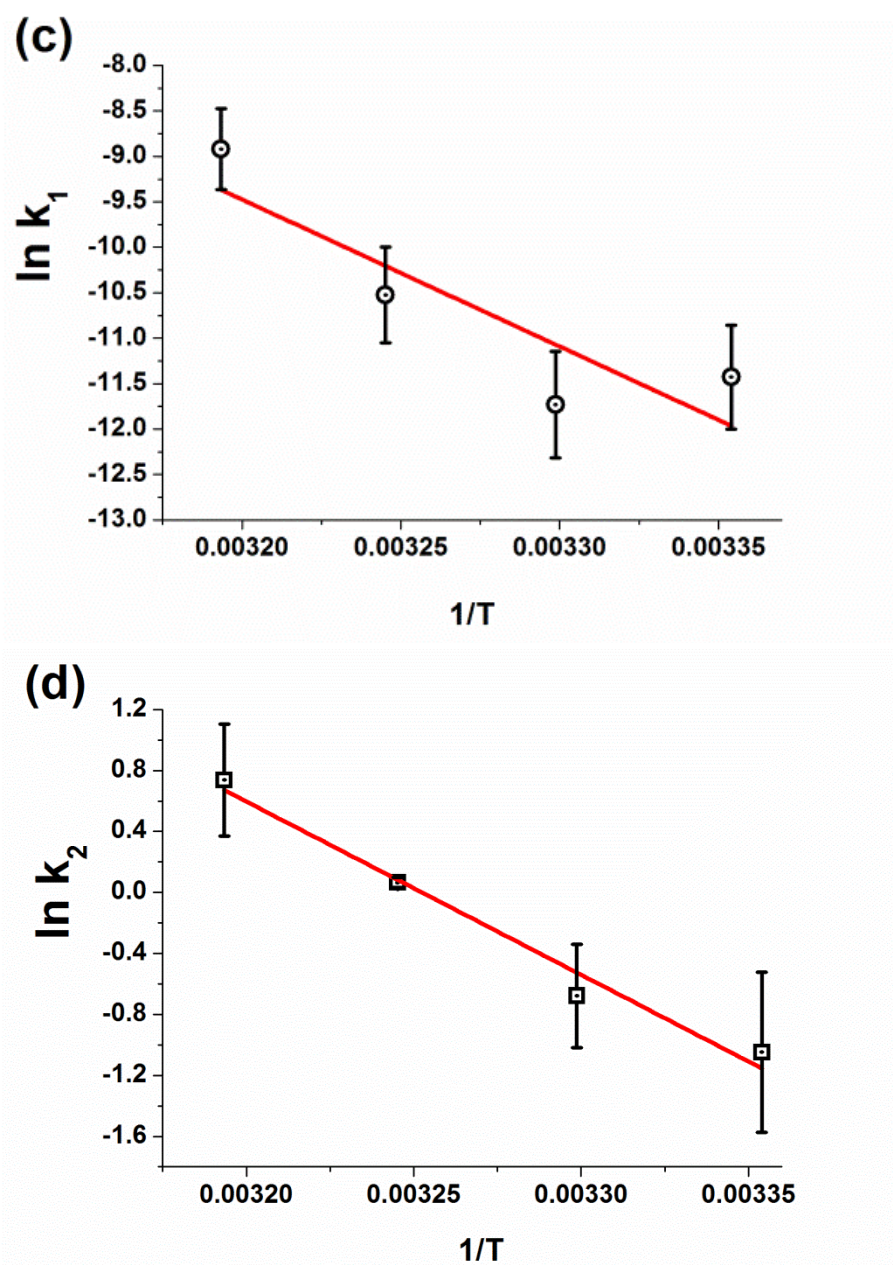
Figure 24. (a) The evolution of equivalent hydrogen per mole of AB versus time plot for the hydrolytic dehydrogenation of AB starting with Ru^{3+}/X-NW precatalyst (0.271 mM Ru) and 100 mM AB at various temperatures, (b) The Arrhenius plot for the *in-situ* generated Ru^{0}/X-NW catalyzed hydrolytic dehydrogenation of AB. $\ln k = -11841.87(1/T) +40.87$, (c) The Arrhenius plot for nucleation of ruthenium(0) nanoparticles, $\ln(k_1) = -16165.01/T + 42.25$, (d) The Arrhenius plot for the autocatalytic surface growth of ruthenium(0) nanoparticles, $\ln(k_2) = -11365.7/T + 36.96$.

The activation energy for the hydrolytic dehydrogenation of AB catalyzed by Ru^{0}/X-NW is also compared by the activation energy which was determined by using *in situ* generated ruthenium(0) nanoparticles supported on xonotlite nanowire during the hydrolysis of AB as catalyst. Fig. 24a shows the evolution of equivalent hydrogen per mole of AB versus time plot for the hydrolytic dehydrogenation of AB starting

with Ru^{3+}/X-NW precatalyst (0.271 mM Ru) and 100 mM AB at different temperatures. Activation energy was determined by evaluating the temperature dependent kinetic data presented in Fig. 24a. The rate constants for the hydrogen generation at different temperatures were calculated from the slope of the linear portion of each plot given in Fig. 24a and used for the calculation of activation energy (Ea = 98 ± 2 kJ mol^{-1}) from the Arrhenius plot in Fig. 24b. The higher activation energy for the hydrolytic dehydrogenation of AB catalyzed by using *in situ* generated ruthenium(0) nanoparticles supported on xonotlite nanowire may be attributed to the aggregation of ruthenium(0) nanoparticles on the surface of xonotlite nanowire (Fig. 25).
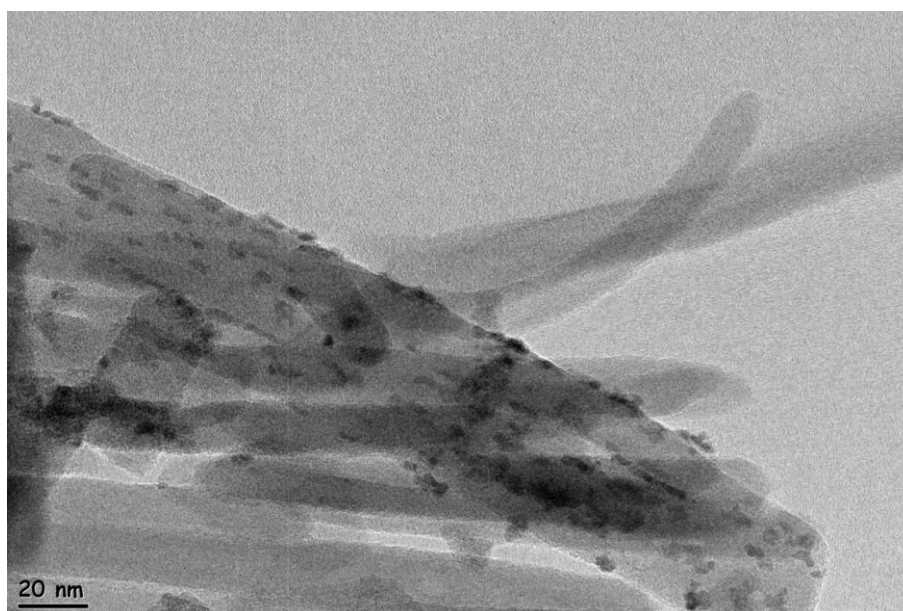
Figure 25. TEM image of *in situ* generated ruthenium(0) nanoparticles supported on xonotlite nanowire during the hydrolysis of AB at room temperature

All the plots in Fig. 24a curve-fit well to the Finke– Watzky two-step mechanism, giving the rate constants k_1 of the slow, continuous nucleation, P $\rightarrow$ Q, and k_2 of the autocatalytic surface growth, P + Q $\rightarrow$ 2Q for the formation of ruthenium(0) nanoparticles catalyst from the ruthenium(III) ions during the hydrolysis of ammonia borane (see Scheme 1). The rate constants, k_1 and k_2, determined from the nonlinear least squares curve-fit in Fig. 24a are shown in Table 5. Note that the mathematically required correction has been made to k_2 for the stoichiometry factor of 369 as described elsewhere [42], but not for the "scaling factor"; that is, no correction has been made for changing the number of ruthenium atoms on the growing metal surface. Although there is no observable correlation between the rate constant k_1 for

nucleation and the reaction temperature because of relatively large uncertainty in the k_1 values, the rate constant k_2 for autocatalytic surface growth increases with the increasing reaction temperature.

Table 5. The rate constants k_1 of the slow, continuous nucleation, P → Q, and k_2 of the autocatalytic surface growth, P + Q → 2Q for the formation of ruthenium(0) nanoparticles catalyst from the reduction of ruthenium(III) ions during the hydrolysis of AB at various temperatures.

Temperature (°C)	k_1 (s^{-1})	k_2 (M^{-1}s^{-1})	k_2 / k_1
25	$1.09 \times 10^{-5} \pm 1.53 \times 10^{-6}$	$0.351 \pm 1.06 \times 10^{-2}$	3.22×10^{4}
30	$8.03 \times 10^{-6} \pm 1.12 \times 10^{-6}$	$0.508 \pm 1.32 \times 10^{-2}$	6.32×10^{4}
35	$2.68 \times 10^{-5} \pm 3.74 \times 10^{-6}$	$1.070 \pm 3.03 \times 10^{-2}$	3.98×10^{4}
40	$8.01 \times 10^{-4} \pm 2.10 \times 10^{-5}$	$2.090 \pm 8.41 \times 10^{-2}$	1.57×10^{4}

From the Arrhenius plots constructed by using the values of rate constants k_1 and k_2 at various temperatures in Fig. 24c and d, one can obtain the activation energy, $E_a = 134 \pm 7$ kJ/mol for the nucleation and $E_a = 94 \pm 2$ kJ/mol for the autocatalytic surface growth of ruthenium(0) nanoparticles, respectively. The large value of k_2/k_1 ratio also given in Table 5 is indicative of the high level kinetic control in the formation of ruthenium(0) nanoparticles from the reduction of the precursor ruthenium(III) ions on the surface of nanowire.

Catalytic lifetime of Ru^0/X-NW was measured by the total turnover number (TTO) in the hydrolytic dehydrogenation of AB (Fig. 26). A catalyst lifetime experiment starting with 20 mg Ru^0/X-NW in 50 mL of solution of AB at 25.0 ± 0.1 °C reveals a minimum TTO value of 134100 turnovers over 166 h in the hydrolytic dehydrogenation of AB before deactivation of the catalyst. Ru^0/X-NW provide remarkable TTO value for the hydrolytic dehydrogenation of ammonia borane as compared to the other reported ruthenium catalysts listed in Table 2 (see chapter 3). The high activity and long lifetime of nanoparticles catalyst supported on xonotlite nanowire can be attributed to the strong adsorption capacity, high surface area and nonporous structure of xonotlite nanowire. After the lifetime experiment the resulting solution was filtered and no leaching of the ruthenium into the solution was detected by ICP-OES, indicating that ruthenium(0) nanoparticles still remain on the surface of xonotlite nanowire after the lifetime experiment. As shown in Fig. 26, the observation that the TOF value decreases as the reaction proceeds indicates the deactivation of ruthenium(0) nanoparticles catalyst. The deactivation of Ru^0/X-NW

catalyst can be attributed to a decrease in accessibility of active sites of ruthenium nanoparticles due to the passivation of metal surface by metaborate ions which accumulate in solution as the reaction proceeds. In addition, the increase in viscosity of the solution as the reaction proceeds might hinder the diffusion of AB, impeding the collision between AB and catalyst, thus decreasing the catalytic activity [34].
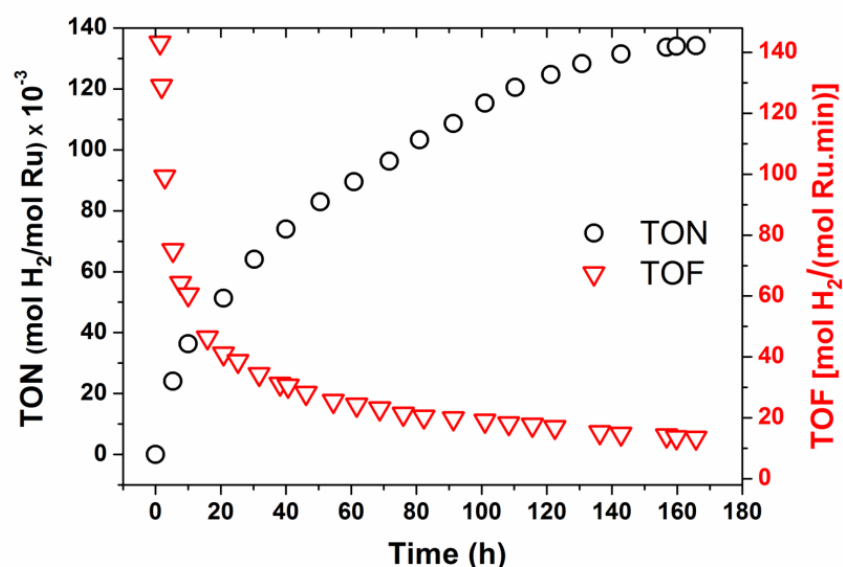
Figure 26. The variation in turnover number (TON) and turnover frequency (TOF) during the catalytic lifetime experiment performed starting with 20 mg Ru^0/X-NW (ruthenium loading = 1.37% wt. Ru, and [Ru] = 0.0542 mM) in 50 mL solution of AB at 25.0 ± 0.1 °C.

The catalytic activity of Ru^0/X-NW after the first run was also tested. After the complete dehydrogenation performed by starting with Ru^0/X-NW (0.271 mM Ru) and 100 mM AB at 25.0 ± 0.1 °C, the catalytic materials were isolated from the reaction solution by centrifugation. The solid materials obtained were redispersed in 10 mL aqueous solution containing 100 mM AB and a second run of hydrolytic dehydrogenation of AB was monitored under the same conditions as the first run. As shown in Fig. 27, the catalytic activity of Ru^0/X-NW in the second run does not differ significantly from the one obtained in the first run. The catalytic activity of the filtrate solution obtained by centrifugation of the solid materials after the first run of hydrolysis was also tested in the hydrolysis of AB (100 mM) under the same conditions. As shown in Fig. 27 the filtrate solution is catalytically silent in hydrolytic dehydrogenation of AB. This observation supports the conclusion that there is no leaching of ruthenium into the solution during the hydrolysis.

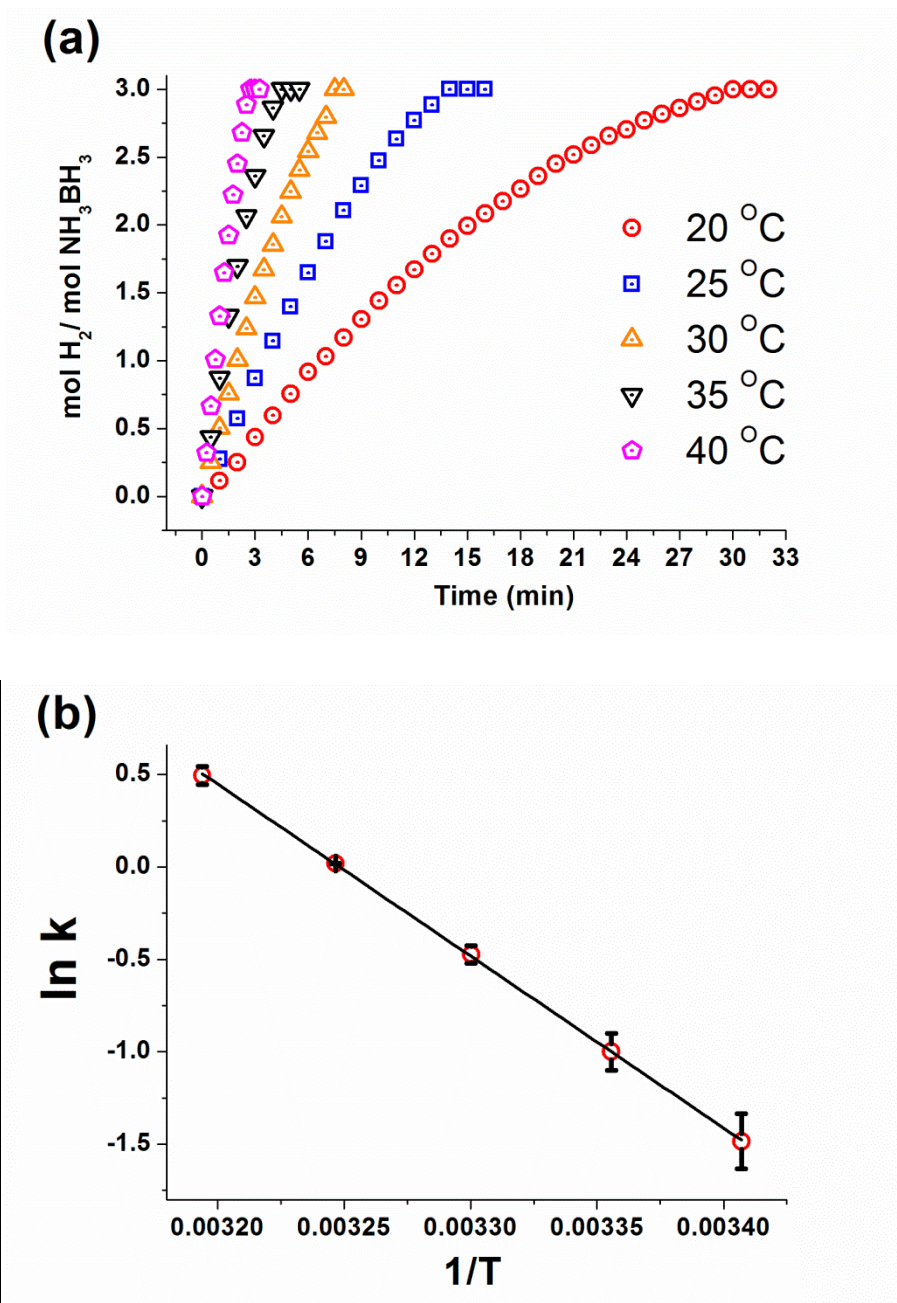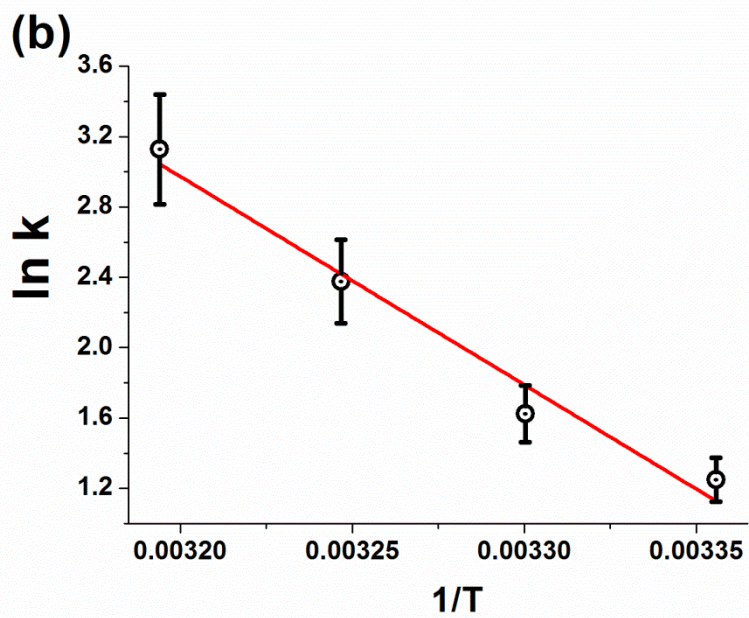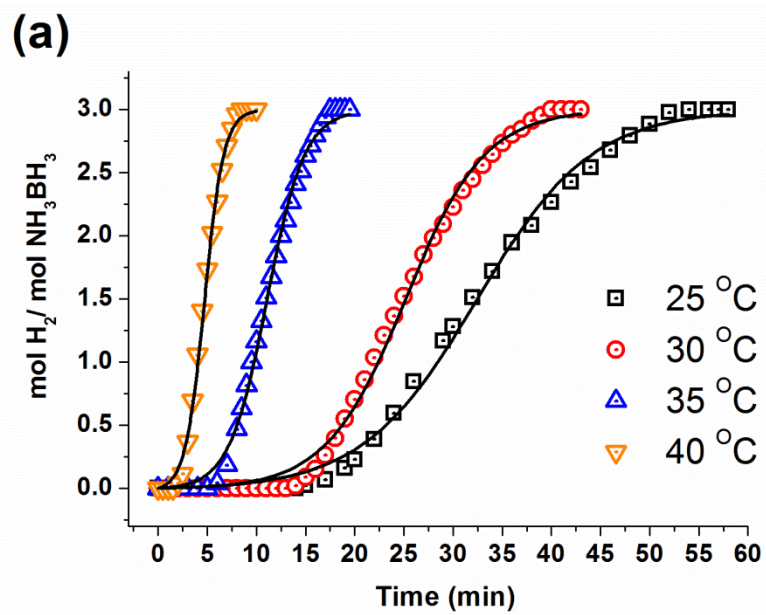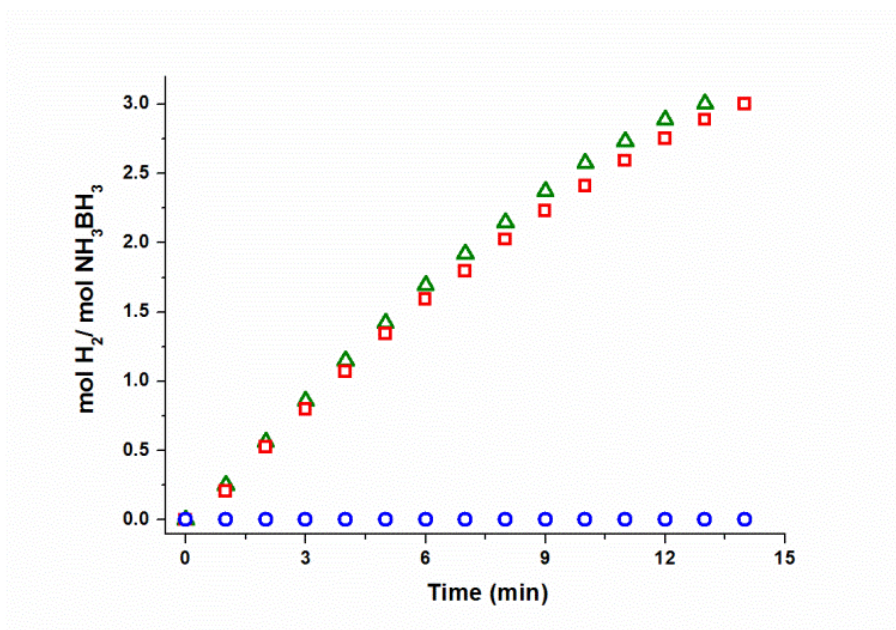**Figure 27.** The evolution of equivalent hydrogen per mole of AB versus time plot for the hydrolytic dehydrogenation of AB (100 mM) starting with Ru^0/X-NW (0.271 mM Ru) (triangle, Δ), Ru^0/X-NW isolated after first run and redispersed (square, □), the filtrate solution obtained by centrifugation of the solid materials after the first run (circle, ○) at room temperature.

CHAPTER 5

Ruthenium(0) Nanoparticles Supported on Hydroxyapatite

Hydroxyapatites, $Ca_{10}(PO_4)_6(OH)_2$, have attracted great interest as a catalyst support due to their high ion exchange ability, high adsorption capacity and nonporous structures that reduce the mass transfer limitations. These unique properties of hydroxypatites encouraged us to use hydroxyapatites as support for ruthenium(0) nanoparticles in developing highly reusable and long lived ruthenium catalysts in hydrogen generation from ammonia borane as compared to the Ru^0/MWCNTs and Ru^0/X-NW.

5.1. Hydrolytic dehydrogenation of ammonia borane catalyzed by Ru^0/HAp

Ruthenium(0) nanoparticles supported on hydroxyapatite were *in situ* generated during the hydrolysis of ammonia borane. Ru^0/HAp are prepared by the ion-exchange of Ru^{3+} ions with Ca^{2+} ions in the lattice of HAp and then reduced by AB at room temperature. When AB solution is added to the suspension of hydoxyapatite containing ruthenium(III) ions, both reduction of ruthenium(III) to ruthenium(0) and hydrogen release from the hydrolysis of AB occur concomitantly. The progress of ruthenium(0) nanoparticles formation and concomitant hydrolytic dehydrogenation of ammonia borane was followed by monitoring the change in H_2 pressure.

The ruthenium(0) nanoparticles supported on hydroxyapatite (Ru^0/HAp), *in situ* formed during the hydrolysis of AB, could be isolated from the reaction solution as powder by filtration and characterized by ICP-OES, XRD, SEM, EDX, TEM and XPS techniques. Ruthenium content of Ru^0/HAp was determined by ICP-OES.
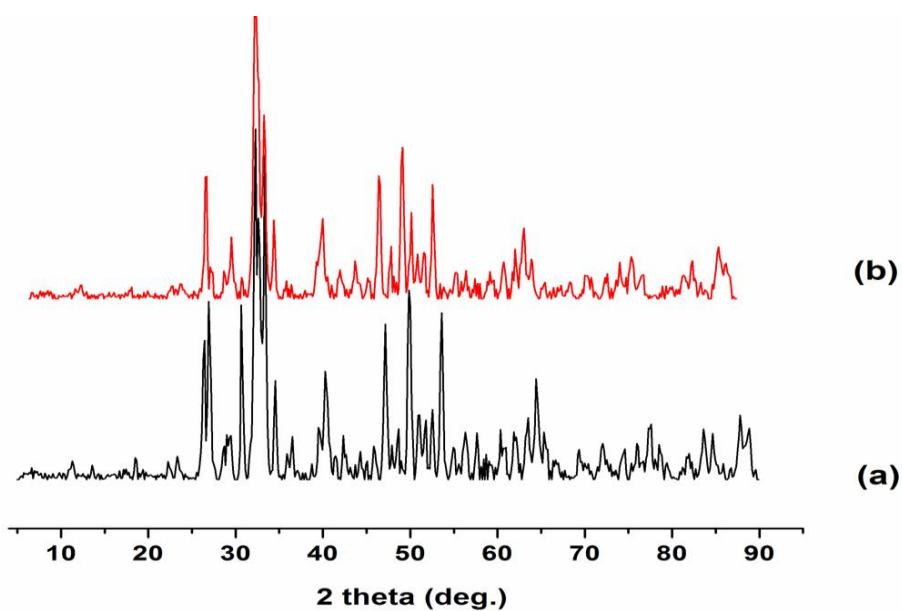
Figure 28. Powder XRD patterns of (a) hydroxapatite, (b) Ru^0/HAp with a 3.96% wt. Ru loading.

The comparison of the XRD patterns of hydroxyapatite and Ru^0/HAp with a ruthenium loading of 3.96% wt. Ru, given in Figure 28a and b, respectively, clearly shows that there is no change in the characteristic diffraction peaks of hydroxyapatite. This observation indicates that the host material remains intact after ion-exchange and reduction of ruthenium(III) ions without noticeable alteration in the framework lattice or loss in the crystallinity. There is no observable peak attributable to ruthenium nanoparticles in Figure 28b, probably as a result of low ruthenium loading of hydroxyapatite.

Figure 29 exhibits the SEM image and SEM-EDX spectrum of Ru^0/HAp with a ruthenium loading of 3.96% wt. indicating that ruthenium is the only element detected in the sample in addition to the framework elements of hydroxyapatite (Ca, P, O).
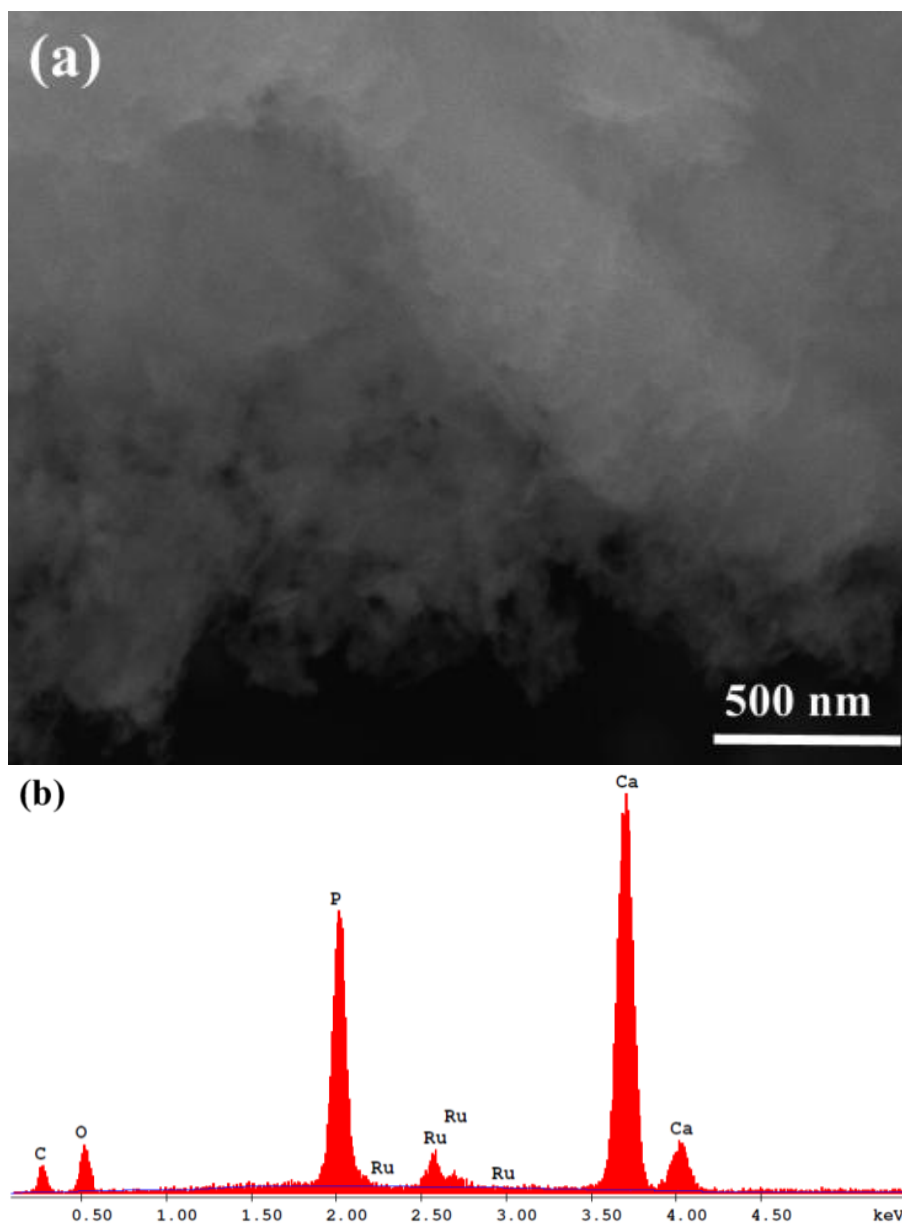
Figure 29. a) SEM image (The scale bar is 500 nm), b) SEM-EDX spectrum of Ru^0/HAp with a 3.96% wt. Ru loading.

Figure 30 shows the TEM images of Ru^0/HAp with a ruthenium loading of 3.96% wt. taken with different magnifications, which indicate that (*i*) highly dispersed ruthenium(0) nanoparticles are formed on the surface of hydroxyapatite with particle size in the range 3.0-5.5 nm (mean diameter: 4.7 ± 0.7 nm, histogram in Fig. 30a inset) and (*ii*) ion-exchange of ruthenium(III) followed by reduction to ruthenium(0) causes no change in the framework lattice of the hydroxyapatite in agreement with the XRD results.
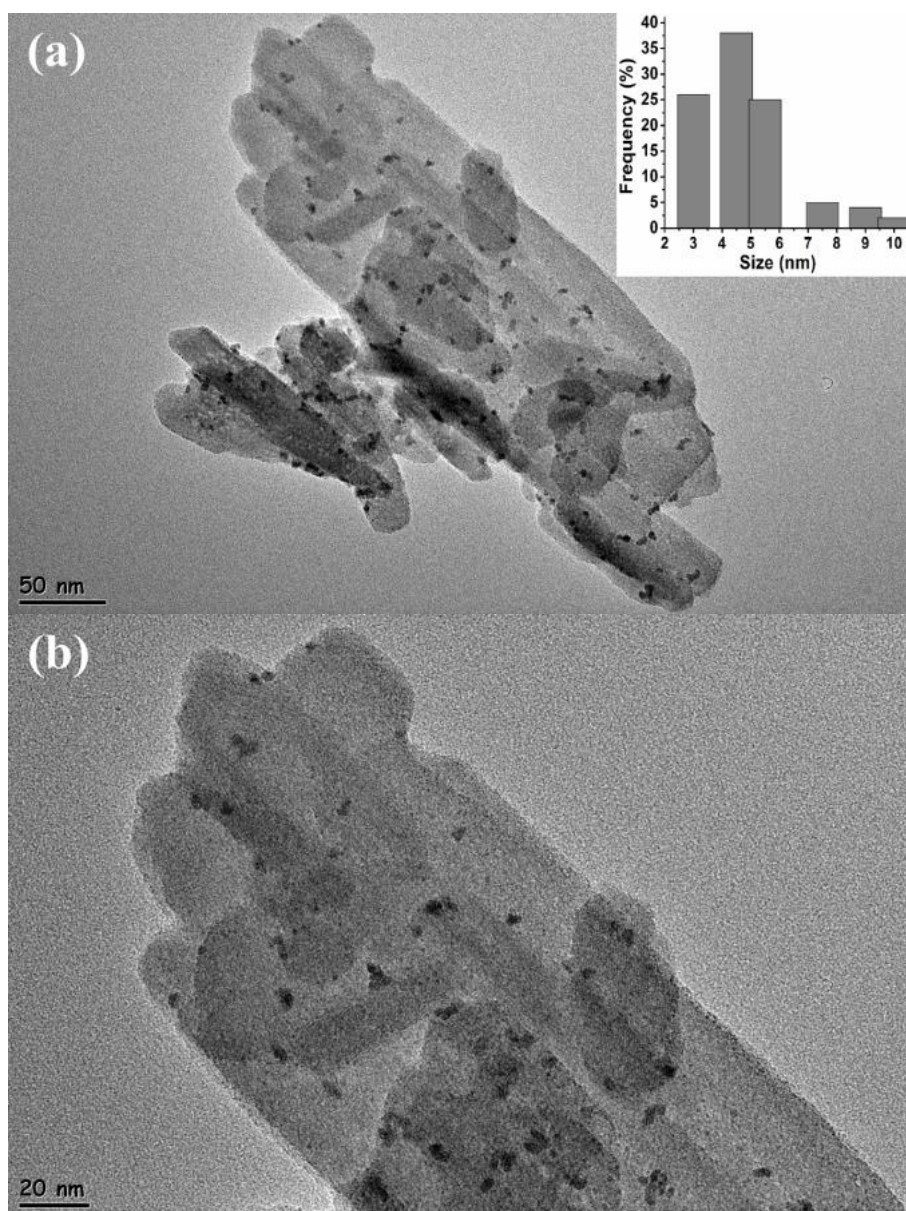
Figure 30. TEM images of Ru⁰/HAp with a 3.96% wt. Ru loading in different magnifications with the scale bar of (a) 50 nm and (b) 20 nm and inset: the corresponding histogram for the particle size distribution.

The composition of Ru^0/HAp formed *in situ* during the hydrolysis of AB and the oxidation state of ruthenium were also studied by XPS technique. The survey-scan XPS spectrum of Ru^0/HAp with a ruthenium loading of 3.96% wt. (Fig. 31) shows the presence of ruthenium in addition to the hydroxyapatite framework elements (Ca, P, O) in agreement with the SEM-EDX result. High resolution X-ray photoelectron spectrum of a Ru^0/HAp sample given in the inset of Figure 31 shows two prominent bands at 284.8 eV and 280.6 eV which can readily be assigned to Ru(0) $3d_{3/2}$ and $3d_{5/2}$, respectively, in the nanoparticles by comparing with the values of ruthenium metal 285 and 280 eV, respectively [47]. It is noteworthy that the Ru(0) $3d_{3/2}$ peak at

284.8 eV overlaps with the C 1s peak at 284.0 eV coming from air with a percent atomic ratio of 9.29 (C 1s /Ru 3d). Because of this overlap, only the peak at 280.6 eV can with certainty be assigned to Ru(0) $3d_{5/2}$.
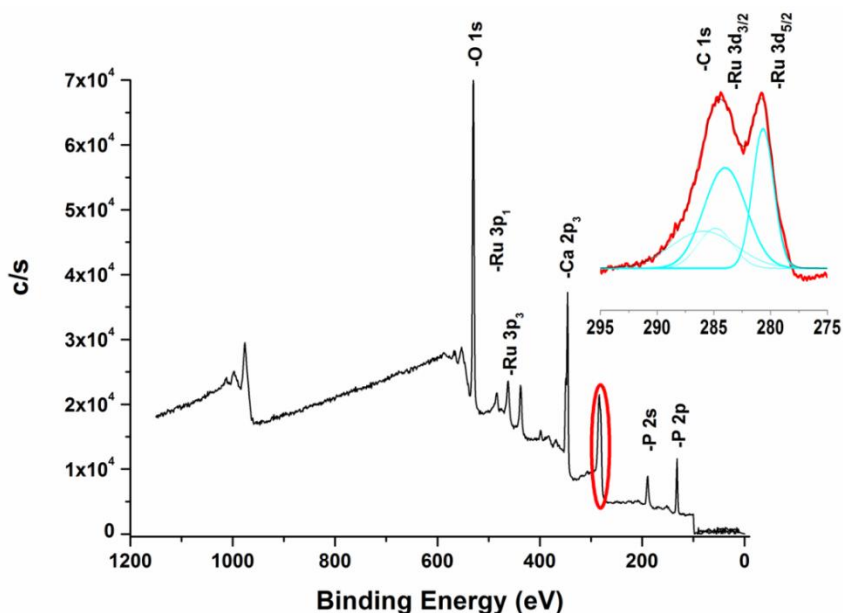
Figure 31. X-ray photoelectron (XPS) spectrum of Ru^0/HAp sample with ruthenium loading of 3.96% wt. Ru. The inset gives the high resolution scan and deconvolution of Ru 3d bands.

5.2. Catalytic activity of Ru^0/HAp in hydrolytic dehydrogenation of ammonia borane

A control experiment was performed to check whether hydroxyapatites show any catalytic activity in the hydrolysis of AB before starting the investigation on the catalytic activity of Ru^0/HAp. In a control experiment starting with 1.0 mmol AB and 10 mg powder of hydroxyapatite (the same amount as the one used in catalytic activity tests) in 10 mL water at 25.0 ± 0.1 ºC or 40.0 ± 0.1 ºC, no hydrogen generation was observed in 1 h at both temperatures. This observation indicates that the hydrolysis of AB does not occur in the presence of hydroxyapatite in the temperature range used in this study.
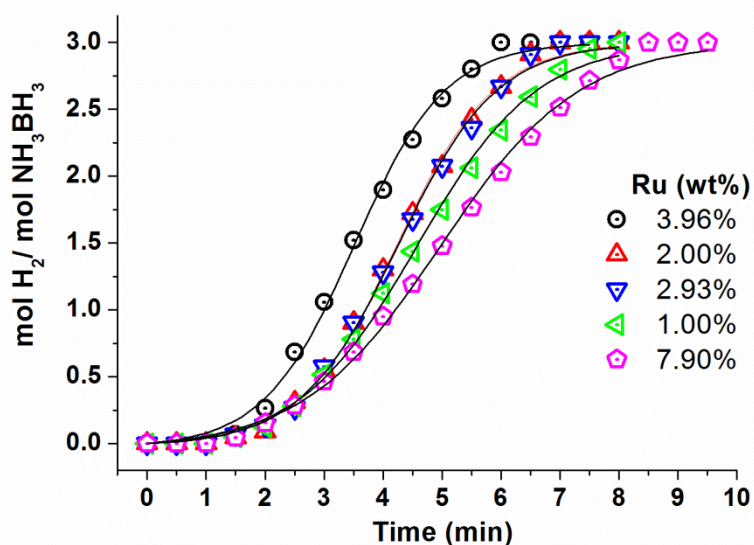
Figure 32. Plot of mol H_2 /mol $H_3N.BH_3$ versus time for the hydrolytic dehydrogenation of AB (100 mM) starting with Ru^{3+}/HAp precatalyst (0.784 mM Ru) with different ruthenium loading at 25.0 ± 0.1 °C.

Ruthenium(0) nanoparticles supported on hydroxyapatite, Ru^0/HAp, are found to be highly active catalyst in the hydrolysis of ammonia borane generating 3.0 equivalent H_2 gas per mol of AB in the same temperature range. Expectedly, the catalytic activity depends on the ruthenium loading of catalyst materials. A series of experiments were performed starting with 10 mL solution of 100 mM AB and 0.784 mM Ru using Ru^{3+}/HAp sample with various ruthenium loading (1.00, 2.00, 2.93, 3.96, 7.90% wt. Ru) in appropriate amount to provide the same ruthenium concentration in all of the experiments. Figure 32 shows the evolution of equivalent hydrogen per mole of AB versus time plot for the hydrolytic dehydrogenation of AB (100 mM) starting with Ru^{3+}/HAp precatalyst (0.784 mM Ru) with different ruthenium loading at 25.0 ± 0.1 °C. All the plots in Figure 32 curve-fit well to the two-step mechanism, giving the rate constants k_1 of the slow, continuous nucleation, P → Q, and k_2 of the autocatalytic surface growth, P + Q → 2Q for the formation of ruthenium(0) nanoparticles catalyst from the ruthenium(III) ions during the hydrolysis of ammonia borane (Table 6) [110].

The catalytic activity of *in situ* generated Ru^0/HAp, measured as turnover frequency (TOF) in the hydrolytic dehydrogenation of AB at 25.0 ± 0.1 °C, shows variation with the ruthenium loading (Table 6). The Ru^0/HAp sample with ruthenium loading of 3.96% wt. Ru provides the highest catalytic activity in hydrogen generation from

the hydrolysis of AB at 25.0 ± 0.1 $^{\circ}$C. Therefore, Ru^0/HAp catalyst with ruthenium loading of 3.96% wt. was used in all of the further experiments performed in this study.

Table 6. The rate constants k_1 of the slow, continuous nucleation, P $\rightarrow$ Q, and k_2 of the autocatalytic surface growth, P + Q $\rightarrow$ 2Q for the formation of ruthenium(0) nanoparticles catalyst from the ruthenium(III) ions during the hydrolysis of AB (100 mM) starting with Ru^0/HAp with different ruthenium loading (0.784 mM Ru) and the turnover frequency (TOF) of hydrogen generation from the catalytic hydrolysis of AB at 25.0 ± 0.1 $^{\circ}$C

Ru loading of HAp (% wt Ru)	k_1 (s^{-1})	k_2 (M^{-1}s^{-1})	TOF (min^{-1})
1.00	$1.72 \times 10^{-4} \pm 2.2 \times 10^{-5}$	$0.698 \pm 2.5 \times 10^{-2}$	83
2.00	$1.13 \times 10^{-4} \pm 1.6 \times 10^{-5}$	$0.863 \pm 2.9 \times 10^{-2}$	118
2.93	$1.19 \times 10^{-4} \pm 1.8 \times 10^{-5}$	$0.847 \pm 3.0 \times 10^{-2}$	112
3.96	$2.20 \times 10^{-4} \pm 3.7 \times 10^{-5}$	$0.915 \pm 4.2 \times 10^{-2}$	123
7.90	$2.01 \times 10^{-4} \pm 2.4 \times 10^{-5}$	$0.596 \pm 2.1 \times 10^{-2}$	84
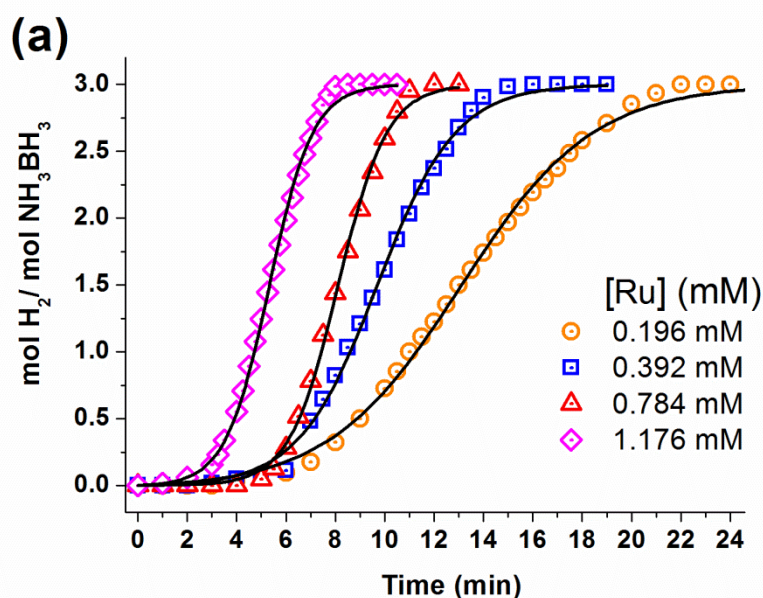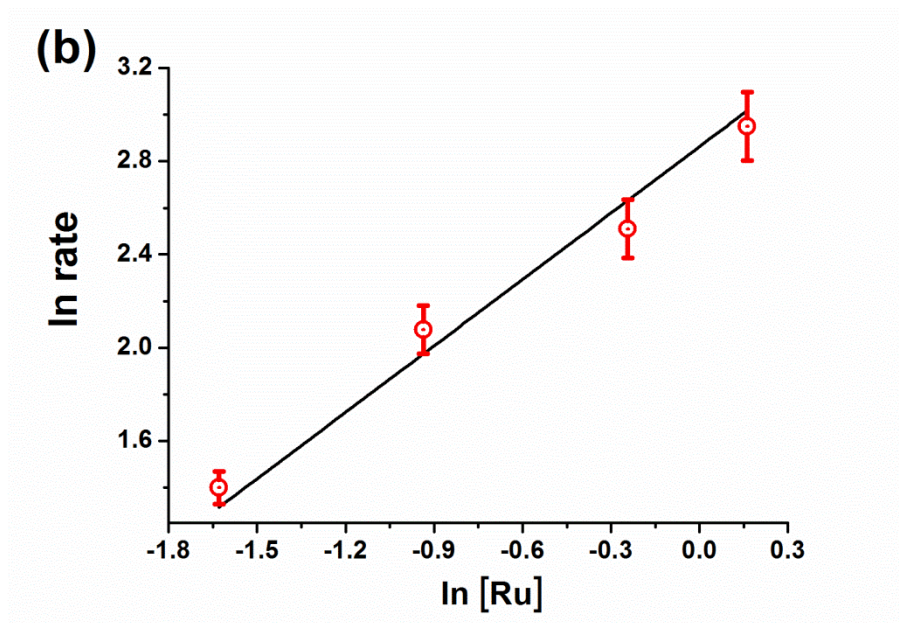
Figure 33. (a) mol H_2 /mol $H_3N.BH_3$ versus time graph depending on the ruthenium concentration in Ru^0/HAp for the hydrolysis of AB (100 mM) at 25.0 ± 0.1 °C. (b) The plot of hydrogen generation rate versus the concentration of Ru, both in logarithmic scale; ln(rate) = 0.95 ln[Ru] + 2.86.

Figure 33a shows the plots of equivalent H_2 gas generated per mole of H_3NBH_3 versus time during the catalytic hydrolysis of 100 mM AB solution using Ru^0/HAp with a loading of 3.96% wt. Ru in different catalyst concentration at 25.0 ± 0.1 °C. In each experiment, hydrogen evolution starts after a short induction period of less than 6 minutes and continues almost linearly until the complete conversion of the substrate giving 3.0 equivalents of H_2 per mole of AB. All the experimental data fit well to sigmoidal curve according to the two-step mechanism, which provides the rate constants k_1 of the slow, continuous nucleation, P $\rightarrow$ Q, and k_2 of the autocatalytic surface growth, P + Q $\rightarrow$ 2Q for the formation of ruthenium(0) nanoparticles catalyst from the ruthenium(III) ions during the hydrolysis of ammonia borane (Table 7) [110]. Although it is not possible to get a direct correlation between the rate constant k_1 for nucleation and the catalyst concentration, the rate constant k_2 for surface growth decreases with the increasing concentration of ruthenium. The hydrogen generation rate was determined from the linear portion of each plot in Figure 33a and plotted versus the initial concentration of ruthenium, both in logarithmic scale, in Figure 33b, which gives straight line with a slope of 0.95 indicating that the catalytic hydrolysis of AB is first order with respect to the ruthenium concentration. The turnover frequency for hydrogen generation from the hydrolysis of AB (100 mM) at 25.0 ± 0.1 °C was determined from the hydrogen

generation rate in the linear portion of plots given in Figure 33 for experiments starting with 100 mM AB plus Ru^0/HAp with a loading of 3.96% wt. Ru. The TOF value of Ru^0/HAp catalyst is as high as 137 min^{-1} (mol H_2/ mol Ru.min) in the hydrolytic dehydrogenation of ammonia borane at 25.0 ± 0.1 °C. TOF values of the reported ruthenium catalysts used in hydrolytic dehydrogenation of ammonia borane are listed in Table 2 (see chapter 3) for comparison.

Table 7. The rate constants k_1 of the slow, continuous nucleation, P → Q, and k_2 of the autocatalytic surface growth, P + Q → 2Q for the formation of ruthenium(0) nanoparticles catalyst from the ruthenium(III) ions during the hydrolysis of AB at various concentration of ruthenium.

[Ru] (mM)	k_1 (s^{-1})	k_2 $(M^{-1}s^{-1})$
0.196	$4.67 \times 10^{-5} \pm 4.0 \times 10^{-6}$	$1.05 \pm 2.2 \times 10^{-2}$
0.392	$2.33 \times 10^{-5} \pm 3.3 \times 10^{-6}$	$0.89 \pm 2.4 \times 10^{-2}$
0.784	$4.62 \times 10^{-6} \pm 9.8 \times 10^{-7}$	$0.72 \pm 2.1 \times 10^{-2}$
1.176	$4.57 \times 10^{-5} \pm 5.3 \times 10^{-6}$	$0.53 \pm 1.2 \times 10^{-2}$

We have carried out the ruthenium nanoparticle formation experiments at various temperature in order to estimate the activation energies for the nucleation and autocatalytic surface growth of ruthenium(0) nanoparticles catalyst. Figure 34a shows the evolution of equivalent hydrogen per mole of AB versus time plot for the hydrolytic dehydrogenation of AB starting with Ru^{3+}/HAp precatalyst (0.392 mM Ru) and 100 mM at five different temperatures. For each temperature, experimental data curve-fit well to the two-step mechanism, giving the rate constants k_1 of the slow, continuous nucleation, P → Q, and k_2 of the autocatalytic surface growth, P + Q → 2Q for the formation of ruthenium(0) nanoparticles catalyst from the ruthenium(III) ions during the hydrolysis of ammonia borane (Table 8) [110]. From the Arrhenius plots constructed by using the values of rate constants k_1 and k_2 at various temperatures in Figure 34b and c, one can obtain the activation energy E_a = 166 ± 7 kJ/mol for the nucleation and $E_a = 59 \pm 2$ kJ/mol for the autocatalytic surface growth of ruthenium(0) nanoparticles, respectively. It is noteworthy that the k_1 values have much higher uncertainty compared to the k_2 values.

Table 8. The rate constants k_1 of the slow, continuous nucleation, P → Q, and k_2 of the autocatalytic surface growth, P + Q → 2Q for the formation of ruthenium(0) nanoparticles catalyst from the reduction of ruthenium(III) ions during the hydrolysis of AB at various temperatures.

Temperature (°C)	k_1 (s^{-1})	k_2 (M^{-1}s^{-1})	k_2 / k_1
20	$5.83 \times 10^{-6} \pm 7.4 \times 10^{-7}$	$0.655 \pm 1.3 \times 10^{-2}$	1.12×10^{3}
25	$2.37 \times 10^{-5} \pm 3.3 \times 10^{-6}$	$0.888 \pm 2.4 \times 10^{-2}$	3.75×10^{3}
30	$1.05 \times 10^{-5} \pm 2.3 \times 10^{-6}$	$1.49 \pm 4.8 \times 10^{-2}$	1.42×10^{3}
35	$7.85 \times 10^{-5} \pm 1.3 \times 10^{-5}$	$2.02 \pm 6.9 \times 10^{-2}$	0.26×10^{3}
40	$5.01 \times 10^{-4} \pm 6.8 \times 10^{-5}$	$2.43 \pm 1.0 \times 10^{-1}$	0.49×10^{3}

Activation energy for the hydrolytic dehydrogenation of ammonia borane catalyzed by Ru^0/HAp could be determined by evaluating the temperature dependent kinetic data presented in Figure 34a. The rate constants for the hydrogen generation at different temperature were calculated from the slope of linear portion of each plot given in Figure 34a and used for the calculation of activation energy ($E_a = 58 \pm 2$ kJ/mol) from the Arrhenius plot in Figure 34d. The activation energy for the hydrolytic dehydrogenation of ammonia borane catalyzed by Ru^0/HAp is comparable to the literature values reported for the other ruthenium catalysts in the same reaction (Table 2, see chapter 3).
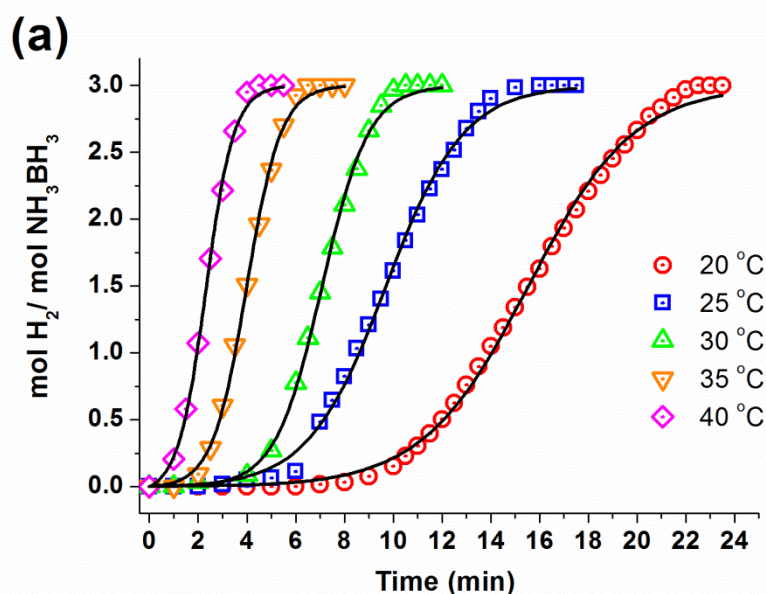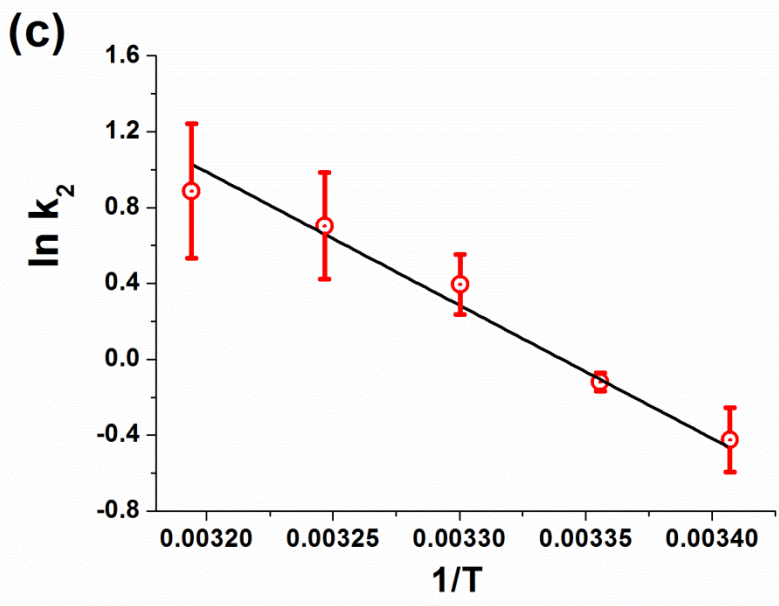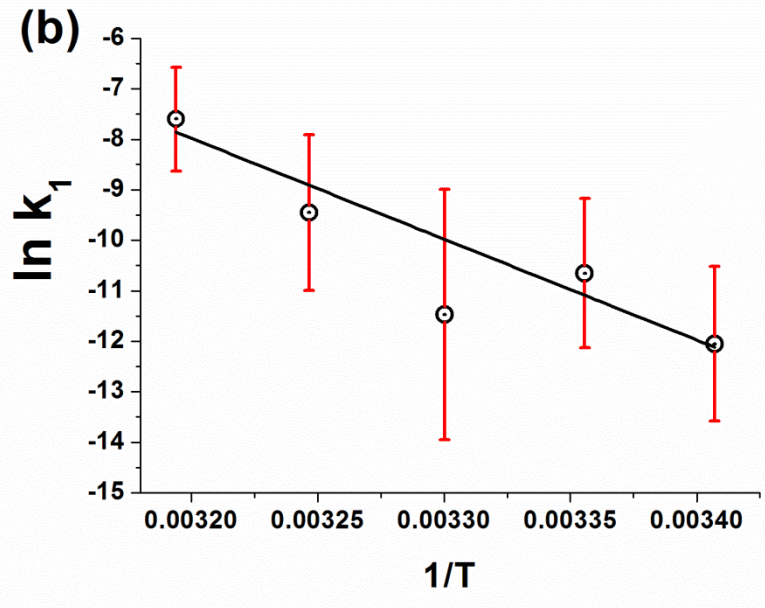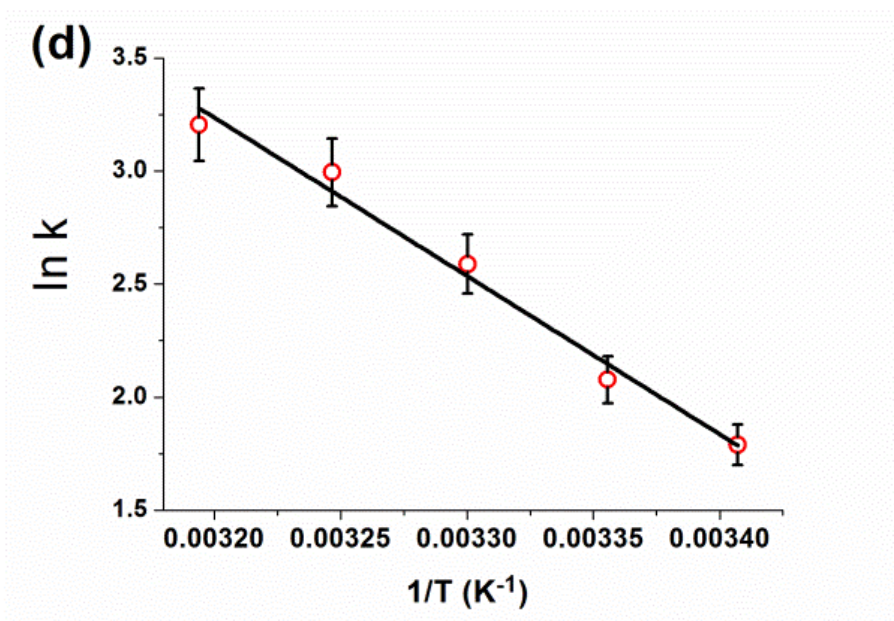
Figure 34. (a) The evolution of equivalent hydrogen per mole of AB versus time plot for the hydrolytic dehydrogenation of AB starting with Ru^{3+}/HAp precatalyst (0.392 mM Ru) and 100 mM AB at various temperatures, (b) The Arrhenius plot for nucleation of ruthenium(0) nanoparticles ($\ln k_1$= -19982.7(1/T) + 55.97), (c) The Arrhenius plot for the autocatalytic surface growth of ruthenium(0) nanoparticles ($\ln k_2$= -7024.02(1/T) + 23.46), (d) The Arrhenius plot for the Ru^0/HAp catalyzed hydrolytic dehydrogenation of AB ($[H_3N.BH_3]$ = 100 mM and [Ru]= 0.392 mM) ($\ln k$ = -7004.83(1/T) +25.65).
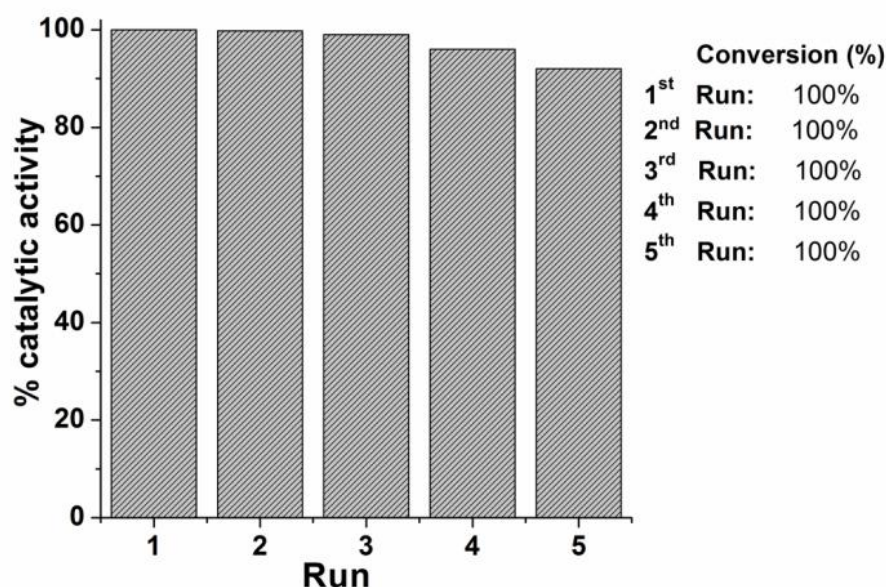
Figure 35. The percentage of initial catalytic activity of Ru^0/HAp ([Ru]=0.567 mM) in successive runs after the reuse for the hydrolytic dehydrogenation of ammonia borane (100 mM).

Reusability of Ru^0/HAp catalyst was tested in successive experiments performed using the catalyst isolated from the reaction solution after a previous run of

hydrolysis of AB. After the completion of hydrogen generation from the hydrolysis of AB starting with 0.567 mM Ru^{3+}/HAp plus 100 mM AB in 10 mL aqueous solution at 25.0 ± 0.1 °C, the catalyst was isolated by centrifugation, washing with water and drying under vacuum (10^{-3} torr) at 80 °C. The whole powder materials were weighed and then redispersed in 10 mL solution containing 100 mM AB and a second run of hydrolysis was started immediately and continued until the completion of hydrogen evolution. This was repeated five times. Fig. 35 shows the percentage of initial catalytic activity of Ru^0/HAp in the subsequent catalytic hydrolysis of 100 mM ammonia borane performed by using the catalyst isolated after the previous run of hydrolysis at 25.0 ± 0.1 °C. The material loss has already been taken into account in calculating the activity in each run during the isolation and redispersion processes. The reusability tests reveal that Ru^0/HAp are still active in the subsequent runs of hydrolytic dehydrogenation of AB providing 100% conversion, *i.e.* a release of 3.0 equivalent H$_2$ per mole of NH$_3$BH$_3$. After the fifth run hydrolytic dehydrogenation of AB, Ru^0/HAp preserve 92% of their initial catalytic activity.
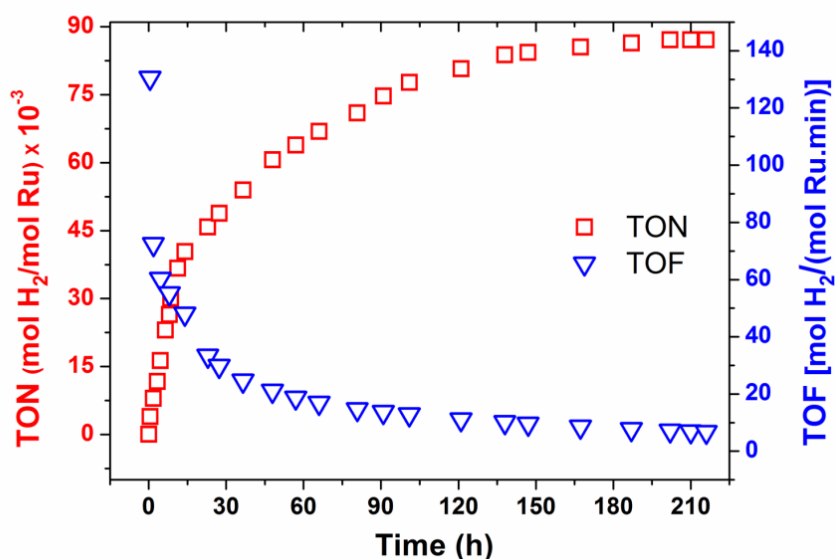
Figure 36. The variation in turnover number (TON) and turnover frequency (TOF) during the catalytic lifetime experiment performed starting with 20 mg Ru^0/HAp (ruthenium loading = 3.96% wt. Ru, and [Ru] = 0.784 mM) in 100 mL solution of AB at 25.0 ± 0.1 °C.

Catalytic lifetime of Ru^0/HAp was determined by measuring the total turnover number (TTO) in the hydrolysis of ammonia borane. A catalyst lifetime experiment was performed starting with 20 mg Ru^0/HAp (ruthenium loading = 3.96% wt. Ru, and [Ru] = 0.784 mM) in 100 mL solution of AB at 25.0 ± 0.1 °C. Figure 36 shows

the variation in turnover number (TON) and turnover frequency (TOF) in the course of reaction. The TOF value decreases expectedly as the ruthenium(0) nanoparticles catalysts are deactivated during the lifetime experiment. Ruthenium(0) nanoparticles supported on hydroxyapatite provide minimum 87000 turnovers over 202 h in the hydrolysis of AB at 25.0 ± 0.1 °C before deactivation of the catalyst (see Table 2 in chapter 3 for the comparison of the TTO values of the reported ruthenium catalysts).

CHAPTER 6

Ruthenium(0) Nanoparticles Supported on Magnetic Silica Coated Cobalt-Ferrite

Recently, much attention has been paid to the magnetically recoverable catalysts in liquid phase reactions due to their easy magnetic separation making the recovery of catalysts much easier than by filtration and centrifugation. In this study, we developed magnetically separable and highly reusable Ru(0) NPs supported on silica coated cobalt ferrite ($Ru^0/SiO_2\text{-}CoFe_2O_4$) as catalyst in hydrogen generation from hydrolysis of ammonia borane. Silica was used to protect the magnetic core material against the chemical attack by reaction solution leaching and agglomeration and to provide high surface area for stabilization of the ruthenium nanoparticles.

6.1. Hydrolytic dehydrogenation of ammonia borane catalyzed by $Ru^0/SiO_2\text{-}CoFe_2O_4$

Ruthenium(0) nanoparticles supported on magnetic silica-coated cobalt ferrite were *in situ* generated from the reduction of $Ru^{3+}/SiO_2\text{-}CoFe_2O_4$ during the catalytic hydrolysis of AB. Ruthenium(III) ions were first impregnated on $SiO_2\text{-}CoFe_2O_4$ from the aqueous solution of ruthenium(III) chloride yielding $Ru^{3+}/SiO_2\text{-}CoFe_2O_4$ and then reduced by AB at room temperature. When AB solution is added to the suspension of $Ru^{3+}/SiO_2\text{-}CoFe_2O_4$, both reduction of ruthenium(III) to ruthenium(0) and hydrogen release from the hydrolysis of AB occur concomitantly.

Ruthenium(0) nanoparticles supported on magnetic silica-coated cobalt ferrite, $Ru^0/SiO_2\text{-}CoFe_2O_4$, *in situ* generated during the hydrolysis of AB, could be isolated from the reaction solution as powder by using a permanent magnet and characterized

by ICP-OES, XRD, TEM, TEM-EDX, and XPS techniques. Ruthenium content of Ru^0/SiO_2-$CoFe_2O_4$ was determined by ICP-OES.

XRD pattern of Ru^{3+}/SiO_2-$CoFe_2O_4$ and Ru^0/SiO_2-$CoFe_2O_4$ in Fig. 37b and c give peaks at $30.3°$, $35.8°$, $43.3°$, $57.4°$ and $62.5°$ assigned to the (220), (311), (400), (511) and (440) diffractions of SiO_2-$CoFe_2O_4$, respectively (PDF Card #22-1086). The comparison of the XRD patterns of SiO_2-$CoFe_2O_4$, Ru^{3+}/SiO_2-$CoFe_2O_4$ and Ru^0/SiO_2-$CoFe_2O_4$ with a ruthenium loading of 1.96% wt. Ru, given in Fig. 37a–c, respectively, clearly shows that there is no change in the characteristic diffraction peaks of silica-coated cobalt ferrite, (SiO_2-$CoFe_2O_4$). This observation indicates that the host material remains intact after impregnation and reduction of Ru^{3+} ions without noticeable alteration in the framework lattice or loss in the crystallinity. There is no observable peak attributable to ruthenium nanoparticles in Fig. 37b and c, probably as a result of low ruthenium loading of silica-coated cobalt ferrite nanoparticles.
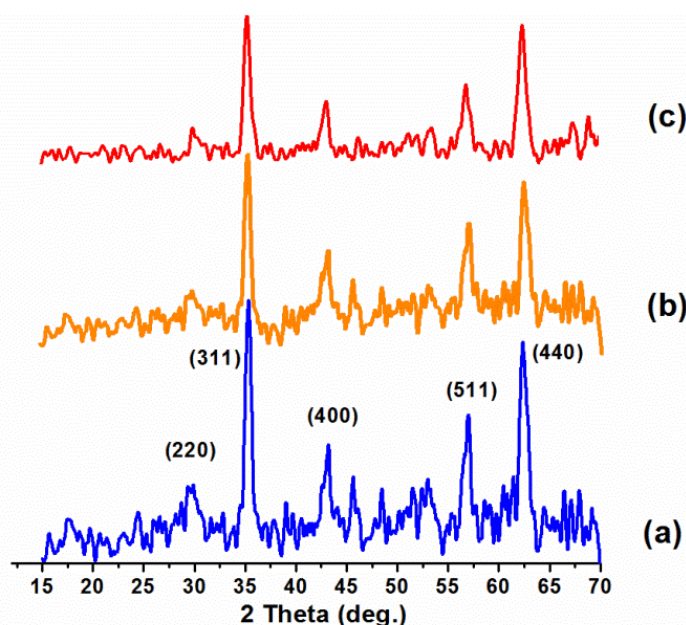
Figure 37. Powder XRD patterns of (a) silica-coated cobalt ferrite, (b) Ru^{3+}/SiO_2-$CoFe_2O_4$ and (c) Ru^0/SiO_2-$CoFe_2O_4$, *in situ* generated during the hydrolysis of AB, with 1.96% wt. Ru loading.

Fig. 38 shows the TEM images of silica-coated cobalt ferrite and Ru^0/SiO_2-$CoFe_2O_4$ with a 1.96% wt. Ru loading taken with different magnifications. The size of SiO_2-$CoFe_2O_4$ nanoparticles used as support is around 15 nm (Fig. 38a and b) and highly dispersed ruthenium nanoparticles are formed on the silica-coated cobalt ferrite (Fig. 38d) as seen from the comparison of the images in Fig. 38b and d taken from the

area indicated with an arrow in Fig. 38a and c, respectively. TEM-EDX spectrum (Fig. 38e) taken from the Ru^0/SiO_2-$CoFe_2O_4$ shown in Fig. 38c and d indicates that ruthenium is the only element detected in the sample in addition to the framework elements of silica-coated cobalt ferrite (Si, O, Co, Fe).

The composition of Ru^0/SiO_2-$CoFe_2O_4$ formed *in situ* during the hydrolysis of AB and the oxidation state of ruthenium also studied by XPS technique. The survey-scan XPS spectrum of Ru^0/SiO_2-$CoFe_2O_4$ with 1.96% wt. Ru loading (Fig. 39a) shows all the framework elements of ruthenium(0) nanoparticles supported on magnetic silica-coated cobalt ferrite in agreement with the TEM-EDX result. High resolution X-ray photoelectron spectrum of a Ru^0/SiO_2-$CoFe_2O_4$ sample given in Fig. 39b shows two prominent bands at 484.9 eV and 462.5 eV which can readily be assigned to Ru(0) $3p_{1/2}$ and $3p_{3/2}$, respectively [111].
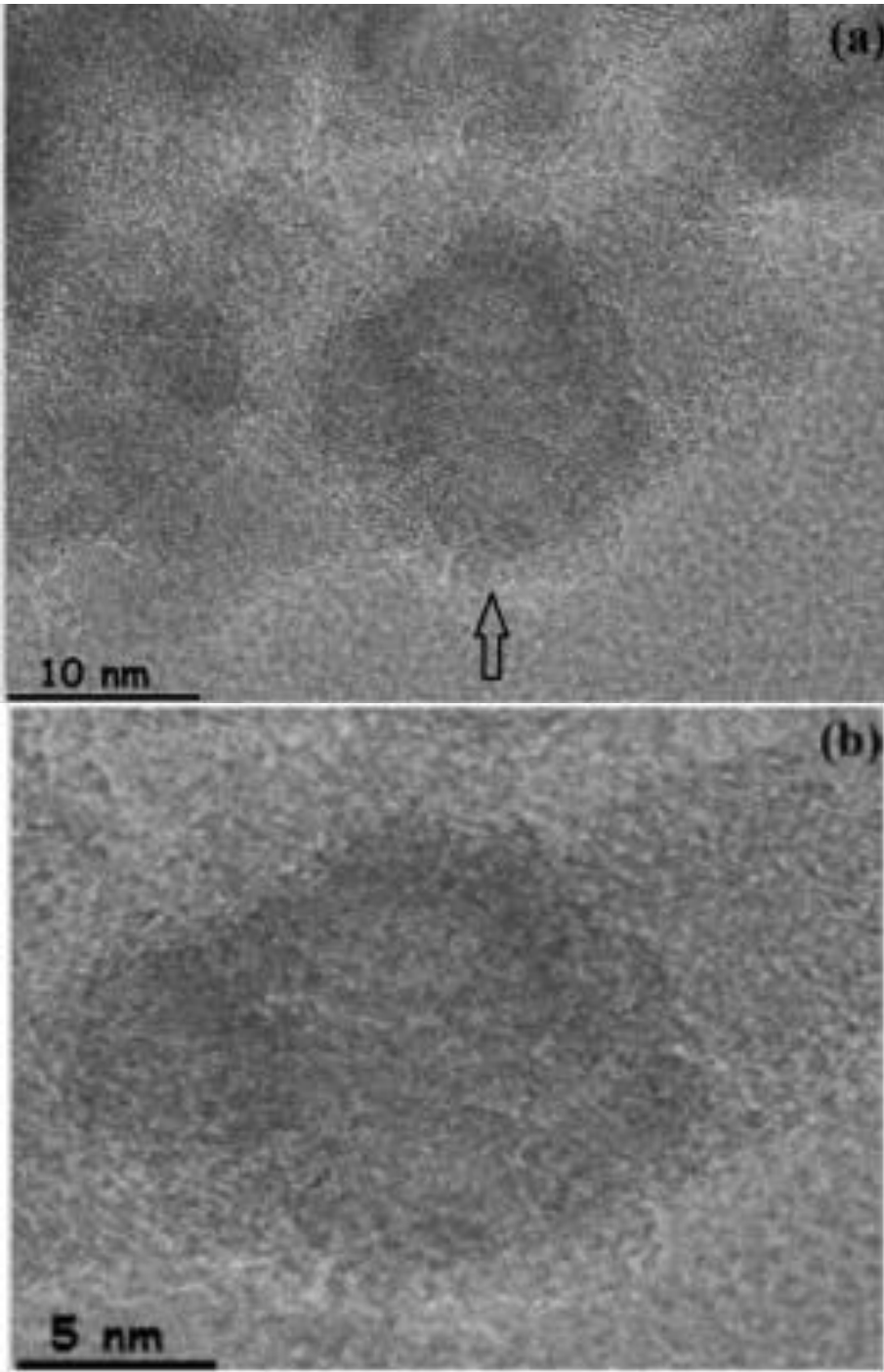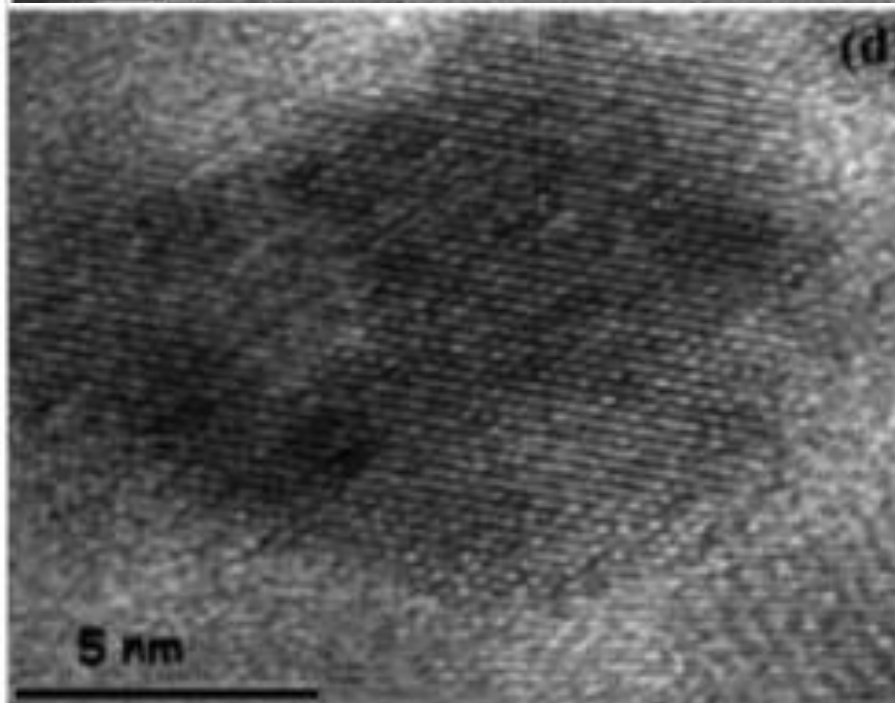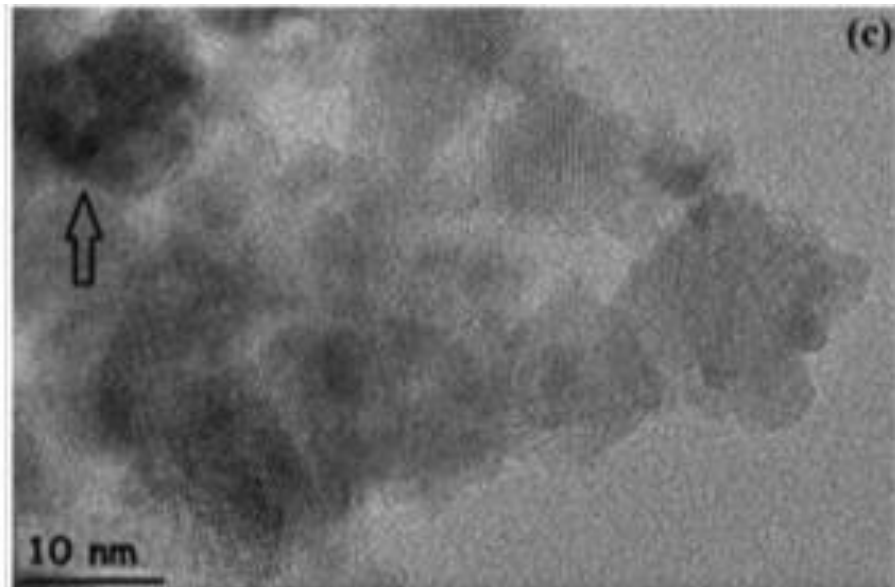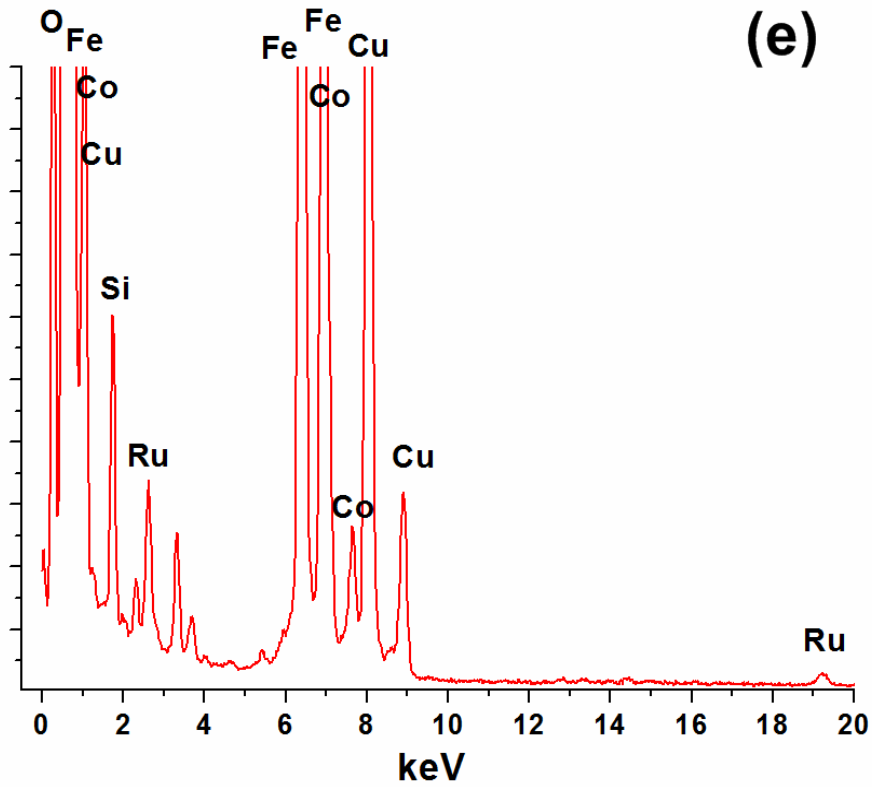
Figure 38. TEM images of silica-coated cobalt ferrite with the scale bar of (a) 10 nm, (b) 5 nm and TEM images of Ru^0/SiO_2-$CoFe_2O_4$ with 1.96% wt. Ru loading with the scale bar of (c) 10 nm, (d) 5 nm and (e) TEM-EDX spectrum of Ru^0/SiO_2-$CoFe_2O_4$.

(b)
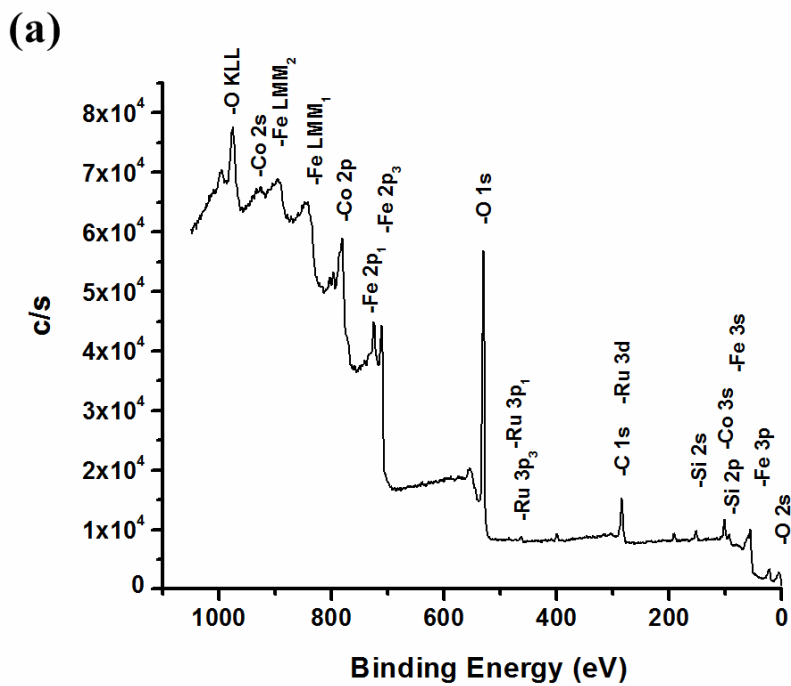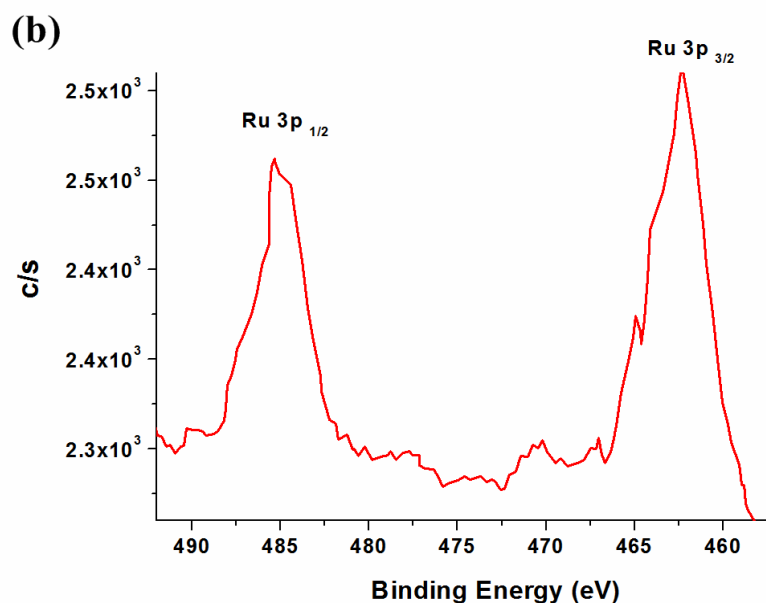
Figure 39. (a) X-ray photoelectron (XPS) spectrum of Ru^0/SiO_2-$CoFe_2O_4$ sample with 1.96% wt. Ru loading, (b) The high resolution scan Ru 3p bands.

6.2. Catalytic activity of Ru^0/SiO_2-$CoFe_2O_4$ in hydrolytic dehydrogenation of ammonia borane

Before starting with the investigation on the catalytic activity of Ru^0/SiO_2-$CoFe_2O_4$ in the hydrolysis of AB, a control experiment was performed to check whether SiO_2-$CoFe_2O_4$ shows any catalytic activity in the hydrolysis of AB at temperatures in the range 25–40 °C. In a control experiment starting with 1.0 mmol of AB and 10 mg of powder of SiO_2-$CoFe_2O_4$ (the same amount as the one used in catalytic activity tests) in 10 mL of water, no hydrogen generation was observed in 1 h. This observation indicates that the hydrolysis of AB does not occur in the presence of SiO_2-$CoFe_2O_4$ in the temperature range used in this study. On the other hand, ruthenium(0) nanoparticles supported on magnetic silica-coated cobalt ferrite are highly active catalyst in the hydrolysis of ammonia-borane generating 3.0 equivalent H_2 gas per mol of AB.

Fig. 40a shows the plots of equivalent H_2 gas generated per mole of H_3NBH_3 versus time during the catalytic hydrolysis of 100 mM AB solution starting with Ru^0/SiO_2-$CoFe_2O_4$ with 1.96% wt. Ru loading in different catalyst concentration at 25.0 ± 0.1 °C. In each experiment, hydrogen evolution starts after a short induction period of

less than 12 min and continues almost linearly until the complete conversion of the substrate giving 3.0 equivalents of H_2 per mole of AB. All the experimental data fit well to sigmoidal curve according to the two-step mechanism, which provides the rate constants k_1 of the slow, continuous nucleation, P → Q, and k_2 of the autocatalytic surface growth, P + Q → 2Q for the formation of ruthenium(0) nanoparticles catalyst from the ruthenium(III) ions during the hydrolysis of ammonia borane (Table 9) [112]. The rate constant k_1 for nucleation increases while the rate constant k_2 for surface growth decreases with the increasing concentration of ruthenium as seen in Table 9.
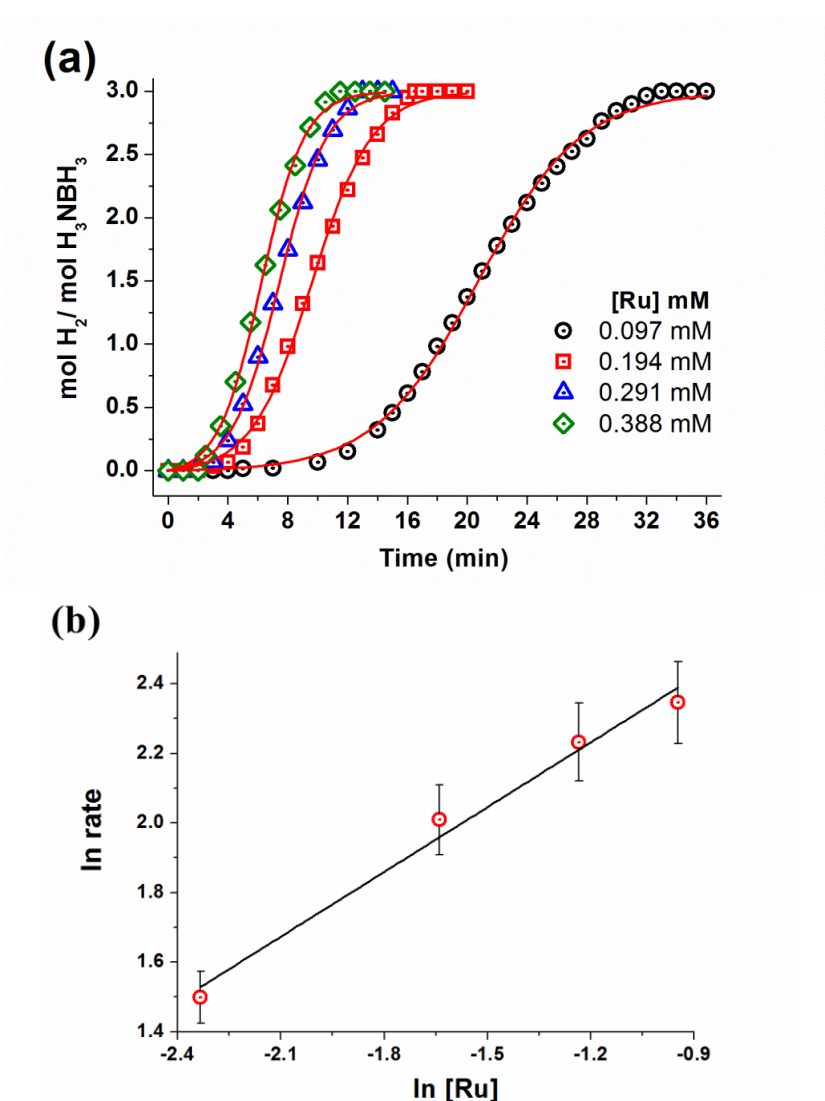
Figure 40. (a) mol H_2/mol H_3NBH_3 versus time graph depending on the ruthenium concentration in Ru^0/SiO_2-$CoFe_2O_4$ for the hydrolysis of AB (100 mM) at 25.0 ± 0.1°C, (b) The plot of hydrogen generation rate versus the concentration of Ru, both in logarithmic scale; ln(*rate*) = 0.62 ln[Ru] + 2.98.

Table 9. The rate constants k_1 of the slow, continuous nucleation, P → Q, and k_2 of the autocatalytic surface growth, P + Q → 2Q for the formation of ruthenium(0) nanoparticles catalyst from the ruthenium(III) ions during the hydrolysis of AB at various concentration of ruthenium.

[Ru] mM	k_1 (s^{-1})	k_2 $(M^{-1}s^{-1})$	Induction time (s)	TOF (min^{-1})
0.097	$1.20 \times 10^{-5} \pm 1.15 \times 10^{-6}$	$1.65 \pm 3.11 \times 10^{-2}$	720	172.5
0.194	$6.95 \times 10^{-5} \pm 8.73 \times 10^{-7}$	$1.41 \pm 4.59 \times 10^{-2}$	240	143.54
0.291	$9.70 \times 10^{-5} \pm 1.14 \times 10^{-5}$	$1.19 \pm 3.73 \times 10^{-2}$	120	119.62
0.388	$1.52 \times 10^{-4} \pm 2.02 \times 10^{-4}$	$0.98 \pm 3.84 \times 10^{-2}$	60	100.48

The hydrogen generation rate was determined from the linear portion of each plot in Fig. 40a and plotted versus the initial concentration of ruthenium, both in logarithmic scale, in Fig. 40b, which gives a straight line with a slope of 0.62 indicating that the catalytic hydrolysis of AB is 0.6 order with respect to the ruthenium concentration. The turnover frequency values, shown in Table 9, for hydrogen generation from the hydrolysis of AB (100 mM) at 25.0 ± 0.1°C were determined from the hydrogen generation rate in the linear portion of plots given in Fig. 40a for experiments starting with 100 mM AB plus Ru^0/SiO_2-$CoFe_2O_4$ with 1.96% wt. Ru loading in various Ru concentration at 25.0 ± 0.1°C. It is noteworthy that the rate constant k_1 correlates well with the induction period while the rate constant k_2 correlates with the rate of hydrogen generation from the hydrolysis of ammonia borane [42]. The rate constant k_1 for the slow, continuous nucleation is inversely proportional to the induction period as seen from Table 9. The rate constant k_2 for the surface growth of ruthenium(0) nanoparticles increases as the TOF value. The TOF value is as high as 172 min^{-1} (mol H_2/mol Ru min). TOF values of the ruthenium catalysts used in hydrolysis of ammonia-borane in the literature are listed in Table 2 (see chapter 3) for comparison.

Table 10. The rate constants k_1 of the slow, continuous nucleation, P → Q, and k_2 of the autocatalytic surface growth, P + Q → 2Q for the formation of ruthenium(0) nanoparticles catalyst from the reduction of ruthenium(III) ions during the hydrolysis of AB at various temperatures.

Temperature (°C)	k_1 (s^{-1})	k_2 (M^{-1}s^{-1})	k_2 / k_1
25	$6.95 \times 10^{-5} \pm 8.73 \times 10^{-6}$	$1.41 \pm 4.59 \times 10^{-2}$	2.03×10^4
30	$9.33 \times 10^{-5} \pm 1.02 \times 10^{-5}$	$2.32 \pm 6.26 \times 10^{-1}$	2.48×10^4
35	$2.25 \times 10^{-4} \pm 3.12 \times 10^{-5}$	$3.01 \pm 1.21 \times 10^{-1}$	1.34×10^4
40	$6.39 \times 10^{-4} \pm 7.87 \times 10^{-5}$	$3.88 \pm 1.78 \times 10^{-1}$	6.06×10^4

Fig. 41a shows the evolution of equivalent hydrogen per mole of AB versus time plot for the hydrolysis starting with Ru^{3+}/SiO_2-$CoFe_2O_4$ precatalyst (0.194 mM Ru) and 100 mM AB at four different temperatures. For each temperature, experimental data curve-fit well to the 2-step mechanism, giving the rate constants k_1 of the slow, continuous nucleation, P → Q, and k_2 of the autocatalytic surface growth, P + Q → 2Q for the formation of ruthenium(0) nanoparticles catalyst from the ruthenium(III) ions during the hydrolysis of ammonia-borane (Table 10). The large value of k_2/k_1 ratio (Table 10) is indicative of the high level kinetic control in the formation of ruthenium(0) nanoparticles from the reduction of the precursor ruthenium(III) ions on the surface of silica-coated cobalt ferrite [110]. From the Arrhenius plots constructed by using the values of rate constants k_1 and k_2 at various temperatures in Fig. 41b and c, respectively, one can obtain the activation energy E_a= 116 ±7 kJ/mol for the nucleation and E_a= 51±2 kJ/mol for the autocatalytic surface growth of ruthenium(0) nanoparticles, which were comparable with the values listed in Table 11.

Activation energy for the hydrolysis of ammonia borane catalyzed by Ru^0/SiO_2-$CoFe_2O_4$ could be determined by evaluating the temperature dependent kinetic data presented in Fig. 41a. The rate constants for the hydrogen generation at different temperature were calculated from the slope of linear portion of each plot given in Fig. 41a and used for the calculation of activation energy (E_a= 45±2 kJ/mol) from the Arrhenius plot in Fig. 41d. The activation energy for the hydrolysis of ammonia-borane catalyzed by Ru^0/SiO_2-$CoFe_2O_4$ is comparable to the literature values reported for the other ruthenium catalysts in the same reaction (Table 2 in chapter 3).
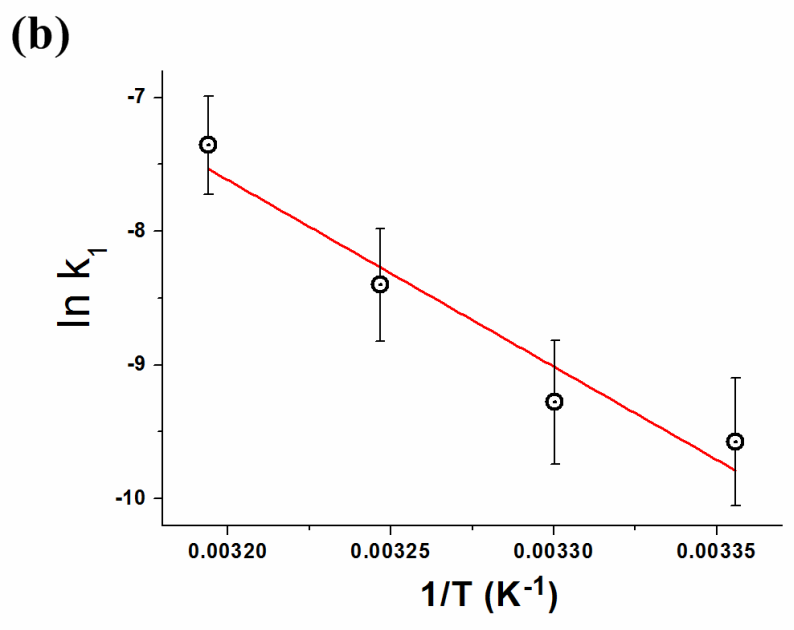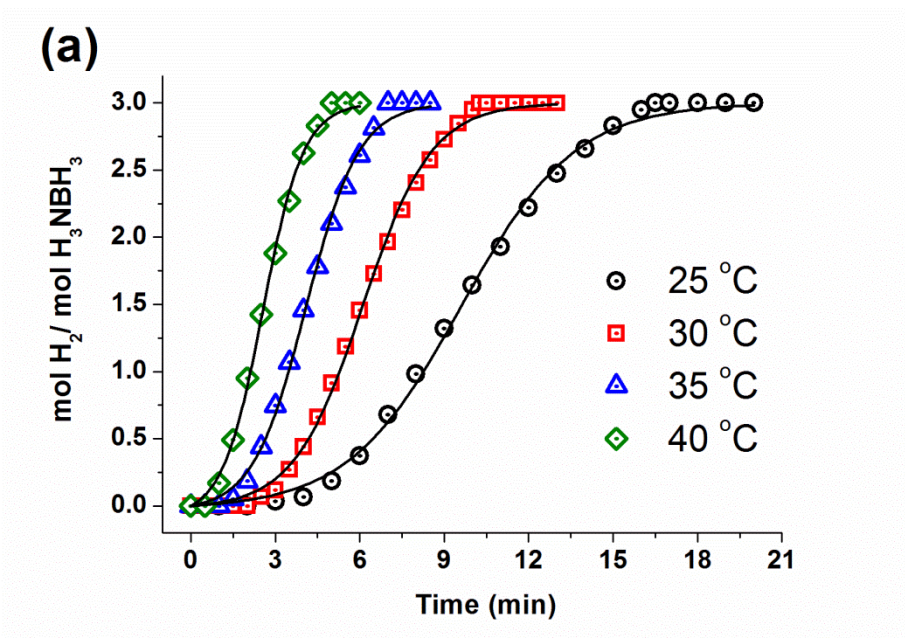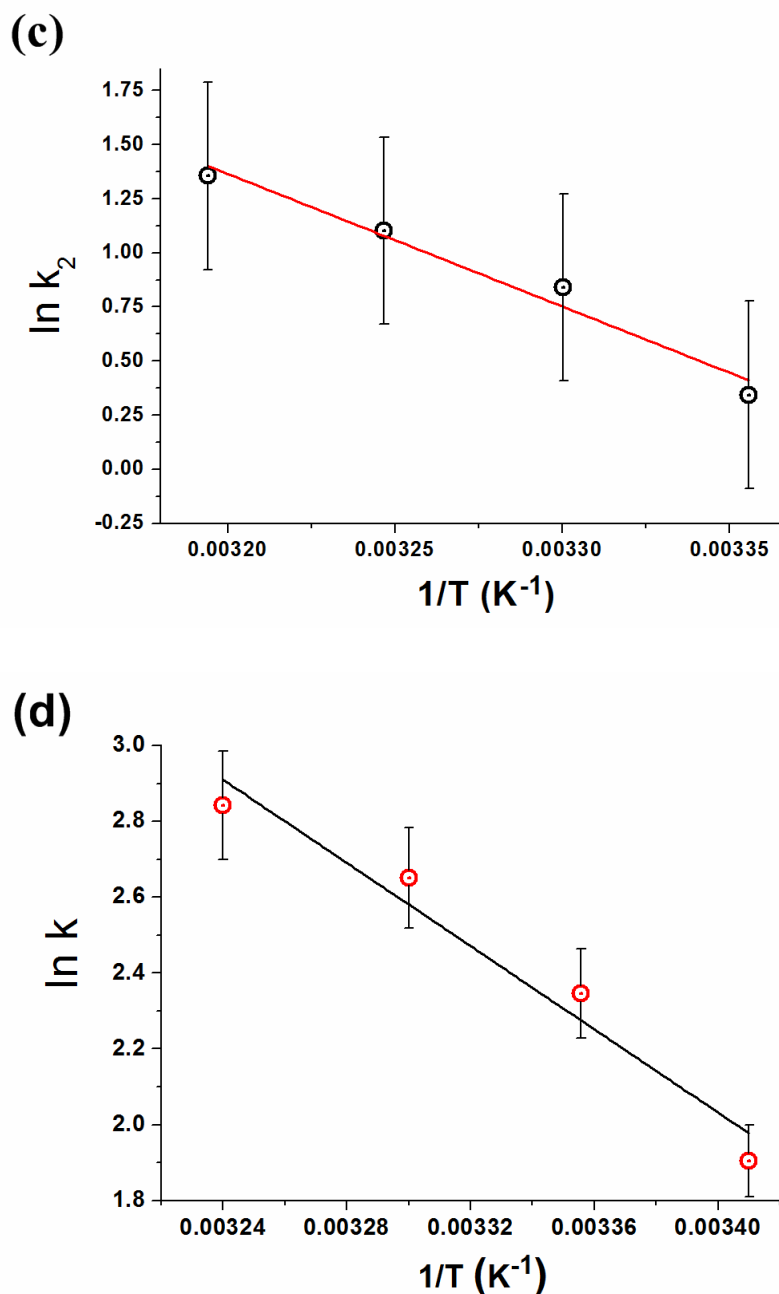
Figure 41. (a) The evolution of equivalent hydrogen per mole of AB versus time plot for the hydrolysis of AB starting with $Ru^{3+}/SiO_2\text{-}CoFe_2O_4$ precatalyst (0.194 mM Ru) and 100 mM AB at various temperatures, (b) The Arrhenius plot for nucleation of ruthenium(0) nanoparticles (In k_1= −13947.9(1/T) + 37.02), (c) The Arrhenius plot for the autocatalytic surface growth of ruthenium(0) nanoparticles (In k_2= −6129.25(1/T) + 20.98), (d) The Arrhenius plot for the $Ru^0/SiO_2\text{-}CoFe_2O_4$ catalyzed hydrolysis of AB ([H_3NBH_3] = 100 mM and [Ru] = 0.194 mM) (ln k = −5490.61 (1/T) + 20.70).

Reusability of $Ru^0/SiO_2\text{-}CoFe_2O_4$ catalyst was tested in successive experiments performed using the catalyst isolated from the reaction solution after a previous run of hydrolysis of AB. After the completion of hydrogen generation from the hydrolysis of AB starting with 0.744 mM $Ru^{3+}/SiO_2\text{-}CoFe_2O_4$ plus 100 mM AB in 10 mL aqueous solution at 25.0 ± 0.1°C, the catalyst was isolated using a permanent

82

magnet (Fig. 42a and b) and washed with 10 mL of water. After washing, the isolated sample of Ru^0/SiO_2-$CoFe_2O_4$ was redispersed in 10 mL solution containing 100 mM AB and a second run of hydrolysis was started immediately and continued until the completion of hydrogen evolution. This was repeated 10 times. After each run, the catalyst was isolated using a permanent magnet and the upper solution was separated. The resulting solutions after each subsequent runs were analyzed by ICP-OES and no leaching of ruthenium into the solution was detected. Therefore, the slight decrease in the catalytic activity of Ru^0/SiO_2-$CoFe_2O_4$ after tenth run in hydrolytic dehydrogenation of AB can be attributed to partial aggregation of nanoparticles on the surface of silica-coated cobalt ferrite. The reusability tests reveal that Ru^0/SiO_2-$CoFe_2O_4$ are still active in the subsequent runs of hydrolysis of AB providing 100% conversion and Ru^0/SiO_2-$CoFe_2O_4$ preserve 94% of their initial catalytic activity even after tenth run (Fig. 43).
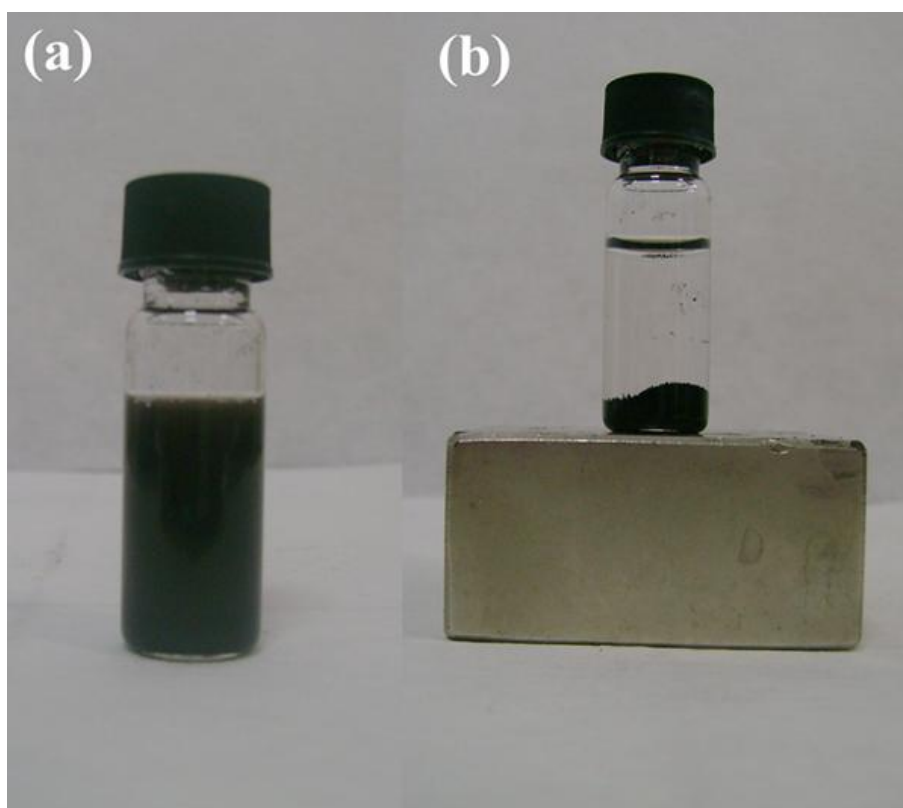
Figure 42. The pictures of (a) dispersed catalyst in water (b) isolated catalyst using a permanent magnet.
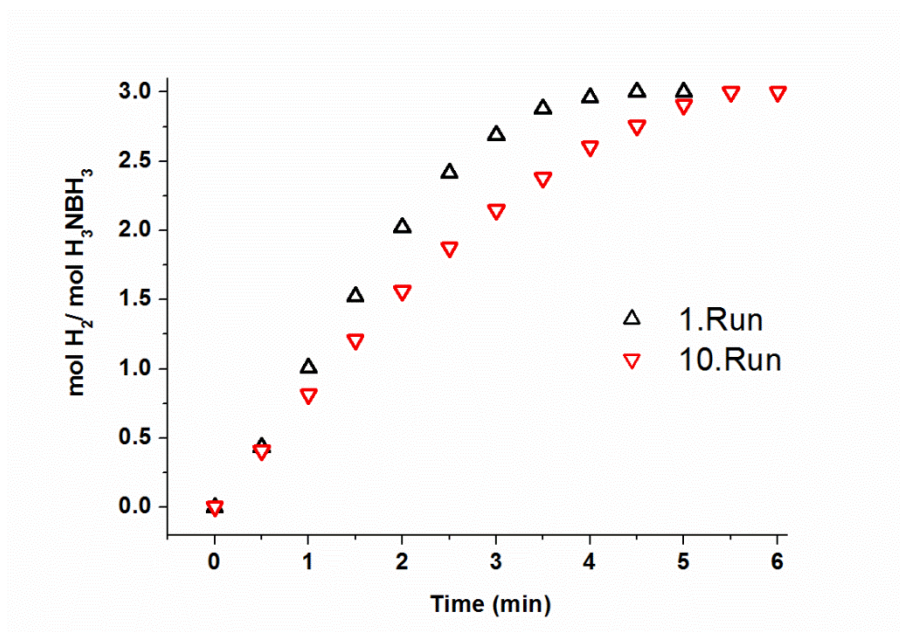
Figure 43. mol H_2/mol H_3NBH_3 versus time graph for the first and tenth use of Ru^0/SiO_2-$CoFe_2O_4$ in hydrolysis of AB.

CHAPTER 7

DISCUSSION

The literature results reveal that carbon based catalysts such as Rh/CNTs [84], Pt/CNTs [85], Ru/CNTs [61], Ru/graphene [59], Ru/Carbon black [34] show very high catalytic activity in hydrolysis of ammonia borane at room temperature. In a recent study [113], Platinum NPs were supported on pristine CNTs (Pt/CNT-P), oxygen-group-rich CNTs (Pt/CNT-O), and defect-rich CNTs (Pt/CNT-D). It is found that the catalytic activity of the catalysts in hydrolysis of AB is in the order of Pt/CNT-D>Pt/CNT-P>Pt/CNT-O. In fact, this study shows that the catalytic activity of a catalyst also depends on the electronic environment or functional groups on the supporting material.

The effect of particle size of nanoparticles on catalytic activity of catalyst has been widely studied. Chen et al [114] reported the relation between platinum particle size and TOF values of the catalysts (Pt/CNTs-OHT, Pt/CNTs, Pt/CNTs-O, Pt/Activated carbon) used in hydrolysis of ammonia borane. The study shows that particle size has a volcano shape in terms of TOF value, which shows also variation according to the catalyst support. Therefore, it is clear that optimum particle size should be determined to achieve the highest catalytic activity.

The effect of particle shape of the Pt nanoparticles on the TOF value was also reported by Chen et al [115]. According to the reported results, fraction of the specific active sites (e.g., corner, edge, (111), or (100) site) on Pt/CNTs have a reasonable effect on TOF value. This study concludes that Pt(111) on the truncated cuboctahedron shape is a dominating catalytically active surface for the hydrolysis of AB.

In this dissertation, we preferred to test first multi-walled carbon nanotube as supporting material for the ruthenium(0) nanoparticles catalysts in hydrogen generation from the hydrolysis of ammonia borane. Indeed, Ru^0/MWCNTs provide remarkable catalytic activity with a TOF value of 329 min^{-1} in hydrogen generation from the hydrolysis of ammonia borane at 25.0 ± 0.1 °C. The comparison of the turnover frequency (TOF) values of the reported catalysts listed in Table 2 (see chapter 3) shows that there is no clear insight explaining the high activity of the catalysts according to the type of supporting material, surface area of the catalyst and the size of metal NPs. The choice of the suitable supporting material seems to be critical as well as the surface area of the catalyst.
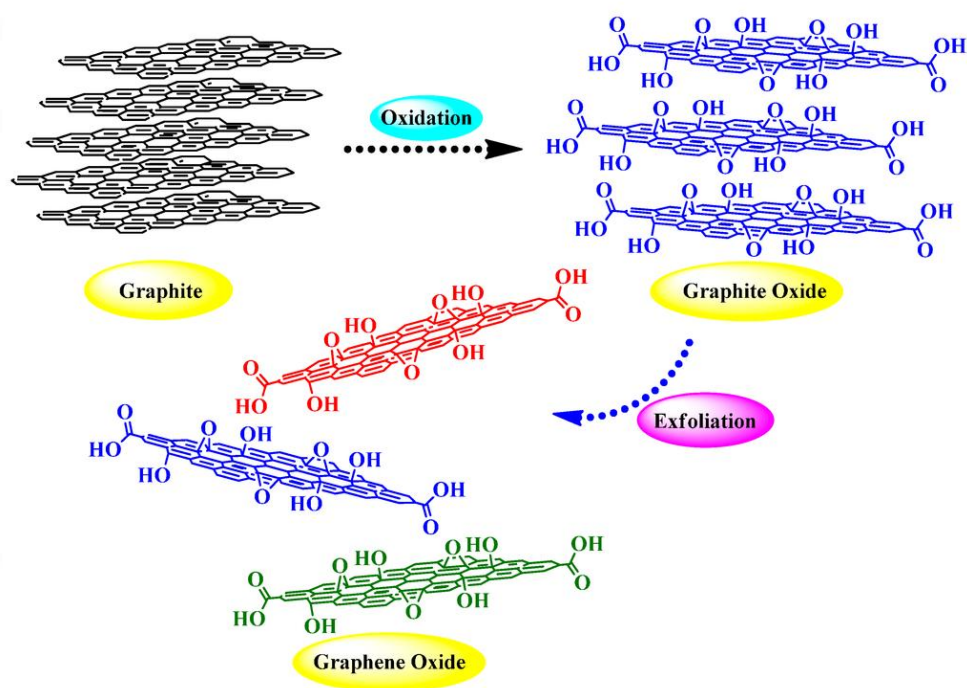
Figure 44. Preparation of graphite oxide and graphene oxide from graphite [117].

For comparision, we aimed to use graphene, a single-layer of graphite, as the support for the ruthenium(0) nanoparticles and had almost successfully prepared Ru/graphene when Cheng research group published the first paper on the same catalyst, reporting the development of a new Ru/graphene catalyst which provides a TOF value of 600 min^{-1} in hydrogen generation from the hydrolysis of AB at room temperature. The catalyst has been prepared by mixing $RuCl_3$, graphene oxide, ethylene glycol and ascorbic acid in an autoclave which was kept at 180 °C for 5h. Although Ru/graphene catalysts have been prepared under harsh conditions, they

have been reported to show remarkable activity in hydrogen generation from hydrolysis of AB due to the the small particle size (average particle size: 1.9 nm) and narrow size distribution of ruthenium nanoparticles dispersed on the graphene sheets.

Although graphene oxide has received considerable attention in literature as a catalyst support due to its outstanding charge carrier mobility, mechanical robustness, and chemical stability [116], the large scale production of uniform graphene oxide (GO) is still a challenge. Chemical reduction of GO is one of the effective method for the large scale preparation [117], which can be achieved by Hummers method [118,119]. Hummers method consists of many steps (Fig. 44 and Fig. 45) including oxidation of graphite, filtration, washing, and exfoliation. In this method, graphite is oxidized by concentrated H_2SO_4, $KMnO_4$ and $NaNO_3$. After the oxidation, the oxidized graphite is filtered and washed with dilute HCl. Than exfoliation of graphite oxide is performed by chemical treatment with hydrazine or DMF [120].
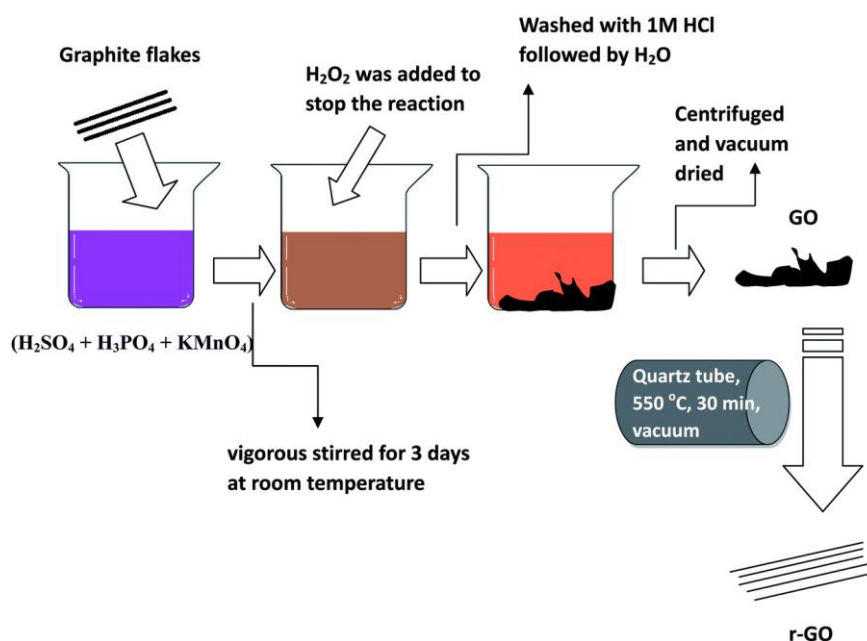
Figure 45. Illustration of the preparation procedures of graphene oxide(GO) and reduced-GO, made by Xavier et al [116].

Although Hummers method is a well known technique for the large scale preparation of graphene oxide, the oxidation conditions such as reaction temperature, stirring time and the type of acids for the oxidation show variation among the reported studies in literature. It is still a challenge to produce graphene sheets of the same quality.

After having missed the opportunity to use graphene as support for the ruthenium nanoparticles we considered to develop various ruthenium catalysts on different supporting materials such as xonotlite nanowire (one dimensional inorganic analog of carbon nanotubes), hydroxyapatite and magnetic silica-coated cobalt ferrite to achieve more active and stable catalysts in hydrolysis of AB as compared to the Ru^0/MWCNTs. We found that the catalytic activity of Ru^0/MWCNTs (TOF=329 min^{-1}) is higher than that of Ru^0/X-NW (TOF=135 min^{-1}), Ru^0/HAp (TOF=137 min^{-1}), Ru^0/SiO_2-$CoFe_2O_4$ (TOF=172 min^{-1}), in hydrogen generation from the hydrolysis of AB. As stated above, it is difficult to give a specific explanation for the high activity of Ru^0/MWCNTs. However, effect of small metal particle size on catalytic activity of the catalysts seems obvious (Table 11).

Table 11. Turnover frequency (TOF), total turnover number (TTO) and activation energy values of the ruthenium catalysts prepared in this dissertation for hydrogen generation from the hydrolysis of ammonia borane at 25.0 ± 0.1 °C.

Catalyst	Ru (mM)	E_a (nucleation)	E_a (surface growth)	E_a (hydrolysis)	TOF (min^{-1})	TTO (mol H_2/mol Ru)	Particle size (nm)
Ru^0/MWCNTs	0.189	77	41	33	329	26 400	2.5
Ru^0/SiO_2-$CoFe_2O_4$	0.194	116	51	45	172	-	-
Ru^0/X-NW	0.271	137	94	98	135	134 100	4.4
Ru^0/HAp	0.392	166	59	58	137	87 000	4.7

The smaller ruthenium(0) nanoparticles could adsorb more B-containing species than the larger ones during the catalytic reaction [115] and the increase of borate ions on the surface of metal nanoparticles may result in activity loss, which might be the main reason for the lower TTO value of Ru^0/MWCNTs (TTO= 26,400) as compared to that of Ru^0/X-NW (TTO= 134, 100) and Ru^0/HAp (TTO= 87,000). Among the ruthenium catalysts prepared in this dissertation, Ru^0/X-NW was found to have the longest life time providing TTO value of 134,100 for hydrogen generation from the

hydrolysis of AB at 25.0 ± 0.1 °C. There exists no strong evidence for the explanation of high catalytic life time of the catalysts.

Apparent activation energy values for the nucleation and surface growth of ruthenium NPs were given in Table 11. It is found that Ru^0/MWCNTs have the lowest nucleation activation energy value (E_a= 77 kJ/mol). Although one is tempted to see an inverse relation between the nucleation activation energy and TOF value or particle size of the ruthenium(0) nanoparticles, further investigation is needed for a concrete suggestion. As shown in Table 11, activation energy values for the surface growth of ruthenium NPs are close to the activation energy values of hydrolysis reaction. However, there is no strong evidence showing a relation between these values and TOF value or particle size of ruthenium NPs.

Since the magnetic separation making the recovery of catalysts much easier than by filtration and centrifugation we developed magnetically separable ruthenium catalysts. Indeed, Ru^0/SiO_2-$CoFe_2O_4$ was the first magnetically separable monometallic ruthenium catalyst used in hydrolysis of AB in literature. Ru^0/SiO_2-$CoFe_2O_4$ shows remarkable reusability as compared to other reported ruthenium catalysts listed in Table 12. This catalyst keeps 94% of initial catalytic activity even after the tenth use in hydrolysis of AB. Ru^0/HAp was also found highly reusable catalyst in the same reaction. Ru^0/HAp retains 92% of the initial catalytic activity even after the fifth use. While, Ru^0/MWCNTs shows a significant catalytic activity loss after the reusability tests due to the aggregation of ruthenium nanoparticles on the surface of carbon nanotubes. Due to the easy aggregation of metal nanoparticles on carbon after multiple use, carbon based ruthenium catalysts such as Ru/g-C_3N_4 [63], Ru/C [34], Ru/graphene [59], Ru/ND (nanodiamond) [68] are less reusable as compared to the metal oxide supported ruthenium catalysts such as Ru^0/SiO_2-$CoFe_2O_4$, Ru^0/HAp, Ru NPs@Al_2O_3[80], Ru NPs@ZK-4 [79] (Table 12).

Table 12. Reusability of the reported ruthenium catalysts used in hydrolysis of AB at room temperature.*Ammonia borane was added into the reaction solution without separating the catalyst from the reaction mixture.

Catalyst	Ru (mM)	TOF (min^{-1})	Reusability (% of retaining initial activity)	Ref
Ru^0/SiO$_2$-CoFe$_2$O$_4$	0.744	100	94% after 10.Run	[72]
Ru^0/HAp	1.175	137	92% after 5.Run	[74]
Ru NPs@Al$_2$O$_3$	1.0	83	90% after 10.Run	[80]
Ru NPs@ZK-4	0.2	91	85 % after 5.Run	[79]
Ru^0/HfO$_2$	1.58	170	75% after 5.Run	[73]
RuNPs@TiO$_2$	0.25	200	65% after 5.Run	[121]
Ru^0/CeO$_2$	0.76	249	60% after 5.Run	[60]
Laurate stabilized Ru NPs	1.0	75	53% after 5.Run	[81]
Ru/g-C$_3$N$_4$	-	313	50% after 4.Run	[63]
Ru^0/X-NW	0.271	135	100% after 2.Run	[75]
Ru/C	0.85	429.5	43.1% after 5.Run	[34]
Ru^0/MWCNTs	0.567	329	41% after 4.Run	[61]
Ru/ND	-	229	40% after 5.Run	[68]
Nanoporous Ru	1.0	26.7	*67% after 5.Run	[82]
Ru@SBA-15 NCs	0.4	316	*100% after 5.Run	[62]
Ru/graphene	-	600	*80% after 5.Run	[59]
Ru@MIL-53(Al)	0.38	266.9	*75% after 5.Run	[65]
Ru/graphene	1.0	100	*72% after 4.Run	[78]
Ru@MIL-53(Cr)	0.39	260.8	*71% after 5.Run	[65]
Ru/MIL-96	0.48	231	*65% after 5.Run	[67]

CHAPTER 8

CONCLUSION

In conclusion, highly active, reusable and long-lived ruthenium catalysts for hydrogen generation from the hydrolysis of ammonia borane were developed: Ruthenium nanoparticles supported on multiwalled carbon nanotubes (Ru^0/MWCNTs), xonotlite nanowire (Ru^0/X-NW), hydroxyapatite (Ru^0/Hap), magnetic silica-coated cobalt ferrite (Ru^0/SiO_2-$CoFe_2O_4$). All the catalysts were *in situ* generated from the reduction of precursor ruthenium(III) ions impregnated on the surface of support during the hydrolysis of ammonia borane at room temperature, isolated from the reaction solution and characterized by using advanced analytical tools including TEM, SEM, EDS, XRD, XPS, ICP-OES. The formation of ruthenium(0) nanoparticles supported on MWCNTs, X-NW, HAp, SiO_2-$CoFe_2O_4$ and the hydrogen generation from the hydrolysis of ammonia borane occur concomitantly in the same medium at room temperature. The use of hydrogen generation from the hydrolysis of AB as reporter reaction gives valuable insights to the formation kinetics of ruthenium(0) nanoparticles. All the kinetic data, collected for the nanoparticles formation and concomitant hydrolytic dehydrogenation of AB catalyzed by Ru^0/MWCNTs, Ru^0/X-NW, Ru^0/HAp, Ru^0/SiO_2-$CoFe_2O_4$ under various experimental conditions, fit well to the 2-step mechanism for the nanoparticles formation: the nucleation (P $\rightarrow$ Q, rate constant k_1) and then autocatalytic surface growth (P + Q $\rightarrow$ 2Q, rate constant k_2) [41,42]. In addition to the activation energy for the catalytic hydrolysis of ammonia borane, the activation energies for the slow nucleation and autocatalytic surface growth of ruthenium(0) nanoparticles could be obtained from the evaluation of individual rate constants for

the slow nucleation (k_1) and autocatalytic surface growth (k_2) (Table 11). They give an idea on the energy barrier for the slow nucleation and autocatalytic surface growth of ruthenium(0) nanoparticles catalysts.

The main findings from this dissertation can be summarized as follows:

Ruthenium(0) nanoparticles supported on multiwalled carbon nanotube (Ru^0/MWCNTs) were easily generated *in situ* during the hydrolysis of ammonia borane. Ruthenium(0) nanoparticles of size in the range 1.4−3.0 nm are well-dispersed on multiwalled carbon nanotubes and they showed remarkable catalytic activity with an initial turn over frequency of 329 min^{-1} at room temperature. The reusability and lifetime experiments show that Ru^0/MWCNTs are still active catalyst in the hydrolysis of ammonia borane even after the fourth run preserving 41% of their initial catalytic activity and also providing 26400 turnovers over 29 h in the hydrolysis of AB at 25.0 ± 0.1 °C before deactivation. Easy preparation and the high catalytic performance of Ru^0/MWCNTs reveal that ruthenium(0) nanoparticles supported on multiwalled carbon nanotubes is a promising catalyst in hydrogen generation from hydrolysis of ammonia borane. Indeed, this study, with more than 50 citations, has become a pioneer publication among the carbon based catalysts used in hydrolysis of ammonia borane

Ruthenium(0) nanoparticles supported on xonotlite nanowire (Ru^0/X-NW) were prepared by the ion exchange of Ru^{3+} ions with Ca^{2+} ions in the lattice of xonotlite nanowire followed by the reduction of the Ru^{3+} exchanged xonotlite nanowire with sodium borohydride in aqueous solution at room temperature. Highly dispersed ruthenium(0) nanoparticles with particle size 4.4 ± 0.4 nm, supported on xonotlite nanowire were reproducibly prepared and characterized by a combination of advanced analytical techniques. Ru^0/X-NW shows high catalytic activity in hydrogen generation from the hydrolysis of AB. It provides a turnover frequency value up to 135 min^{-1} at 25.0 ± 0.1 °C. Ru^0/X-NW provides remarkable catalytic life-time (TTO = 134 100) for hydrogen generation from the hydrolysis of AB at 25.0 ± 0.1 °C. Long lifetime of nanoparticles catalyst supported on xonotlite nanowire are likely due to the strong adsorption capacity, high surface area and nonporous structure of xonotlite nanowire, which makes xonotlite nanowire an attractive candidate as supporting material in the catalysis field.

Ruthenium(0) nanoparticles supported on hydroxyapatite (Ru^0HAp) were prepared by the ion-exchange of Ru^{3+} ions with Ca^{2+} ions in the lattice of HAp and then reduced by AB at room temperature. Highly dispersed ruthenium(0) nanoparticles with particle size 4.7 ± 0.7 nm, on hydroxyapatite, were reproducibly prepared from the reduction of ruthenium(III) ions on the surface of hydroxyapatite during the catalytic hydrolysis of ammonia borane. They could be isolated from the reaction solution by filtration and characterized by a combination of advanced analytical techniques. Ru^0/HAp shows high catalytic activity in hydrogen generation from the hydrolysis of AB providing a turnover frequency value up to 137 min^{-1} at 25.0 ± 0.1 °C. Ru^0/HAp is long lived and reusable catalyst providing 87,000 turnovers for hydrogen generation from the hydrolysis of ammonia borane and maintaining 92% of their initial catalytic activity even after the fifth run of hydrolysis of ammonia borane at 25.0 ± 0.1 °C. Indeed, high ion exchange ability, high adsorption capacity and nonporous structures of hydroxyapatites could be main reason of high stability of Ru^0/HAp in hydrogen generation from hydrolysis of ammonia borane.

Since the isolation of these catalysts from the reaction medium by filtration and centrifugation is difficult and material loss is inevitable during isolation process, a magnetically separable ruthenium catalyst was developed. Ruthenium(0) nanoparticles supported on magnetic silica-coated cobalt ferrite were *in situ* generated from the reduction of $Ru^{3+}/SiO_2\text{-}CoFe_2O_4$ during the catalytic hydrolysis of ammonia-borane. $Ru^0/SiO_2\text{-}CoFe_2O_4$ was magnetically isolated from the reaction solution by using a permanent magnet. $Ru^0/SiO_2\text{-}CoFe_2O_4$ is reusable catalyst in hydrogen generation from the hydrolysis of ammonia-borane retaining 94% of the original catalytic activity after the tenth use providing the evolution of 3.0 equivalent H_2 per mole of ammonia-borane. $Ru^0/SiO_2\text{-}CoFe_2O_4$ provides a turnover frequency value up to 172 min^{-1} at room temperature. $Ru^0/SiO_2\text{-}CoFe_2O_4$ catalyst is the first magnetically separable ruthenium catalyst developed for hydrogen generation from ammonia borane in literature.

The comparison of the ruthenium catalysts developed in this dissertation shows that i) $Ru^0/MWCNTs$ have the highest catalytic activity in hydrogen generation from the hydrolysis of ammonia borane at 25.0 ± 0.1 °C, ii) Ru^0/X-NW has the longest life time in this reaction, iii) Ru^0/HAp and $Ru^0/SiO_2\text{-}CoFe_2O_4$ are highly reusable

catalysts in hydrolytic dehydrogenation of ammonia borane. These catalysts can be employed in developing highly efficient, portable hydrogen generation systems using AB.

REFERENCES

[1]   Eberle U, Felderhoff M, Schüth F. Chemical and physical solutions for hydrogen storage. Angew Chemie - Int Ed 2009;48:6608–30.

[2]   Hamilton CW, Baker RT, Staubitz A, Manners I. B–N compounds for chemical hydrogen storage. Chem Soc Rev 2009;38:279–93.

[3]   Rosi NL. Hydrogen Storage in Microporous Metal-Organic Frameworks. Science 2003;300:1127–9.

[4]   Chen P, Xiong Z, Luo J, Lin J, Tan KL. Interaction of hydrogen with metal nitrides and imides. Nature 2002;420:302–4.

[5]   Lu Z-H, Xu Q. Recent Progress In Boron- And Nıtrogen-Based Chemıcal Hydrogen Storage. Functional Materials Letters 2012;5:1230001-9.

[6]   Yadav M, Xu Q. Liquid-phase chemical hydrogen storage materials. Energy & Environmental Science 2012;5:9698-9725.

[7]   Dillich, S. *2009 DOE Hydrogen Program & Vehicle Technologies Program* http://www.hydrogen.energy.gov/pdfs/review09/st_0_dillich.pdf. DOE has recently lowered the 2015 gravimetric total system target to only 5.5 total system weight %. (accessed July 29, 2016)

[8]   OE Targets for Onboard Hydrogen Storage Systems for Light-Duty Vehicles | Department of Eenergy http://energy.gov/eere/fuelcells/downloads/doe-targets-onboard-hydrogen-storage-systems-light-duty-vehicles (accessed July 29, 2016).

[9]   Staubitz A, Robertson APM, Manners I. Ammonia-Borane and related compounds as dihydrogen sources. Chem Rev 2010;110:4079–124.

[10]   Sanyal U, Demirci UB, Jagirdar BR, Miele P. Hydrolysis of Ammonia Borane as a Hydrogen Source: Fundamental Issues and Potential Solutions Towards Implementation. ChemSusChem 2011;4:1731–9.

[11]   Chandra M, Xu Q. A high-performance hydrogen generation system: Transition metal-catalyzed dissociation and hydrolysis of ammonia–borane. Journal of Power Sources 2006;156:190–4.

[12]   Rachiero GP, Demirci UB, Miele P. Bimetallic RuCo and RuCu catalysts supported on γ-Al_2O_3. A comparative study of their activity in hydrolysis of ammonia-borane. Int J Hydrogen Energy 2011;36:7051-65.

[13]   Rachiero GP, Demirci UB, Miele P. Facile Synthesis by polyol method of a ruthenium catalyst supported on γ-Al_2O_3 for hydrolytic dehydrogenation of ammonia borane. Catal Today 2011;170:85-92.

[14]   Zahmakıran M, Özkar S. Metal nanoparticles in liquid phase catalysis; from recent advances to future goals. Nanoscale 2011;3:3462–81.

[15]   Anastas JH, Warner J. Green Chemistry: Theory and Practice, Oxford Uni. Press, 2000, ISBN 0-19-850698-8

[16]   Demirci UB. How green are the chemicals used as liquid fuels in direct liquid-feed fuel cells? Environment International 2009;35:626–31.

[17]   Nanotechnology Design: The Future of Building n.d. http://edavisndf2015.blogspot.com.tr/2015/09/the-future-of-building.html (accessed July 30, 2016).

[18]   Material synthesis and characterization | whynano n.d. https://whynano.wordpress.com/material-synthesis-and-characterization/ (accessed July 30, 2016).

[19]   O'Neill BJ, Jackson DHK, Lee J, Canlas C, Stair PC, Marshall CL, et al. Catalyst Design with Atomic Layer Deposition. ACS Catalysis 2015;5:1804–25.

[20]   Virkutyte J, Varma RS. Green synthesis of metal nanoparticles: Biodegradable polymers and enzymes in stabilization and surface functionalization. Chem Sci 2011;2:837–46.

[21]   Hunter, R.J., *Foundations of Colloid Science*, Vol. 1, Oxford Univ. Press, New York, 1987.

[22]   Bard, A.J., Faulkner, L.R., *Electrochemical Methods*, Wiley, New York, 1980.

[23]   Jia C-J, Schüth F. Colloidal metal nanoparticles as a component of designed catalyst. Physical Chemistry Chemical Physics 2011;13:2457-2487.

[24]   Özkar S. Transition metal nanoparticles as catalyst in hydrogen generation from the boron based hydrogen storage materials. In: Suib SL, editor. New and future developments in catalysis. Batteries, hydrogen storage and fuel cells. Elsevier; 2013. p. 165-89 [Chapter 7].

[25]   Regalbuto JR, editor. Catalyst preparation: science and engineering. Boca Raton: Taylor & Francis; 2007; 9

[26]   Coleman JN, Khan U, Blau WJ, Gun'ko YK. Small but strong: A review of the mechanical properties of carbon nanotube–polymer composites. Carbon 2006;44:1624–52.

[27]   Choudhary V, Gupta A. Polymer / Carbon Nanotube Nanocomposites. Intech 2001:65–90.

[28]   Zheng SF, Hu JS, Zhong LS, Wan LJ, Song WG. In situ one-step method for preparing carbon nanotubes and Pt composite catalysts and their performance for methanol oxidation. J Phys Chem C 2007;111:11174–9.

[29]   Metin Ö, Kayhan E, Özkar S, Schenieder JJ. Palladium nanoparticles supported on chemically derived graphene:highly active and reusable catalyst for the dehydrogenation of ammonia borane. Int J Hydrogen Energy 2012;37:8161-9.

[30]   Köckritz A, Sebek M, Dittmar A, Radnik J, Brückner A, Bentrup U, et al. Ru-catalyzed oxidation of primary alcohols. Journal of Molecular Catalysis A: Chemical 2006;246:85–99.

[31]   Zahmakıran M, Kodaira T, Özkar S. Ruthenium(0) nanoclusters stabilized by zeolite framework as superb catalyst for the hydrogenation of neat benzene under mild conditions: Additional studies including cation site occupancy, catalytic activity, lifetime, reusability and poisoning. Applied Catalysis B: Environmental 2010;96:533–40.

[32] Li Y, Zhang Q, Zhang N, Zhu L, Zheng J, Chen BH. Ru–RuO$_2$/C as an efficient catalyst for the sodium borohydride hydrolysis to hydrogen. International Journal of Hydrogen Energy 2013;38:13360–7.

[33] Akbayrak S, Tonbul Y, Özkar S. Ceria-supported ruthenium nanoparticles as highly active and long-lived catalysts in hydrogen generation from the hydrolysis of ammonia borane. Dalton Trans 2016;45:10969–78.

[34] Liang H, Chen G, Desinan S, Rosei R, Rosei F, Ma D. In situ facile synthesis of ruthenium nanocluster catalyst supported on carbon black for hydrogen generation from the hydrolysis of ammonia-borane. Int J Hydrogen Energy 2012;37:17921-7

[35] Lin K, Chang J, Chen G, Ruan M, Ning C. A simple method to synthesize single-crystalline β-wollastonite nanowires. Journal of Crystal Growth 2007;300:267–71.

[36] Choi J, Kim JC, Lee YB, Kim IS, Park YK, Hur NH. Fabrication of silica-coated magnetic nanoparticles with highly photoluminescent lanthanide probes. Chemical Communications 2007:1644-46..

[37] Kaya M, Zahmakiran M, Özkar S, Volkan M. Copper(0) Nanoparticles Supported on Silica-Coated Cobalt Ferrite Magnetic Particles: Cost Effective Catalyst in the Hydrolysis of Ammonia-Borane with an Exceptional Reusability Performance. ACS Applied Materials & Interfaces 2012;4:3866–73.

[38] Stöber W, Fink A, Bohn E. Controlled growth of monodisperse silica spheres in the micron size range. Journal of Colloid and Interface Science 1968;26:62–9.

[39] Planeix JM, Coustel N, Coq B, Brotons V, Kumbhar PS, Dutartre R, et al. Application of Carbon Nanotubes as Supports in Heterogeneous Catalysis. J Am Chem Soc 1994;116:7935–6.

[40] Lu J. Effect of surface modifications on the decoration of multi-walled carbon nanotubes with ruthenium nanoparticles. Carbon 2007;45:1599–605.

[41] Watzky MA, Finke RG. Transition metal nanocluster formation kinetic and mechanistic studies. A new mechanism when hydrogen is the reductant: Slow, continuous nucleation and fast autocatalytic surface growth. J Am Chem Soc 1997;119:10382–400.

[42] Widegren JA, Aiken JD, Özkar S, Finke RG. Additional investigations of a new kinetic method to follow transition-metal nanocluster formation, including the discovery of heterolytic hydrogen activation in nanocluster nucleation reactions. Chem Mater 2001;13:312–24.

[43] Widegren JA, Bennett MA, Finke RG. Is it homogeneous or heterogeneous catalysis? Identification of bulk ruthenium metal as the true catalyst in benzene hydrogenations starting with the monometallic precursor, Ru(II)(η^6-C$_6$Me$_6$)(OAc)$_2$, plus kinetic characterization of the heterogeneous nucleation, then autocatalytic surface-growth mechanism of metal film formation. J Am Chem Soc 2003;125:10301–10.

[44] Jin C, Xia W, Nagaiah TC, Guo J, Chen X, Bron M, et al. On the role of the thermal treatment of sulfided Rh/CNT catalysts applied in the oxygen reduction reaction. Electrochim Acta 2009;54:7186–93.

[45]   Sun Z, Zhang X, Na N, Liu Z, Han B, An G. Synthesis of ZrO_2-carbon nanotube composites and their application as chemiluminescent sensor material for ethanol. J Phys Chem B 2006;110:13410–4.

[46]   Zhang H, Chu W, Zou C, Huang Z, Ye Z, Zhu L. Promotion effects of platinum and ruthenium on carbon nanotube supported cobalt catalysts for Fischer-Tropsch synthesis. Catal Letters 2011;141:438–44.

[47]   Wagner, C.; Muilenber, G. E.; Riggs, W. M.; Davis, L. E.; Moulder, J. F. Handbook of X-ray Photoelectron Spectroscopy; Physical Electronic Division, Perkin-Elmer: Eden Prairie, MN, 1979; Vol. 55.

[48]   López E, Kim J, Shanmugharaj AM, Ryu SH. Multiwalled carbon nanotubes-supported Nickel catalysts for the steam reforming of propane. Journal of Materials Science 2012;47:2985–94.

[49]   Özhava D. Özkar S. Rhodium(0) nanoparticles supported on nanosilica: Highly active and long lived catalyst in hydrogen generation from the methanolysis ofammonia borane. Appl Catal B: Environmental, 2016;181:716–26.

[50]   Watzky MA, Finney EE, Finke RG. Transition-Metal Nanocluster Size vs Formation Time and the Catalytically Effective Nucleus Number: A Mechanism-Based Treatment. Journal of the American Chemical Society 2008;130:11959–69.

[51]   Crooks AB, Yih KH, Li L, Yang JC, Özkar S, Finke RG. Unintuitive Inverse Dependence of the Apparent Turnover Frequency on Precatalyst Concentration: A Quantitative Explanation in the Case of Ziegler-Type Nanoparticle Catalysts Made from $[(1,5\text{-}COD)Ir(\mu\text{-}O_2C_8H_{15})]_2$ and $AlEt_3$. ACS Catal 2015;5:3342−53.

[52]   Shmidt FK, Nindakova LO, Shainyan BA, Saraev VV, Chipanina NN, Umanetz VA. Hydrogenation catalysts formation in the system $AlEt_3$-$Co(acac)_{2,3}$. J Mol Catal A: Chem 2005;235:161–72.

[53]   Steinhoff BA, Fix SR, Stahl SS. Mechanistic Study of Alcohol Oxidation by the $Pd(OAc)_2/O_2/DMSO$ Catalyst System and Implications for the Development of Improved Aerobic Oxidation Catalysts. J Am Chem Soc 2002;124:766–67.

[54]   Sanchez-Delgado RA, Andriollo A, Puga J, Martin G. Homogeneous catalysis by metal clusters. 2. Tetranuclear osmium complexes as catalyst precursors in the hydrogenation of styrene. Inorg Chem 1987;26:1867–70.

[55]   Reetz MT, De Vries JG. Ligand-free Heck reactions using low Pd-loading. Chem Comm 2004;14:1559-63.

[56]   De Vries AHM, Mulders JMCA, Mommers JHM, Henderickx HJW, De Vries JG. Homeopathic Ligand-Free Palladium as a Catalyst in the Heck Reaction. A Comparison with a Palladacycle, Org Lett 2003;5:3285–88.

[57]   Doll KM, Finke RG. Adenosylcobinamide Plus Exogenous, Sterically Hindered, Putative Axial Bases: A Reinvestigation into the Cause of Record Levels of Co−C Heterolysis, Inorg Chem 2004;43:2611-23.

[58] Mori K, Miyawaki K, Yamashita H. Ru and Ru–Ni Nanoparticles on TiO$_2$ Support as Extremely Active Catalysts for Hydrogen Production from Ammonia–Borane. ACS Catal 2016:3128–35.

[59] Du C, Ao Q, Cao N, Yang L, Luo W, Cheng G. Facile synthesis of monodisperse ruthenium nanoparticles supported on graphene for hydrogen generation from hydrolysis of ammonia borane. Int J Hydrogen Energy 2015;40:6180–7.

[60] Akbayrak S, Tonbul Y, Özkar S. Ceria-supported ruthenium nanoparticles as highly active and long-lived catalysts in hydrogen generation from the hydrolysis of ammonia borane. Dalton Trans 2016;45:10969–78.

[61] Akbayrak S, Özkar S. Ruthenium(0) nanoparticles supported on multiwalled carbon nanotube as highly active catalyst for hydrogen generation from ammoniaeborane. ACS Appl Mat Interfaces 2012;4:6302-10.

[62] Yao Q, Lu Z-H, Yang K, Chen X, Zhu M. Ruthenium nanoparticles confined in SBA-15 as highly efficient catalyst for hydrolytic dehydrogenation of ammonia borane and hydrazine borane. Sci Rep 2015;5:15186.

[63] Fan Y, Li X, He X, Zeng C, Fan G, Liu Q, et al. Effective hydrolysis of ammonia borane catalyzed by ruthenium nanoparticles immobilized on graphic carbon nitride. Int. J. Hydrogen Energy 2014;39:19982–9.

[64] Xiong X, Zhou L, Yu G, Yang K, Ye M, Xia Q. Synthesis and catalytic performance of a novel RuCuNi/CNTs nanocomposite in hydrolytic dehydrogenation of ammonia borane. Int J Hydrogen Energy 2015;40:15521–8.

[65] Yang K, Zhou L, Yu G, Xiong X, Ye M, Li Y, et al. Ru nanoparticles supported on MIL-53(Cr, Al) as efficient catalysts for hydrogen generation from hydrolysis of ammonia borane. Int J Hydrogen Energy 2016;41:6300–9.

[66] Akbayrak S, Tanyildizi S, Morkan I, Özkar S. Ruthenium(0) nanoparticles supported on nanotitania as highly active and reusable catalyst in hydrogen generation from the hydrolysis of ammonia borane. Int J Hydrogen Energy 2014;39:9628–37.

[67] Wen L, Su J, Wu X, Cai P, Luo W, Cheng G. Ruthenium supported on MIL-96: An efficient catalyst for hydrolytic dehydrogenation of ammonia borane for chemical hydrogen storage. Int J Hydrogen Energy 2014;39:17129–35.

[68] Fan G, Liu Q, Tang D, Li X, Bi J, Gao D. Nanodiamond supported Ru nanoparticles as an effective catalyst for hydrogen evolution from hydrolysis of ammonia borane. Int J Hydrogen Energy 2016;41:1542–9.

[69] Yao Q, Shi W, Feng G, Lu ZH, Zhang X, Tao D, et al. Ultrafine Ru nanoparticles embedded in SiO$_2$ nanospheres: Highly efficient catalysts for hydrolytic dehydrogenation of ammonia borane. J Power Sources 2014;257:293–9.

[70] Metin Ö, Şahin Ş, Özkar S. Water-soluble poly(4-styrenesulfonic acid-co-maleic acid) stabilized ruthenium(0) and palladium(0) nanoclusters as highly active catalysts in hydrogen generation from the hydrolysis of ammonia-borane. Int J Hydrogen Energy 2009;34:6304–13.

[71]   Roy S, Pachfule P, Xu Q. High Catalytic Performance of MIL-101-Immobilized NiRu Alloy Nanoparticles towards the Hydrolytic Dehydrogenation of Ammonia Borane. Eur J Inorg Chem 2016:1–6.

[72]   Akbayrak S, Kaya M, Volkan M, Özkar S. Ruthenium(0) nanoparticles supported on magnetic silica coated cobalt ferrite: Reusable catalyst in hydrogen generation from the hydrolysis of ammonia-borane. J Mol Catal A Chem 2014;394:253–61.

[73]   Kalkan E-B, Akbayrak S, Özkar S. Ruthenium(0) Nanoparticles Supported on Nanohafnia: A Highly Active and Long-Lived Catalyst in Hydrolytic Dehydrogenation of Ammonia Borane Submitted to J Mol Catal A Chem.

[74]   Akbayrak S, Erdek P, Özkar S. Hydroxyapatite supported ruthenium(0) nanoparticles catalyst in hydrolytic dehydrogenation of ammonia borane: Insight to the nanoparticles formation and hydrogen evolution kinetics. Appl Catal B Environ 2013;142-143:187–95.

[75]   Akbayrak S, Özkar S. Ruthenium(0) nanoparticles supported on xonotlite nanowire: a long-lived catalyst for hydrolytic dehydrogenation of ammonia-borane. Dalton Trans 2014;43:1797–805.

[76]   Cao N, Hu K, Luo W, Cheng G. RuCu nanoparticles supported on graphene: A highly efficient catalyst for hydrolysis of ammonia borane. J Alloys Compd 2014;590:241–6.

[77]   Basu S, Brockman A, Gagare P, Zheng Y, Ramachandran PV, Delgass WN, et al. Chemical kinetics of Ru-catalyzed ammonia borane hydrolysis. Journal of Power Sources 2009;188:238–43.

[78]   Cao N, Luo W, Cheng GZ. One-step synthesis of graphene supported Ru nanoparticles as efficient catalysts for hydrolytic dehydrogenation of ammonia borane. Int J Hydrogen Energy 2013;38:11964-72.

[79]   Zahmakiran M. Preparation and characterization of LTA-type zeolite framework dispersed ruthenium nanoparticles and their catalytic application in the hydrolytic dehydrogenation of ammonia-borane for efficient hydrogen generation. Mater Sci Eng B Solid-State Mater Adv Technol 2012;177:606–13.

[80]   Can H, Metin Ö. A facile synthesis of nearly monodisperse ruthenium nanoparticles and their catalysis in the hydrolytic dehydrogenation of ammonia borane for chemical hydrogen storage. Appl Catal B Environ 2012;125:304–10.

[81]   Durap F, Zahmakiran M, Özkar S. Water soluble laurate-stabilized ruthenium(0) nanoclusters catalyst for hydrogen generation from the hydrolysis of ammonia-borane: High activity and long lifetime. Int J Hydrogen Energy 2009;34:7223–30.

[82]   Zhou Q, Yang H, Xu C. Nanoporous Ru as highly efficient catalyst for hydrolysis of ammonia borane. Int J Hydrogen Energy 2016:1–8.

[83]   Abo-Hamed EK, Pennycook T, Vaynzof Y, Toprakcioglu C, Koutsioubas A, Scherman OA. Highly active metastable ruthenium nanoparticles for hydrogen production through the catalytic hydrolysis of ammonia borane. Small 2014;10:3145–52.

[84]   Yao Q, Lu Z-H, Jia Y, Chen X, Liu X. In situ facile synthesis of Rh nanoparticles supported on carbon nanotubes as highly active catalysts for H_2 generation from NH_3BH_3 hydrolysis. International Journal of Hydrogen Energy 2015;40:2207–15.

[85]   Chen W, Ji J, Duan X, Qian G, Li P, Zhou X, et al. Unique reactivity in Pt/CNT catalyzed hydrolytic dehydrogenation of ammonia borane. Chem Commun 2014;50:2142-4.

[86]   Wang J, Qin Y-L, Liu X, Zhang X-B. In situ synthesis of magnetically recyclable graphene-supported Pd@Co coreshell nanoparticles as efficient catalysts for hydrolytic dehydrogenation of ammonia borane. J Mater Chem. 2012;22:12468-70.

[87]   Cao N, Su J, Luo W, Cheng G. Graphene supported Ru@Co coreeshell nanoparticles as efficient catalysts for hydrogen generation from hydrolysis of ammonia borane and methylamine borane. Catal Commun 2014;43:47-51.

[88]   Cao N, Su J, Luo W, Cheng G. Hydrolytic dehydrogenation of ammonia borane and methylamine borane catalyzed by graphene supported Ru@Ni coreeshell nanoparticles. Int. J. Hydrogen Energy 2014;39:426-35.

[89]   Cao N, Su J, Hong X, Luo W, Cheng G. In situ facile synthesis of Ru-based coreeshell nanoparticles supported on carbon black and their high catalytic activity in the dehydrogenation of amine-boranes. Chem Asian J 2014;9:562-71.

[90]   Basu S, Brockman A, Gagare P, Zheng Y, Ramachandran PV, Delgass WN, et al. Chemical kinetics of Ru-catalyzed ammonia borane hydrolysis. Journal of Power Sources 2009;188:238–43.

[91]   Yang L, Luo W, Cheng G. Graphene-Supported Ag-Based Core–Shell Nanoparticles for Hydrogen Generation in Hydrolysis of Ammonia Borane and Methylamine Borane. ACS Appl Mater Interfaces 2013;5:8231–40.

[92]   Güngörmez K, Metin Ö. Composition-controlled catalysis of reduced graphene oxide supported CuPd alloy nanoparticles in the hydrolytic dehydrogenation of ammonia borane. Applied Catalysis A: General 2015;494:22–8.

[93]   Çiftci NS, Metin Ö. Monodisperse nickel–palladium alloy nanoparticles supported on reduced graphene oxide as highly efficient catalysts for the hydrolytic dehydrogenation of ammonia borane. International Journal of Hydrogen Energy 2014;39:18863–70.

[94]   Kılıç B, Şencanlı S, Metin Ö. Hydrolytic dehydrogenation of ammonia borane catalyzed by reduced graphene oxide supported monodisperse palladium nanoparticles: High activity and detailed reaction kinetics. Journal of Molecular Catalysis A: Chemical 2012;361–362:104–10.

[95]   Zhang J, Chen C, Yan W, Duan F, Zhang B, Gao Z, et al. Ni nanoparticles supported on CNTs with excellent activity produced by atomic layer deposition for hydrogen generation from the hydrolysis of ammonia borane. Catal Sci Technol 2016;6:2112–9.

[96]   Zhao G, Zhong J, Wang J, Sham T-K, Sun X, Lee S-T. Revealing the synergetic effects in Ni nanoparticle-carbon nanotube hybrids by scanning transmission X-ray microscopy and their application in the hydrolysis of ammonia borane. Nanoscale 2015;7:9715–22.

[97]   Sun D, Mazumder V, Metin O, Sun S. Catalytic Hydrolysis of Ammonia Borane *via* Cobalt Palladium Nanoparticles. ACS Nano 2011;5:6458–64.

[98]   Yang Y, Zhang F, Wang H, Yao Q, Chen X, Lu Z-H. Catalytic Hydrolysis of Ammonia Borane by Cobalt Nickel Nanoparticles Supported on Reduced Graphene Oxide for Hydrogen Generation. Journal of Nanomaterials 2014;2014:1–9.

[99]   Feng W, Yang L, Cao N, Du C, Dai H, Luo W, et al. In situ facile synthesis of bimetallic CoNi catalyst supported on graphene for hydrolytic dehydrogenation of amine borane. International Journal of Hydrogen Energy 2014;39:3371–80.

[100]   Yang L, Su J, Meng X, Luo W, Cheng G. In situ synthesis of graphene supported Ag@CoNi core–shell nanoparticles as highly efficient catalysts for hydrogen generation from hydrolysis of ammonia borane and methylamine borane. Journal of Materials Chemistry A 2013;1:10016.

[101]   Yang L, Cao N, Du C, Dai H, Hu K, Luo W, et al. Graphene supported cobalt(0) nanoparticles for hydrolysis of ammonia borane. Materials Letters 2014;115:113–6.

[102]   Du C, Su J, Luo W, Cheng G. Graphene supported Ag@Co core–shell nanoparticles as e fficient catalysts for hydrolytic dehydrogenation of amine boranes. Journal of Molecular Catalysis A: Chemical 2014;383–384:38–45.

[103]   Yan JM, Wang ZL, Wang HL, Jiang Q. Rapid and energy efficient synthesis of a graphene CuCo hybrid as a high performance catalyst. J Mater Chem 2012;22:10990-3.

[104]   Metin O, Mazumder V, Özkar S, Sun S. Monodisperse Nickel Nanoparticles and Their Catalysis in Hydrolytic Dehydrogenation of Ammonia Borane. Journal of the American Chemical Society 2010;132:1468–9.

[105]   Du Y, Cao N, Yang L, Luo W, Cheng G. One-step synthesis of magnetically recyclable rGO supported Cu@Co core–shell nanoparticles: highly efficient catalysts for hydrolytic dehydrogenation of ammonia borane and methylamine borane. New Journal of Chemistry 2013;37:3035.

[106]   Xi P, Chen F, Xie G, Ma C, Liu H, Shao C, et al. Surfactant free RGO/Pd nanocomposites as highly active heterogeneous catalysts for the hydrolytic dehydrogenation of ammonia borane for chemical hydrogen storage. Nanoscale 2012;4:5597-5601.

[107]   Wen M, Sun B, Zhou B, Wu Q, Peng J. Controllable assembly of Ag/C/Ni magnetic nanocables and its low activation energy dehydrogenation catalysis. Journal of Materials Chemistry 2012;22:11988-11993

[108]   Yang Y, Lu Z-H, Hu Y, Zhang Z, Shi W, Chen X, et al. Facile in situ synthesis of copper nanoparticles supported on reduced graphene oxide for hydrolytic dehydrogenation of ammonia borane. RSC Advances 2014;4:13749-52.

[109]   (a) Shen JY, Adnot A, Kaliaguine S. An ESCA study of the interaction of oxygen with the surface of ruthenium. Applied Surface Science 1991;51:47–60. (b) Suñol JJ, Bonneau ME, Roué L, Guay D, Schulz R. XPS surface study of nanocrystalline Ti–Ru–Fe materials. Applied Surface Science 2000;158:252–62.

[110]   Watzky MA, Finke RG. Nanocluster size-control and "Magic Number" investigations. experimental tests of the "Living-metal polymer" concept and of mechanism-based size-control predictions leading to the syntheses of iridium (0) nanoclusters centering about four sequential magic numbers. Chemistry of Materials 1997;9:3083–3095.

[111]   Park KC, Jang IY, Wongwiriyapan W, Morimoto S, Kim YJ, Jung YC, et al. Carbon-supported Pt–Ru nanoparticles prepared in glyoxylate-reduction system promoting precursor–support interaction. Journal of Materials Chemistry 2010;20:5345-5354.

[112]   Chen G, Desinan S, Rosei R, Rosei F, Ma D. Synthesis of Ni–Ru Alloy Nanoparticles and Their High Catalytic Activity in Dehydrogenation of Ammonia Borane. Chem Eur J 2012;18:7925–30.

[113]   Chen W, Duan X, Qian G, Chen D, Zhou X. Carbon Nanotubes as Support in the Platinum-Catalyzed Hydrolytic Dehydrogenation of Ammonia Borane. ChemSusChem 2015;8:2927–31.

[114]   Chen W, Ji J, Duan X, Qian G, Li P, Zhou X, et al. Unique reactivity in Pt/CNT catalyzed hydrolytic dehydrogenation of ammonia borane. Chemical Communications 2014;50:2142-44.

[115]   Chen W, Ji J, Feng X, Duan X, Qian G, Li P, et al. Mechanistic Insight into Size-Dependent Activity and Durability in Pt/CNT Catalyzed Hydrolytic Dehydrogenation of Ammonia Borane. Journal of the American Chemical Society 2014;136:16736–9.

[116]   Xavier P, Sharma K, Elayaraja K, Vasu KS, Sood AK, Bose S. Reduced graphene oxide induced phase miscibility in polystyrene–poly(vinyl methyl ether) blends. RSC Advances 2014;4:12376-87.

[117]   Garg B, Bisht T, Ling Y-C. Graphene-Based Nanomaterials as Heterogeneous Acid Catalysts: A Comprehensive Perspective. Molecules 2014;19:14582–614.

[118]   Hummers WS, Offeman RE. Preparation of graphitic oxide J Am Chem Soc 1958;80:39-1339

[119]   Kovtyukhova NI, Ollivier PJ, Martin BR, Mallouk TE, Chizhik SA, Buzaneva EV, et al. Layer-by-layer assembly of ultrathin composite films from micron-sized graphite oxide sheets and polycations. Chem Mater 1999;11:771-8.

[120]   Ai KL, Liu YL, Lu LH, Cheng XL, Huo LH. A novel strategy for making soluble reduced graphene oxide sheets cheaply by adopting an endogenous reducing agent. J Mater Chem 2011;21:3365-70.

[121]   Konuş N, Karataş Y, Gulcan M. In Situ Formed Ruthenium(0) Nanoparticles Supported on TiO$_2$ Catalyzed Hydrogen Generation from Aqueous Ammonia-Borane Solution at Room Temperature Under Air. Synthesis and Reactivity in Inorganic, Metal-Organic, and Nano-Metal Chemistry 2016; 46:534–542

APPENDIX

All curve fit analysis has been made by following the steps given below:

1. Open Origin 8 Program
2. Click "Analysis-Nonlinear Curve Fit-Code-Function" to open the dialog given in Fig A1.
3. Add the function shown in Fig A1.
4. Click "Parameters" and fix the A value as 3 shown in Fig. A2 (since 3 equivalent H_2 generation)
5. Click "fit"
6. The data obtained as K1 and K2 are the rate constants for the slow nucleation and autocatalytic surface growth of metal(0) nanoparticles, respectively.
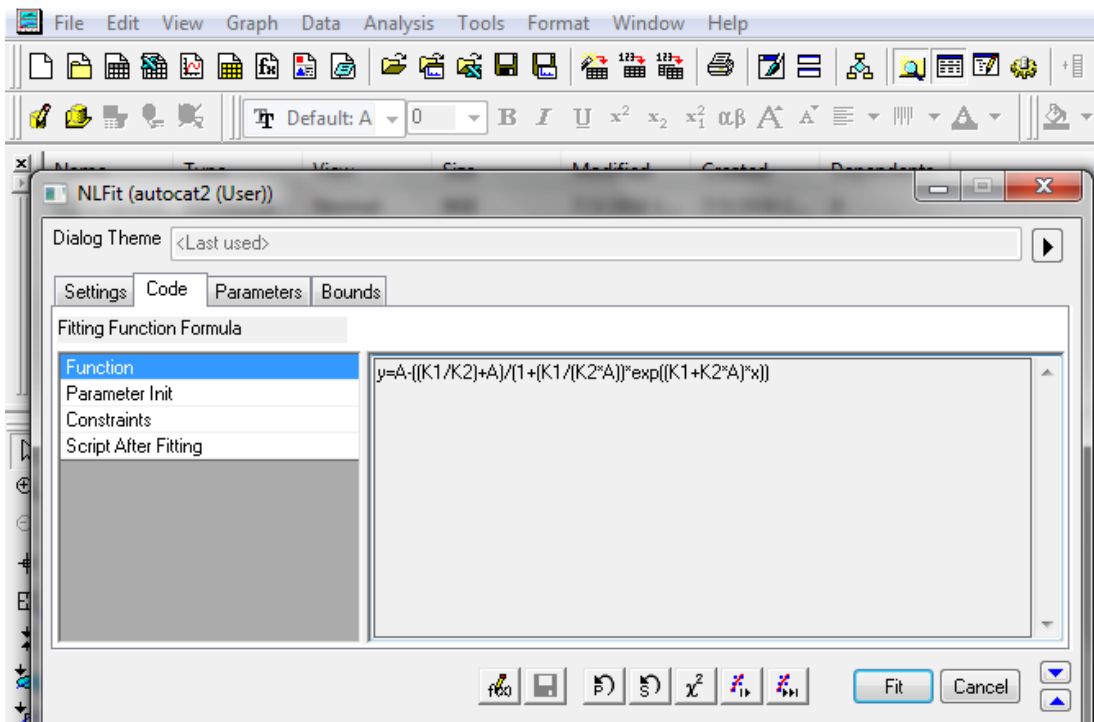
Figure A1: Function for the Finke-Watzky 2-step mechanism
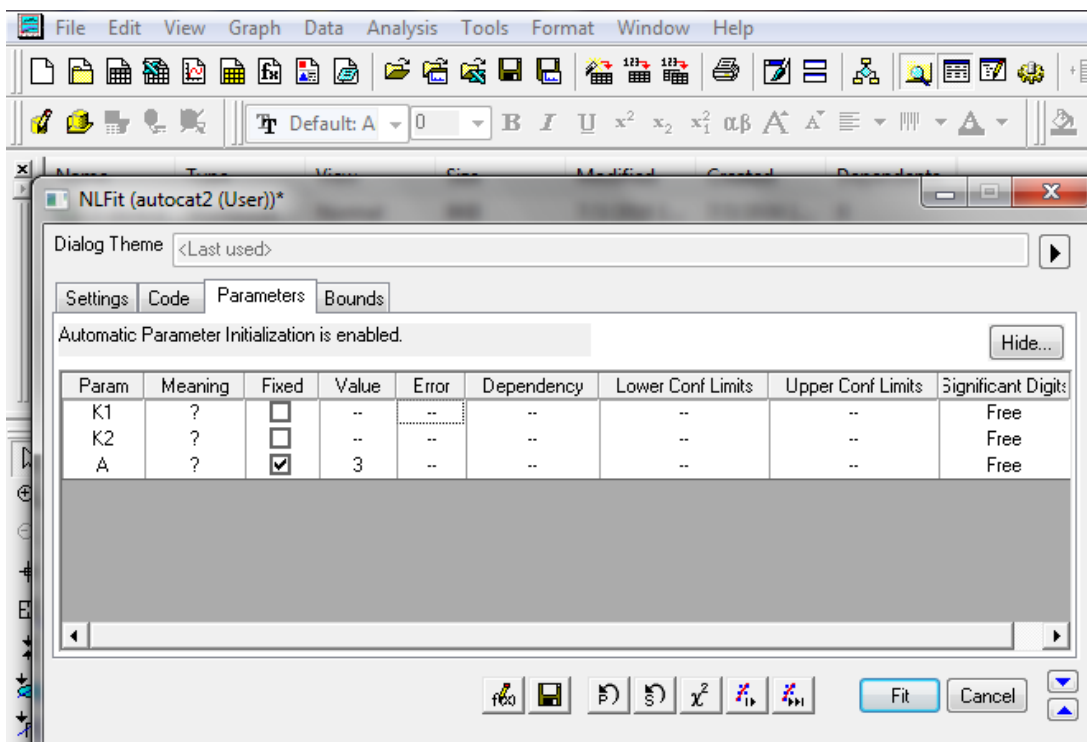
Figure A2: Parameters for the Finke-Watzky 2-step mechanism

Calculation of initial TOF value

TOF value (min^{-1})= (mmol H_2) (mmol Ru)$^{-1}$ (time)$^{-1}$

mmol H_2: mmol of collected hydrogen gas in the time range where the rate of hydrogen evolution is the highest

mmol Ru: total mol number of Ru atoms (no correction has been made for the number of active surface Ru atoms)

time: the time interval where the rate of hydrogen evolution is the highest
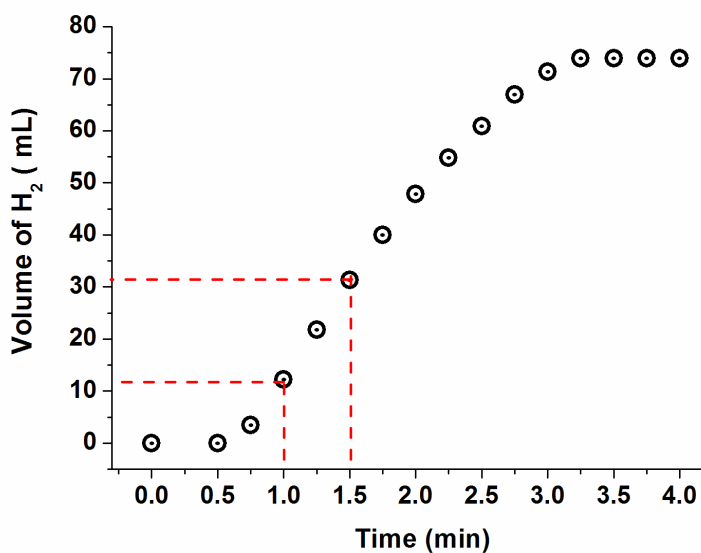
Figure A3: Hydrogen generation from the hydrolysis of ammonia borane (100 mM) using Ru^0/MWCNT ([Ru]= 0.567 mM which corresponds ≈0.00567 mmol Ru) at 25.0 ± 0.1°C.

ΔV= 19.14 mL $H_2 \approx$ 0.714 mmol H_2

Δt= 0.5 min

TOF value (min^{-1})= (0.714 mmol H_2) (0.00567 mmol Ru)$^{-1}$ (0.5 min)$^{-1}$ = 252 min^{-1}

CURRICULUM VITAE

Personal Data

Name   Serdar AKBAYRAK

Date of Birth   February 25, 1984

Status   Married

E-mail   serdar2730@gmail.com

Mobile   0544 468 14 99

Education

2011-present   Graduate School Natural and Applied Sciences, Middle East

Technical University, Turkey (Ph.D. in Chemistry)

2008-2011   Graduate School Natural and Applied Sciences, Middle East

Technical University, Turkey (M.S in Chemistry)

Thesis Title: "Synthesis and Characterization of Os(0)
Nanoclusters and Their Use in Aerobic Alcohol Oxidation"

2003-2008   Graduate School Natural and Applied Sciences, Middle East

Technical University, Turkey (B.S in Chemistry)

Positions

2014-2015   Visiting Researcher at Northwestern University, USA (12 months)

(Host Scientist: **Prof. Dr. Tobin Jay Marks**)

2011-2014   Teaching Assistant In Inorganic Chemistry, METU, Turkey

2010-2011   Visiting Researcher in Laboratory of Inorganic Chemistry at the
Technische Universität Darmstadt, Germany (3 months)

(Host Scientist: **Prof. Dr. Jörg Schneider**)

2010-2011   Teaching Assistant In Inorganic Chemistry, METU, Turkey

2009-2010   Teaching Assistant In General Chemistry Laboratory, METU,
Turkey

Awards

2010-2011   METU Graduate Courses Performance Award

The most successful student in the Ph.D.

Program of Department of Chemistry (CGPA: 3.71/4.00)

Scholarships

2010   Research Fellowship during IntenC exchange program between
METU and TU Darmstadt (Germany) by The Scientific and
Technological Research Council of Turkey (**TUBITAK**)

2014   Research Fellowship by The Scientific and Technological Research Council of Turkey (**TUBITAK**) for the special studies in Tobin Jay Marks' Lab at Northwestern University (USA)

Patent Application

2015   **Title of Invention:** Selective Benzene Hydrogenation by Bimetallic Nanoparticles Supported on Metal Oxides

Inventors: Massimiliano Delferro, Tobin J Marks, <u>Serdar Akbayrak</u>

Patent Number: Northwestern University 2015-025-01

Provisional Serial No: 62/156,726 (Filing Date: May 4, 2015)

Publications

1. "Osmium(0) Nanoclusters Stabilized by Zeolite Framework; Highly Active Catalyst in the Aerobic Oxidation of Alcohols Under Mild Conditions"

Mehmet Zahmakıran, **Serdar Akbayrak**, Tetsuya Kodaira and Saim Özkar

Dalton Trans., 2010, 39, 7521–7527

2. "Zeolite Framework Stabilized Nickel(0) Nanoparticles: Active and Long-lived Catalyst for Hydrogen Generation from the Hydrolysis of Ammonia-Borane and Sodium Borohydride"

Mehmet Zahmakıran, Tugce Ayvalı, **Serdar Akbayrak**, Salim Calıskan, Derya Celik, Saim Özkar

Catalysis Today 170 (2011) 76– 84

3. " Ruthenium(0) Nanoparticles Supported on Multiwalled Carbon Nanotube   As Highly Active Catalyst for Hydrogen Generation from Ammonia-Borane"

Serdar Akbayrak, Saim Özkar

ACS Appl. Mater. Interfaces 2012, 4, 6302−6310

4. "Dihydroxylation of Olefins Catalyzed by Zeolite-Confined Osmium(0) Nanoclusters: An Efficient and Reusable Method for the Preparation of 1,2-cis-diols"

Önder Metin, Nurdan Alcan Alp, **Serdar Akbayrak**, Abdullah Biçer, Mehmet Serdar Gültekin, Saim Özkar and Uğur Bozkaya

Green Chem. 2012, 14, 1488–1492

5. "Hydroxyapatite supported ruthenium(0) nanoparticles catalyst in hydrolytic dehydrogenation of ammonia borane: Insight to the nanoparticles formation and hydrogen evolution kinetics"

Serdar Akbayrak, Pelin Erdek, Saim Özkar

Applied Catalysis B: Environmental 142– 143 (2013) 187– 195

6. "One–Pot Synthesis of 1,2/3-triols from the Allylic Hydroperoxides Catalyzed by Zeolite-Confined Osmium(0) Nanoclusters"

Haydar Göksu, Diğdem Dalmızrak, **Serdar Akbayrak**, Mehmet Serdar Gültekin, Saim Özkar, Önder Metin

Journal of Molecular Catalysis A: Chemical 378 (2013) 142– 147

7. "Ruthenium(0) nanoparticles supported on xonotlite nanowire as long-lived catalyst for hydrolytic dehydrogeneration of ammonia-borane"

Serdar Akbayrak, Saim Özkar

Dalton Trans. 43 (2014) 1797-1805

8. "Palladium(0) nanoparticles supported on silica-coated cobalt ferrite: A highly active,magnetically separable and recyclable catalyst for hydrolytic dehydrogenation of ammonia-borane"

Serdar Akbayrak, Murat Kaya, Saim Özkar, Mürvet Volkan

Applied Catalysis B: Environmental 147 (2014) 387-393

9. "Rhodium(0) nanoparticles supported on nanotitania as highly active catalyst in hydrogen generation from the hydrolysis of ammonia borane"

<u>Serdar Akbayrak</u>, Serap Gençtürk, İzzet Morkan, Saim Özkar

RSC Advances 4 (2014) 13742-13748

10. "Immobilization of dioxomolybdenum(VI) complex bearing salicylidene 2-picoloyl hydrazone on chloropropyl functionalized SBA-15: A highly active, selective and reusable catalyst in olefin epoxidation"

Mojtaba Bagherzadeh, Maryam Zare, Taghi Salemnoush, Saim Özkar, **<u>Serdar Akbayrak</u>**

Applied Catalysis A: General 475 (2014) 55– 62

11. "Ruthenium(0) nanoparticles supported on nanotitania as highly active and reusable catalyst in hydrogen generation from the hydrolysis of ammonia borane"

<u>Serdar Akbayrak</u>, Seda Tanyıldızı, İzzet Morkan, Saim Özkar

International Journal of Hydrogen Energy 39 (2014) 9628-9637

12. "Ruthenium(0) nanoparticles supported on magnetic silica coated cobalt ferrite: Reusable catalyst in hydrogen generation from the hydrolysis of ammonia-borane"

<u>Serdar Akbayrak</u>, Murat Kaya, Saim Özkar, Mürvet Volkan

Journal of Molecular Catalysis A: Chemical 394 (2014) 253–261

13. "Epoxidation of olefins catalyzed by a molybdenum-Schiff base complex anchored in the pores of SBA-15"

Mojtaba Bagherzadeh, Maryam Zare, Taghi Salemnoush, **<u>Serdar Akbayrak</u>**, Saim Özkar

Journal of Molecular Catalysis A: Chemical 395 (2014) 470–480

14. "Immobilization of a molybdenum complex on the surface of magnetic nanoparticles for the catalytic epoxidation of olefins"

Maryam Zare, Zeinab Moradi-Shoeili, Mojtaba Bagherzadeh, **<u>Serdar Akbayrak</u>**, Saim Özkar

New Journal of Chemistry 40 (2016) 1580-1586.

15. "Synthesis, characterization and catalytic activity of supported molybdenum Schiff base complex as a magnetically–recoverable nanocatalyst in epoxidation reaction"

Zeinab Moradi-Shoeili, Maryam Zare, Mojtaba Bagherzadeh, Saim Özkar **<u>Serdar Akbayrak</u>**,

*Journal of Coordination Chem.*69(4) (2016) 668-677

16. "Palladium(0) nanoparticles supported on ceria: Highly active and reusable catalyst in hydrogen generation from the hydrolysis of ammonia borane

Yalçın Tonbul, **<u>Serdar Akbayrak</u>**, Saim Özkar

(International Journal of Hydrogen Energy 41 (2016) 11154-11162

17. "Ceria supported rhodium nanoparticles: Superb catalytic activity inhydrogen generation from the hydrolysis of ammonia borane

<u>Serdar Akbayrak</u>, Yalçın Tonbul, Saim Özkar

Applied Catalysis B: Environmental 198 (2016) 162–170

18. "Ceria-supported ruthenium nanoparticles as highly active and long-lived catalysts in hydrogen generation from the hydrolysis of ammonia borane"

<u>Serdar Akbayrak</u>, Yalçın Tonbul, Saim Özkar

Dalton Transactions 45 (2016) 10969–10978

19. "Facile Synthesis of Three-Dimensional Pt-TiO$_2$ Nanonetworks: Highly Active Catalyst for Hydrolytic Dehydrogenation of Ammonia Borane"

Mohammad Aref Khalily, Hamit Eren, **Serdar Akbayrak**, Hepi Hari Susapato, Necmi Biyikli, Saim Özkar, Mustafa O. Guler

(*Angewandte Chemie Int. Ed.* DOI:10.1002/anie.201605577R1)

20. "Inverse dependence of the catalytic activity on catalyst concentration for the ruthenium(0) nanoparticles supported on xonotlite nanowire in hydrogen generation from the hydrolysis of sodium borohydride"

Serdar Akbayrak, Saim Özkar

Journal of Molecular Catalysis A: Chemical 424 (2016) 254–260

21. "Oxazine containing molybdenum(VI)–oxodiperoxo complex immobilized on SBA-15 as highly active and selective catalyst in the oxidation of alkenes to epoxides under solvent-free conditions"

Maryam Zare, Zeinab Moradi-Shoeili, Parvin Esmailpour, **Serdar Akbayrak**, Saim Özkar

(Submitted to *RSC Advances*)

22. "Nanoceria Supported Palladium(0) Nanoparticles: Superb Catalyst in Dehydrogenation of Formic Acid at Room Temperature"

Serdar Akbayrak, Yalçın Tonbul, Saim Özkar

(Submitted to *Applied Catalysis B: Environmental)*

23. "Ruthenium(0) Nanoparticles Supported on Nanohafnia: A Highly Active and Long-Lived Catalyst in Hydrolytic Dehydrogenation of Ammonia Borane"

Elif Betül Kalkan, **Serdar Akbayrak**, Saim Özkar

(Submitted to *Journal of Molecular Catalysis A: Chemical*)

24. "Palladium nanoparticles supported on polydopamine coated Fe_3O_4 as magnetically recoverable and highly active catalyst for hydrolytic dehydrogenation of ammonia borane**"**

Joydev Manna, **Serdar Akbayrak**, Saim Özkar

(Submitted to *RSC Advances*)

25. "Ammonia Synthesis Using Hydrogen Migrating on the Surface of Ru/Zeolite-Y at Room Temperature"

Mustafa Yasin Aslan, **<u>Serdar Akbayrak</u>**, Deniz Üner, Saim Özkar (*Article in Preparation*)

26. "Bimetallic Palladium-Group 11 (Cu, Ag, Au) Metal Nanoparticles Supported on Alumina: Highly Benzene-Selective Catalysts for Competitive Arene Hydrogenation"

<u>Serdar Akbayrak</u>, Saim Özkar, James R. Gallagher, Jeffrey T. Miller, Alessandro Motta, Robertino Zanoni, Massimiliano Delferro and Tobin J. Marks (*Article in Preparation*)

Conferences

2016   "Ruthenium(0) nanoparticles supported on xonotlite nanowire as long-lived catalyst for hydrolytic dehydrogeneration of ammonia-borane" (*Oral presentation*)

   <u>Serdar Akbayrak</u>, Saim Özkar

   National Catalysis Conferences

   April 27-30, 2016, Bursa-Turkey

2012   "Dihydroxylation of Olefins Catalyzed by Zeolite-Confined Osmium(0) Nanoclusters: An Efficient and Reusable Method for the Preparation of 1,2-cis-diols" (Poster presentation)

   Önder Metin, Nurdan Alcan Alp, **<u>Serdar Akbayrak</u>**, Abdullah Biçer, Mehmet Serdar Gültekin, Saim Özkar and Uğur Bozkaya

   National Catalysis Conferences

March 21-24, 2012, Kocaeli-Turkey

2011   "Preparation and Characterization of Ruthenium(0) Nanoparticles Supported on Hydroxyapatite and Their Use in Hydrolysis of Sodium Borohydride" (Poster presentation)

Serdar Akbayrak, Saim Özkar

III. National Inorganic Chemistry Conference

May 19-22, 2011, Çanakkale-Turkey

2009   "Osmium(0) Nanoclusters Stabilized by Zeolite Framework; Highly Active Catalyst in the Aerobic Oxidation of Alcohols Under Mild Conditions" (Poster presentation)

Serdar Akbayrak, Mehmet Zahmakıran, Tetsuya Kodaira and Saim Özkar

13th European Conference on Applications of Surface and Interface Analysis

October 13-23, 2009, Antalya-Turkey